NONFLAMMABLE PERFLUOROPOLYETHER ELECTROLYTES FOR SAFER LITHIUM-BASED BATTERIES

Kevin Raymond Olson

A dissertation submitted to the faculty at the University of North Carolina at Chapel Hill in partial fulfillment of the requirements for the degree of Doctor of Philosophy in the Department of Chemistry.

Chapel Hill
2017

Approved by:

Joseph M. DeSimone

Frank A. Leibfarth

Amy C. Marschilok

Sergei S. Sheiko

R. Mark Wightman

ABSTRACT

Kevin Raymond Olson: Nonflammable Perfluoropolyether Electrolytes for Safer Lithium-Based Batteries
(Under the direction of Joseph M. DeSimone)

The importance of batteries to sustainable energy is widely recognized. Lithium-ion batteries (LIBs) not only power handheld electronics but also are increasingly being implemented in electric vehicles and "smart-grid" applications to store energy from intermittent solar and wind sources, making sustainable energy a reality. Unfortunately, LIBs contain a highly flammable solvent and can exhibit catastrophic failure, as was brought to the public's attention by the Boeing 787, Samsung Galaxy Note 7, hoverboard, and Tesla battery fires. Thus, realizing the full potential of LIBs in large-scale systems requires the development of nonflammable electrolytes.

Perfluoropolyether (PFPE)-based electrolytes address many of the shortcomings of conventional carbonate-based electrolytes or polymer electrolytes such as poly(ethylene oxide). PFPE-based electrolytes transport lithium more efficiently than conventional electrolytes, which has important implications on long-term battery performance. PFPEs make interesting electrolyte solvents because they are nonflammable, nonvolatile, liquid across a broad temperature range, chemically stable, and interact favorably with the anion of fluorinated salts. In this work, the molecular underpinnings for ion transport in PFPE electrolytes will be established by systematically probing how PFPE structure affects electrolyte performance including ionic conductivity, diffusivity, and transference number. End group polarity, end group concentration, and PFPE molecular weight all have important implications on electrolyte performance.

To my mother, Pam, who lost her battle with cancer 10 years ago. She instilled in me a love of learning and science, and I continue to strive to live in a way that would make her proud.

ACKNOWLEDGMENTS

I would like to acknowledge Dr. Mahati Chintapalli, Ksenia Timachova, Deep Shah, and Jiefu Yin, who did tremendous work to characterize ion transport and battery performance of these systems. It has truly been a pleasure for me to work with a group of such talented and personable researchers. I would also like to thank the principal investigators and research associates leading this collaboration—Dr. Nitash Balsara, Dr. Amy Marschilok, Dr. Esther Takeuchi, and Dr. Kenneth Takeuchi—for their insightful contributions to the work herein. I thank Dr. Sue Mecham, Dr. Bob Pinschmidt, and Dr. Ali Nebipasagil for their insightful and stimulating conversation and for continuing to nurture my growth as a scientist. I appreciate the time and insights of my other committee members as well—Dr. Frank Leibfarth, Dr. Sergei Sheiko, and Dr. Mark Wightman.

I'd like to express my sincere gratitude to my principal investigator, Professor Joseph DeSimone. I am humbled by the opportunity Professor DeSimone gave me to become a part of his research group, and I consider it an honor to have been guided both scientifically and professionally by him. I also appreciate all of my previous research advisors and mentors who instilled an enjoyment of the sciences in me and gave me the confidence to pursue a career in the sciences. I particularly thank Dr. Moses Lee and Dr. Tom Guarr for their wisdom that continues to influence me both personally and in my scientific career.

I thank my family and friends for their continued encouragement throughout this journey, which kept me going—my father and stepmother, Kurt and Crista, and my siblings, Jenny, Steve, and Lara. Finally, I thank my wonderful wife Stephanie for her endless support to pursue my passions as we take this journey together.

TABLE OF CONTENTS

LIST OF TABLES

LIST OF FIGURES

LIST OF CHEMICAL REACTION SCHEMES

LIST OF ABBREVIATIONS AND SYMBOLS

$(CD_3)_2CO$	deuterated acetone
1D	one-dimensional
2,2-DMPA	2,2-dimethoxy-2-phenylacetophenone
Å	angstroms
A	constant proportional to the number of charge carriers
a	cross-sectional area of electrolyte
AC	alternating current
amu	atomic mass unit
ASTM	American Society for Testing and Materials
ATR	attenuated total reflectance
B	activation energy for ion transport
c	molar salt concentration
C_8-X	perfluorinated octane; X represents terminal functional group
cm^{-1}	wavenumbers
cP	centipoise
CV	cyclic voltammetry

D_-	anion diffusion coefficient
D	diffusion coefficient
D_+	cation diffusion coefficient
d1	NMR relaxation time
DAC	di(allyl carbonate)
DAE	di(allyl ether)
DEC	diethyl carbonate or as end group, di(ethylene carbonate)
DFT	density functional theory
DMAP	4-dimethylaminopyridine
DMC	dimethyl carbonate or as end group, di(methyl carbonate)
DMF	N,N-dimethylformamide
DMSO	dimethyl sulfoxide
DN	donor number
DP	degree of polymerization
DPC	di(propargyl carbonate)
DSC	differential scanning calorimetry
E	voltage

EBC	ethylene biscarbonate
EC	ethylene carbonate
e_i	ionic charge
EO	ethylene oxide
exp	exponent
f	degree of functionality
F	Faraday's constant
FTIR	Fourier transform infrared spectroscopy
g	gradient strength
g/mol	grams per mole
GPC	gel permeation chromatography
H_f	enthalpy of fusion
HFP	hexafluoropropylene
HFPO	hexafluoropropylene oxide
HMIS	hazardous material identification system
HOMO	highest occupied molecular orbital
HSAB	hard soft acid base theory

I	current (for electrochemical measurements)
I	observed intensity (for spectroscopy)
IL	ionic liquid
IR	infrared spectroscopy
J	Joules
j	square root of -1
K	Kelvin
kDa	kiloDalton
l	length
Li	lithium
Li^+/Li-ion	lithium-ion
LIB	lithium-ion battery
LiBETI	lithium bis(pentafluoroethanesulfonyl)amide
LiFSI	lithium bis(fluorosulfonyl)amide
LiPFESI	lithium perfluoroetherbis(sulfonylamide)
LiTFSI	lithium bis(trifluoromethane)sulfonamide
LUMO	lowest unoccupied molecular orbital

M_c	critical molar mass for entanglements
MHz	megahertz
min	minutes
mm	millimeter
M_n	number-average molecular weight
$MTPEG_4$	tetraethylene glycol mono-thiol
M_v	viscosity-average molecular weight
MW	molecular weight
N	degree of polymerization
N_2	nitrogen gas
n_i	charge carrier concentration
nm	nanometer
Pa s	Pascal seconds
PEG	poly(ethylene glycol)
PEO	poly(ethylene oxide)
$PFEG_{\#}X$	perfluoroethylene glycol; # represents number of perfluoroethylene oxide repeat units; X represents terminal functional group
pfg-NMR	pulsed-field gradient nuclear magnetic resonance spectroscopy

PFPE	perfluoropolyether (if used generically, refers to Fluorolink D-based materials)
$PFPE_{D10H}$-X	materials synthesized from Fluorolink D10H (1400 g/mol); X represents terminal functional group
$PFPE_{D10}$-X	materials synthesized from Fluorolink D10 (1000 g/mol); X represents terminal functional group
$PFPE_{E10H}$-X	materials synthesized from Fluorolink E10H (1960 g/mol, EO end groups); X represents terminal functional group off of EO
$PFPE_{E10}$-X	materials synthesized from Fluorolink E10 (1200 g/mol, EO end groups); X represents terminal functional group off of EO
PTFE	polytetrafluoroethylene
R	ideal gas constant
R	resistance (for electrochemical calculations)
rf	radio frequency
R_{max}	maximum number of lithium ions per end group
r_{max}	maximum number of lithium ions per polymer repeat unit
ROP	ring-opening polymerization
RTIL	room-temperature ionic liquid
S/cm	Siemens per centimeter
SAXS	small-angle x-ray scattering
SEC	size exclusion chromatography

SEI	solid electrolyte interphase
SEO	polystyrene-block-poly(ethylene oxide)
SHE	standard hydrogen electrode
SPE	solid polymer electrolyte
T	temperature
t	time
t^+	transference number
T_c	crystallization temperature
$T_{d(5\%)}$	5% degradation temperature
TEA	triethylamine
TFE	tetrafluoroethylene
TFME	trifluoromethyl ester
T_g	glass transition temperature
TGA	thermogravimetric analysis
THF	tetrahydrofuran
T_m	melting temperature
$T_{ML(5\%)}$	5% mass loss temperature (caused by simple evaporation or degradation)

UV	ultraviolet
V	Volt
VFT	Vogel-Fulcher-Tammann (equation)
WAXS	wide-angle x-ray scattering
wt.%	weight percent
Z	impedance
β	iconicity
γ	gyromagnetic ratio
δ	chemical shift (in NMR spectra)
δ	duration of gradient pulse
Δ	interval between gradient pulses
ε	dielectric constant
ζ	friction coefficient
η	viscosity
η_D	refractive index
μ_i	ionic mobility
σ	ionic conductivity

τ	separation between gradient pulses
φ	phase shift
χ	Flory-Huggins interaction parameter

Chapter 1: Introduction to Lithium-Ion Battery Electrolytes

1.1 Importance of Batteries in the Global Energy Landscape

As the worldwide population grows, nonrenewable energy resources such as fossil fuels are being depleted. Furthermore, combustion of petroleum, fossil fuels, and coal releases carbon dioxide and other greenhouse gases that contribute to global warming.[1,2] These three fuel sources account for over 80% of energy consumption in the United States, as shown in Figure 1.1.[3]

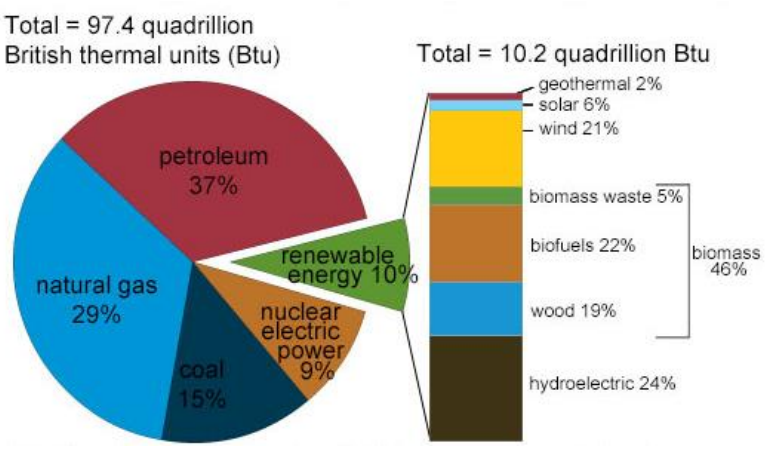

Figure 1.1 U.S. energy consumption by source in 2016. Reprinted from ref. [3].

In contrast, renewable energy sources such as wind and solar are sustainable and environmentally friendly. This has led the United States to take urgent steps toward shifting its energy usage to renewable sources. Following Executive Order 13693, the Department of Energy must triple the federal governments' renewable energy usage within the next 8 years, achieving 30% renewable energy consumption by the year 2025.[4] (This mandate remains in effect despite environmental policy changes made by the current administration in Executive Order 13783.)

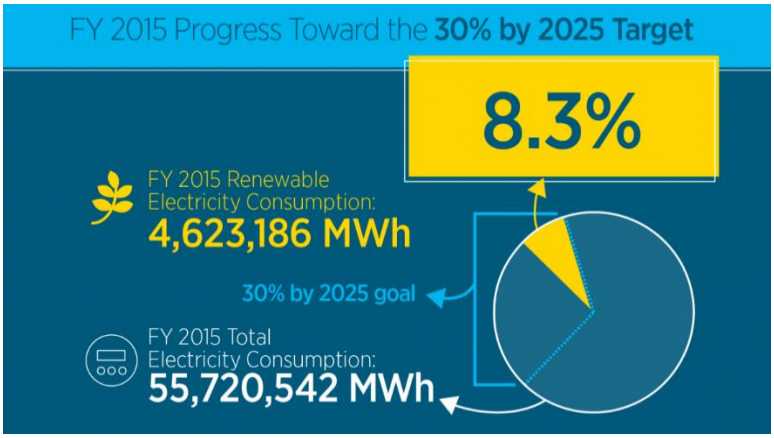

Figure 1.2 Curent and projected federal government energy consumption. Reprinted from ref. [4].

A major issue with renewable energy sources is their intermittent nature. Solar energy is only available when the sun is shining, and wind energy is only available when the wind is blowing. While fossil fuels can be stored for on-demand electricity production, sunshine and wind cannot be captured. Instead, the *electricity* generated by these energy sources must be stored for later use. Battery storage is one solution to this problem: excess electricity produced during peak hours can be stored for use at a time when the energy source is less abundant.[5]

Clearly, the emerging role of rechargeable batteries in our society goes beyond powering portable electronic devices like smartphones and laptops. Aside from grid energy storage, automobiles and aircraft are increasingly shifting toward electrification, reducing our dependence on fossil fuels and cutting greenhouse gas emissions. However, these developments can only be realized with a rechargeable battery that is safe, has high energy densities, and delivers energy quickly on-demand.

1.2 Development of Lithium-Ion Batteries

Lithium is both the most electropositive (-3.04 V vs. SHE) and lightest (6.94 amu) metal, making it a desirable active material for high-energy batteries. After initial demonstration of primary (single-use) batteries containing a metallic lithium anode in 1970,[6] scientists at Exxon

developed a secondary (rechargeable) battery containing a lithium negative electrode and titanium disulfide positive electrode.[7] TiS_2 was already known to reversibly intercalate lithium, theoretically allowing a battery to charge and discharge repeatedly. However, these batteries were not viable due to uneven plating of metallic lithium, resulting in dendrite formation and catastrophic battery failure. A short time later, John Goodenough made his seminal contribution to the battery, proposing lithium metal oxides with the formula LiM_xO_2 as positive electrode materials.[8] Scientists then demonstrated that carbonaceous secondary insertion materials could be substituted for lithium as the negative electrode material, solving the issue of metallic dendrite formation.[9] The first lithium-ion battery (LIB) was commercialized by Sony in 1992. It contained a graphite anode and $LiCoO_2$ cathode, the materials still found in the vast majority of LIBs today.[6] As a culmination of these technological developments, LIBs exhibit long life cycles and high power densities. Therefore, lithium-ion batteries are ubiquitous in today's society, powering laptops, smartphones, and other handheld portable electronics.[10] The lithium-ion battery market is currently valued at about $30 billion and is projected to grow to about $75 billion by 2025.[11]

1.3 Principles of Lithium-Ion Battery Operation

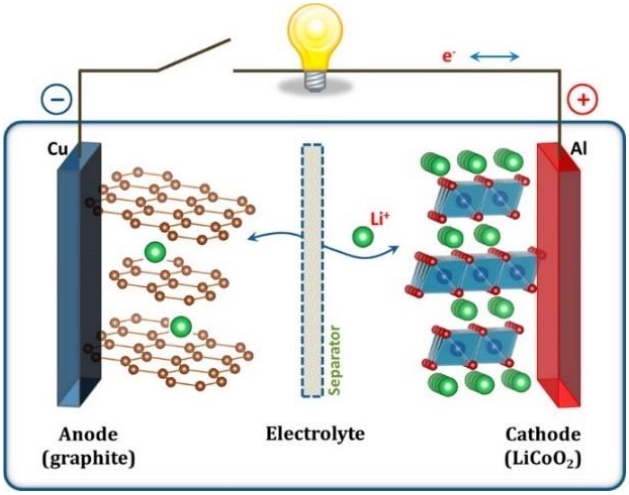

Figure 1.3 Schematic of a lithium-ion battery cell. Reprinted with permission from ref. [10]. Copyright (2013) American Chemical Society.

As shown in Figure 1.3, a lithium-ion battery cell consists of an anode and a cathode connected by an external circuit and separated internally by a separator that is swollen with electrolyte. The electrolyte conducts the ionic component of these reactions (Li^+), yet it is necessarily electronically insulating in order to avoid self-discharge and internal short circuits: the current is forced through the external circuit where work is performed.

LIB cathodes are typically composed of transition metal oxides like $LiCoO_2$ and $LiMn_2O_4$, while anodes primarily consist of carbon-based compounds such as graphite.[12] These layered, secondary insertion materials allow lithium ions to reversibly intercalate into the host electrode structures upon charge and discharge. The half reactions that occur at the graphite anode and the $LiCoO_2$ cathode are provided in Eqn. (1.1) and (1.2).

$$C_6 + x\,e^- + x\,Li^+ \leftrightarrow Li_xC_6 \quad (1.1)$$

$$LiCoO_2 \leftrightarrow x\,Li^+ + x\,e^- + Li_{1-x}CoO_2 \quad (1.2)$$

Commercial LIB electrolytes typically consist of a lithium salt like $LiPF_6$ dissolved in a mixture of small molecule alkyl carbonates such as ethylene carbonate (EC), dimethyl carbonate (DMC), and diethyl carbonate (DEC).[13] The separator consists of a thin, porous polyolefin, generally a trilayer polypropylene-polyethylene-polypropylene film for reasons that will be discussed in further detail in Section 1.4.2 .

In LIBs, alkyl carbonate solvent molecules are placed in contact with highly energetic active materials. Alkyl carbonates are not thermodynamically stable at the operating potentials of the electrodes. Fortunately, EC sacrificially reacts at electrode surfaces, forming a thin polymer network known as the solid-electrolyte interphase (SEI).[14] The SEI is electronically insulating and impermeable to solvent molecules, preventing further breakdown of the electrolyte. Li^+ is conductive through the SEI, enabling the desired galvanic reactions to occur within the electrodes.

1.4 Electrolyte Hazards

Unfortunately, the lithium-ion battery is plagued by safety hazards. Carbonate solvents, the main components of LIB electrolytes, are highly flammable and have low flash points.[15] Dimethyl carbonate (DMC) has an HMIS flammability rating of 3 on a scale from 0 to 4, designating it as a material capable of ignition under almost all normal temperature conditions. This electrolyte flammability issue has resulted in several well-publicized, catastrophic battery failures causing systems like the Samsung Galaxy Note 7, Tesla, hoverboards, e-cigarettes, and the Boeing Dreamliner to burst into flames.

1.4.1 Failure Rates

It is convenient here to distinguish between a "battery cell" and a "battery" (sometimes referred to as a "battery pack"). A battery cell is the basic electrochemical unit that derives electrical energy from chemical energy, as schematically shown in Figure 1.3. A battery consists of a stack of several cells, the wiring that interconnects them electrically, and the battery housing. A rechargeable battery may also contain a temperature sensor to prevent overcharging of the device.

The failure rate of a single lithium-ion cell is about 1 in 10 million, generally considered acceptable for use in handheld devices and other small applications. But for large-scale applications, batteries may contain up to several thousands of cells, exacerbating failure rates of the battery to more than 1 in 10 thousand.[16] Indeed, it has been reported that a Tesla Model S battery contains 8,256 cells. Additionally, these larger batteries may store up to 1,000 times more energy, increasing the likelihood that a single battery malfunction will result in significant property damage, injury, or even fatality. Thus, the hazards associated with lithium-based batteries are unacceptable for large-scale applications.

Because the safety hazards of the LIB itself have not been eliminated to this point, car manufacturers currently use expensive engineering controls to circumvent the issue. For example, both GM and Tesla Motors integrate sophisticated thermal management systems into their batteries, relying on glycol coolant to prevent thermal runaway of the battery.[17,18] Ballistic aluminum and titanium shielding on the underbody of the car is also employed to avoid battery puncture, adding significant mass to the car.[19] Addressing battery hazards at the source, rather than engineering around them, would simultaneously reduce the mass and cost of batteries while increasing consumer confidence in electric vehicles and grid storage.[20]

1.4.2 Failure Mechanism

In batteries, thermal runaway occurs when the heat of the system cannot be dissipated by heat radiation and convection processes. The rise in temperature accelerates exothermic chemical reactions over the desired galvanic ones, eventually leading to uncontrolled heat generation. Although the chemical reactions contributing to thermal runaway may occur in any order, it roughly proceeds as follows, with each reaction releasing heat that fuels the following process:[21]

1. Moderate initial overheating occurs from excessive currents, overcharging, or elevated external temperatures.
2. The SEI layer decomposes due to either physical penetration or elevated temperatures (above 68°C), forming lithium carbonate and gaseous products.
3. Intercalated lithium reacts with organic electrolyte to release flammable hydrocarbons such as ethane and methane, pressurizing the cell. Though the temperature is above the flash point of these gases, combustion does not occur because no oxygen is present in the cell.

4. The polymer separator melts, allowing the electrodes to contact each other and short-circuit the battery.
5. The metal oxide cathode breaks down and releases oxygen, enabling flammable alkyl carbonates and hydrocarbons to combust.
6. Cell pressurization leads to venting, causing a stream of flammable gas to emit from the battery.

To improve battery safety, two mechanisms have been built into LIBs. First, the polymer separator consists of a trilayered polypropylene-polyethylene-polypropylene film. The polyethylene film melts at 130°C, and polypropylene melts at 155°C. In the case of rapid heating, the polyethylene film melts first, clogging the pores of the unmelted polypropylene film and shutting down the battery, in theory. Second, a safety vent is implemented to prevent uncontrolled cell rupture under cases of extreme pressurization. Despite these protections, thermal runaway still causes catastrophic failure in LIBs. Even well-constructed battery cells fail, and small errors in manufacturing, testing, and inspection increase the rate of these failures.[22,23]

1.5 Criteria for Evaluating Novel Battery Electrolytes

Significant research efforts have aimed to identify nonflammable electrolytes in order to enhance the viability of LIBs for large-scale applications.[24,25] To assess novel electrolyte performance, several parameters must be evaluated.

1.5.1 Flammability and Temperature Range

In modern LIBs, highly energetic active materials are placed in contact with volatile, flammable carbonate solvents. Thermal decomposition, oxidation, and reduction of the electrolyte are all exothermic reactions that can trigger thermal runaway,[21] resulting in combustion processes fueled by carbonate solvents. Replacing the electrolyte with a nonflammable material, such as a

polymer or oligomer, would dramatically improve battery safety. Additional consideration should be given to the fact that the electrolyte should be able to operate in a broad temperature range: a battery electrolyte solvent that is crystalline or gaseous provides insufficient ion transport.[13]

Several techniques may be used to evaluate the operating temperature range of an electrolyte. To determine the lower temperature limit, crystallization and glass transition temperatures can be identified by differential scanning calorimetry (DSC). Rheological measurements can also be made to establish the temperature range over which an electrolyte's viscosity is sufficiently low to transport ions efficiently.

Thermogravimetric analysis (TGA) is often used to establish an upper temperature limit by means of the material's volatility or degradation profile, characterized by the $T_{d\ (5\%)}$—the temperature at which 5% mass loss is observed. Mass loss may occur as a result of either direct evaporation of the sample (low molecular weight systems) or by degradation of the backbone followed by evaporation of the degraded components (nonvolatile or polymeric systems).

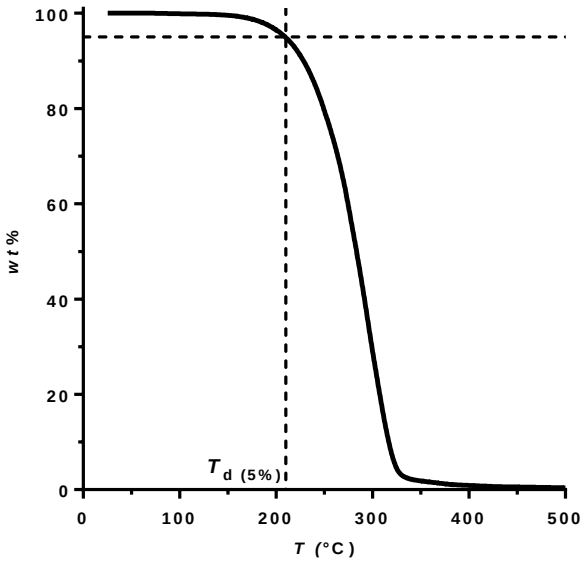

Figure 1.4 TGA curve showing determination of 95% degradation temperature.

A material's flammability characteristics can be evaluated using a combination of flash point and sustained burning measurements. Closed-cup flash point measurements involve heating

a sealed cup of material to periodically increasing temperatures before applying a flame to the sample to test for a flash, as described in ASTM D3278. Sustained burning measurements test whether a material continues to produce sufficient flammable vapor at a given temperature to burn when the ignition source is removed, as described in ASTM D4206. Two materials may exhibit the same flash point but different sustained burning characteristics.

Figure 1.5 Small-scale closed-cup apparatus for flash point and sustained burning measurements.

1.5.2 Electrochemical Stability

Nonflammability is not necessarily indicative of a safe solvent under conditions of abuse in an electrochemical environment.[24] Electrolytes must exhibit stability across an electrochemical potential window that is larger than the operating potential window of the anode and the cathode (≈4V)[12] to prevent the exothermic reactions described in Section 1.4.2 . If the highest occupied molecular orbital (HOMO) of the electrolyte is above the Fermi energy of the cathode, the electrolyte will be oxidized; if the lowest unoccupied molecular orbital (LUMO) of the electrolytes is below the Fermi energy of the anode, the electrolyte will be reduced. Although it is often infeasible to design electrolytes that have such a large HOMO-LUMO gap, electrolyte stability fortunately depends on the formation of a stable SEI layer: electrolyte stability is kinetically, rather than thermodynamically, controlled.[26]

Cyclic voltammetry can be used to evaluate the anodic and cathodic stability of a given electrolyte. Reduction and oxidation potentials are measured as the potential at which the current density reaches a pre-selected cutoff value—0.2 mA/cm^2 for the example shown below.[27] The electrochemical window is defined as the difference between these two potentials.

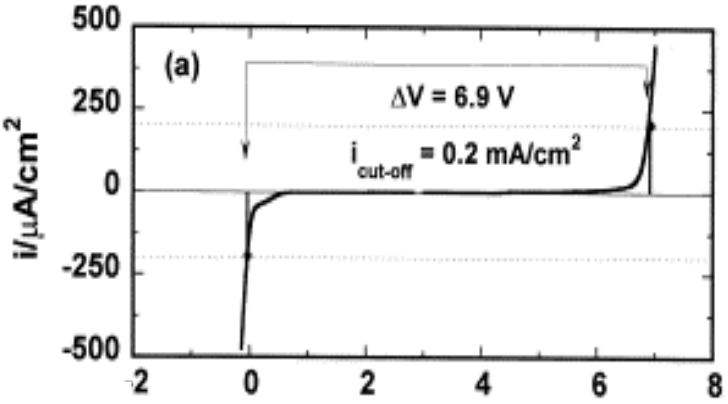

Figure 1.6 Cyclic voltammogram of electrolyte showing electrochemical stability window. Reprinted from ref. [27] with permission from Elsevier.

1.5.3 Cyclability

The long-term stability of a battery can be assessed by measuring the capacity of the battery over extended cycling.[28] An ideal electrolyte should form a passivation layer that remains stable despite electrode volume changes upon cycling, preventing further decomposition of the electrolyte and corresponding capacity loss. Many commercialized LIBs maintain at least 80% of their capacity after 1,000 cycles.[29]

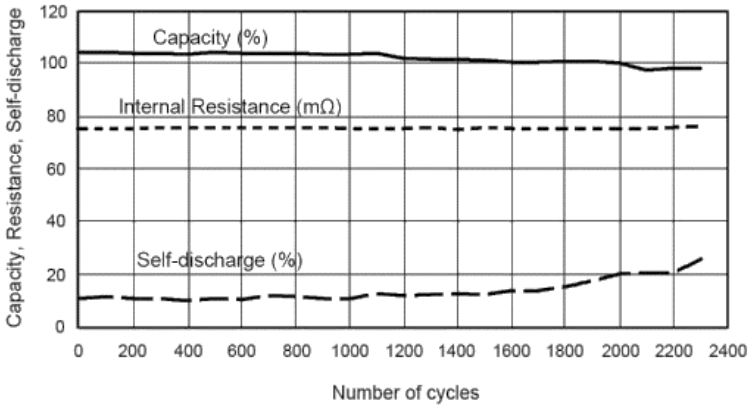

Figure 1.7 Battery capacity retention over extended cycling. Reprinted from ref. [28].

1.5.4 Ionic Conductivity

The ionic conductivity of an electrolyte determines how quickly the energy stored in the LIB can be delivered. The equation for ionic conductivity (σ) is given below:

$$\sigma = \sum_i n_i e_i \mu_i \tag{1.3}$$

where n_i is the concentration of charge carriers, e_i is the ionic charge, and μ_i is the ionic mobility. It is generally accepted that ionic conductivities on the order of 10^{-3} S cm^{-1} are necessary for most high-power applications.[10] Alkyl carbonate electrolytes exhibit $\sigma \approx 10^{-2}$ S cm^{-1}.

Ionic conductivity is determined experimentally using AC impedance spectroscopy, which involves applying a small, sinusoidal potential to an electrochemical cell and measuring the current response. The resulting AC current is shifted in phase from the excitation potential. Impedance—the ratio of voltage to current—can then be expressed as a complex function that contains real (in-phase) and imaginary (out-of-phase) components:

$$Z(\omega) = \frac{E}{I} = Z_0 \exp(j\varphi) = Z_0(\cos\varphi + j\sin\varphi) \tag{1.4}$$

where Z is the impedance, E is the applied voltage, I is the measured current, j is equal to the square root of -1, and φ is the phase shift.

The real component of equation (1.4) corresponds to resistance, while the imaginary component corresponds to reactance (which includes capacitance and inductance). Plotting the imaginary vs. real components of the impedance produces a Nyquist plot, as shown in Figure 1.8.[30] The impedance can be modeled by an equivalent circuit to extract the relevant sources of resistance, capacitance, and inductance in the system. The (extrapolated) x-intercept of the Nyquist plot corresponds to the bulk electrolyte resistance from which ionic conductivity may be calculated.

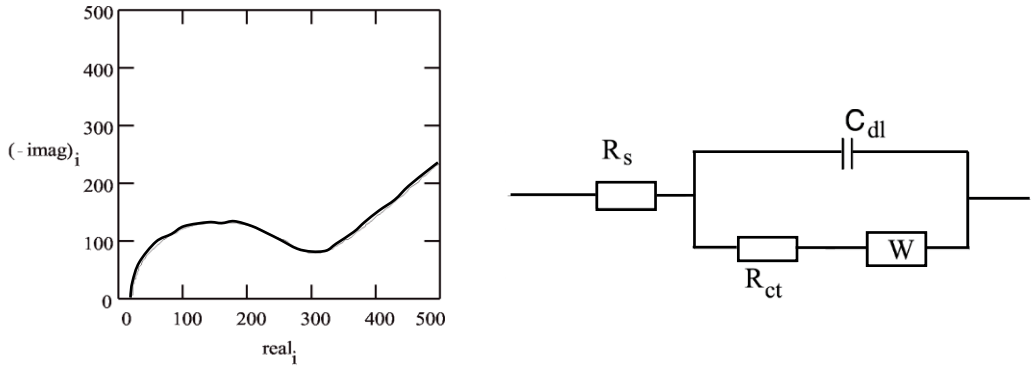

Figure 1.8 Nyquist plot and equivalent circuit used to model data. Reprinted from ref. [30].

1.5.5 Transference Number

For LIBs, only Li^+ intercalates into the electrode materials and participates in redox reactions that ultimately result in work being performed. To gain an accurate representation of the "effective" ionic conductivity flowing through an electrolyte, the charge transport of the redox-active Li^+ ion must be quantified. For an ideal solution, the cation transference number (t^+) is the fraction of the total current carried by the cation:

$$t^+ = \frac{I_+}{I_0} = \frac{\mu_+}{\mu_0} = \frac{\lambda_+}{\lambda_0} = \frac{D_+}{D_+ + D_-} \qquad (1.5)$$

where I, μ, λ, and D denote the current, mobility, ionic conductivity, and diffusion coefficients, and the subscripts $_+$, $_-$, and $_0$ represent the values for the cation, anion, and total electrolyte, respectively.[31] For non-ideal solutions with ion aggregation, equation (1.5) becomes invalid.

Mobility of higher-order ion aggregates (e.g. triplets) must be considered, and negative transference numbers are possible.[32]

Electrolytes with $t^+ << 1$, in which the anion is more mobile than Li^+, experience strong polarization due to anion (salt) enrichment and depletion near the electrode surfaces, impairing long-term battery performance significantly. In fact, Doyle and coworkers showed that electrolytes with a unity transference number outperform systems with 10x higher ionic conductivity but $t^+ = 0.2$ because cells with t^+ near unity have higher energy densities and peak-power densities.[33] In most nonaqueous electrolytes—including commercialized alkyl carbonate solvents—t^+ is between 0.20 and 0.40.[13]

Several methods for the measurement of cation transference numbers in LIB electrolytes exist. An insightful review of these methods is provided by Zugmann and Gores in reference 31. The two methods used in this work for characterization of the transference number—potentiostatic polarization and pulsed-field gradient nuclear magnetic resonance (pfg-NMR)—are described here briefly.

1.5.5.1 Potentiostatic Polarization Method for Measurement of t^+

In the potentiostatic polarization method, a constant potential is applied to a symmetric cell with non-blocking lithium electrodes, and the current response is measured over time. The initial current arises from the flux of both cations and anions. Because anions do not participate in redox reactions at the electrodes, anions (or more accurately, salts) build up near one electrode and are depleted near the other. The salt concentration gradient creates a diffusion force that opposes the migration force from the applied potential. The anion current vanishes when migration is exactly counteracted by diffusion. Thus, the steady-state current is carried only by the cation, which

reversibly reacts at the electrode surfaces. Conceptually, the transference number is given by the ratio between the steady-state (cation) current and the initial (total) current.

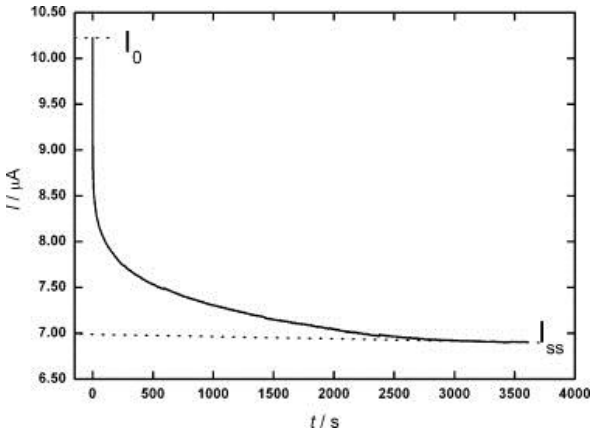

Figure 1.9 Chronoamperogram of $LiPF_6$ electrolyte in ethylene carbonate/diethyl carbonate with an applied voltage of 10 mV. Reprinted from ref. [35] with permission from Elsevier.

An additional correction must be applied because lithium is reactive with nearly all electrolyte materials, creating a passivation layer that changes the cell resistance over the course of the measurement. Accounting for changes in the electrode surface resistances over time, the transference number is given by:

$$t^+ = \frac{I_{SS}(\Delta V - I_0 R_0)}{I_0(\Delta V - I_{SS} R_{SS})} \tag{1.6}$$

where I, ΔV, and R are the current, applied potential, and resistance and the subscripts $_0$ and $_{SS}$ denote the initial and steady state conditions, respectively.[34] The correction for changing resistance is important, as evidenced by Figure 1.9 above: the simple ratio of steady-state to initial current from the chronoamperogram is nearly 0.7, whereas t^+ is known to be < 0.4 for the given electrolyte.[35]

1.5.5.2 Pulsed-Field Gradient NMR (pfg-NMR) Method for Measuring *t+*

Nuclear magnetic resonance can be used to measure the self-diffusion coefficients of different nuclei in an electrolyte. The pulse sequence for a pulsed-field gradient NMR experiment

is given in Figure 1.10. Similar to a standard 1D NMR experiment, the pfg-spin echo experiment begins with a 90° rf pulse (pulse 1), shifting the bulk magnetization vector from the z-axis to the x-y plane, perpendicular to the static field. Pulse 2 is an rf gradient pulse with an intensity that is a linear function of position in the z-direction. The rotation of the magnetization vector is different at each spatial position in the z-direction, canceling the net magnetization. Nuclear diffusion is allowed to occur for a short period, and then a 180° rf pulse (pulse 3) is applied to the sample to invert the magnetization. The gradient pulse (pulse 4) is applied once again to refocus the magnetization.[36]

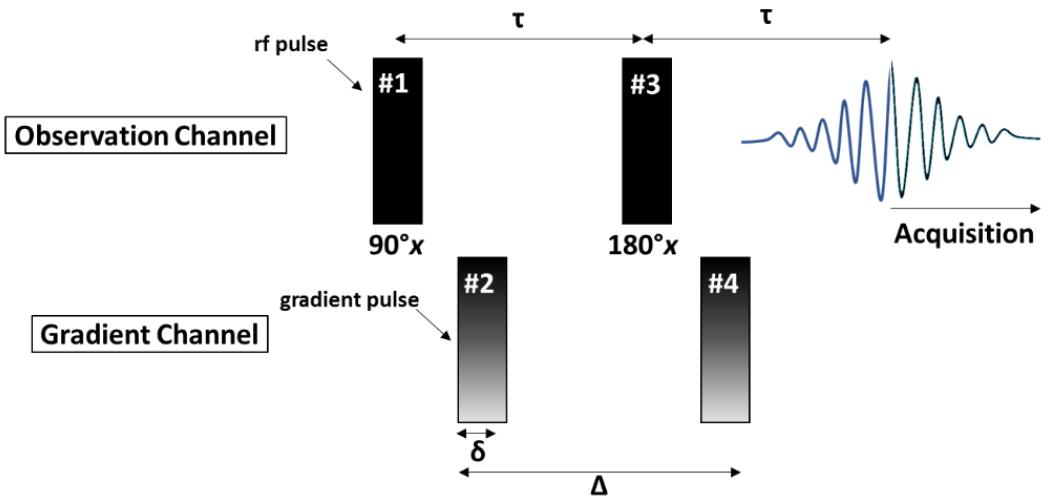

Figure 1.10 Schematic representation of pfg-NMR pulse sequence.

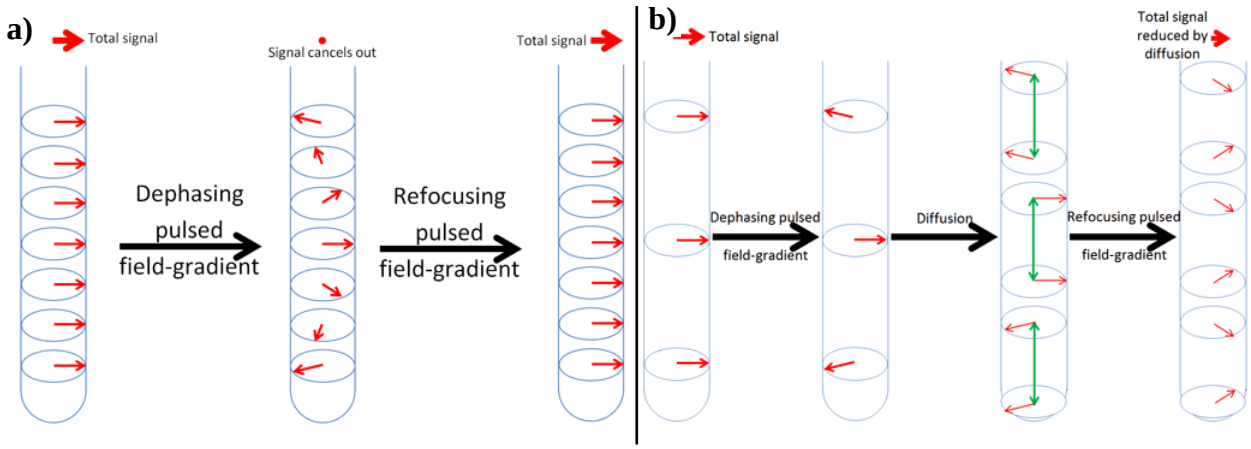

Figure 1.11 Schematic representation of pfg-NMR dephasing and signal recovery a) in the absence of nuclear diffusion and b) with nuclear diffusion. Reprinted from ref. [37].

In the absence of nuclear diffusion, the effects of pulses 2 and 4 exactly cancel each other out and the full signal intensity is recovered, as shown schematically in Figure 1.11a.[37] In contrast, translational motion of a nucleus causes it to experience a different magnetic field strength during pulses 2 and 4 due to the spatial dependence of gradient intensity. In the presence of nuclear diffusion, the effects of pulses 2 and 4 on a nucleus do not exactly cancel each other out and the magnetization is not fully refocused. This "blurring" of phases results in a loss of signal intensity (Figure 1.11b and Figure 1.12).

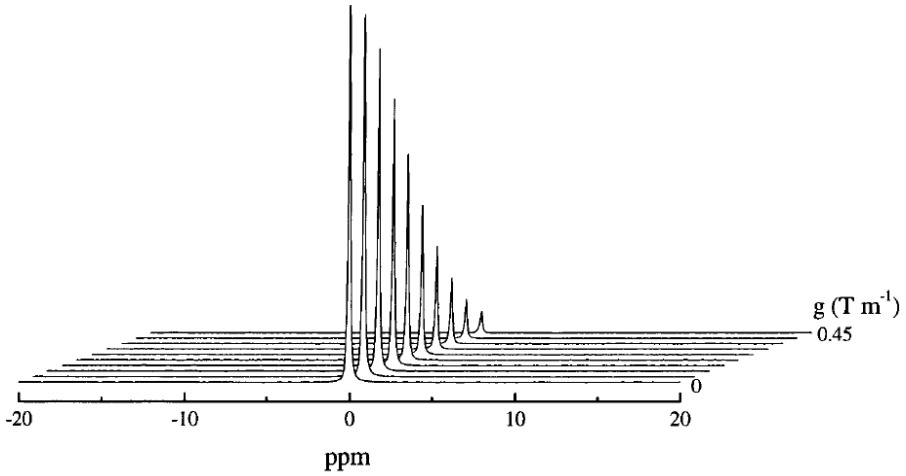

Figure 1.12 ^{13}C pfg-NMR spectra of $^{13}CCl_4$. Peak intensity decreases as gradient field strength increases. Reprinted from ref. [36] with permission from John Wiley and Sons.

The amplitude of the attenuated signal E as a function of gradient strength can be fit to obtain the diffusion coefficient of a given species using equation (1.7):

$$E = e^{-\gamma^2 g^2 \delta^2 {D_i}^{NMR}(\Delta - \frac{\delta}{3} - \frac{\tau}{2})} \quad (1.7)$$

where γ is the gyromagnetic ratio, g is the gradient strength, δ is the duration of the gradient pulse, D_i^{NMR} is the diffusion coefficient, Δ is the interval between gradient pulses, and τ is the separation between pulses.[38] Ultimately, determination of the cation (D_+^{NMR}) and anion (D_-^{NMR}) diffusion coefficients enables calculation of the transference number.

$$t^+ = \frac{{D_+}^{NMR}}{{D_+}^{NMR} + {D_-}^{NMR}} \quad (1.8)$$

For electrolytes containing fluorinated lithium salts, as is common in LIBs, ^{7}Li NMR is used to probe the cation diffusivity while ^{19}F NMR can be used to probe the anion diffusivity. Considering pfg-NMR measures the diffusion of nuclei rather than free ions, this method is only valid for ideal, dilute solutions in which no ion association occurs.

1.6 Current Research in LIB Electrolytes

No single electrolyte to date excels in all of the above criteria—safe (nonflammable), electrochemically stable, cyclable, highly conductive, and high transference number. Each electrolyte comes with its own compromises and therefore should be considered appropriate only for certain applications. For example, the principal shortcomings of small-molecule carbonate-based electrolytes are low transference number and poor safety. Yet because of their low cost, high ionic conductivity, and broad electrochemical stability window, these electrolytes have been deemed suitable for most small-scale applications requiring high energy density.

In a contrasting example, Xu and coworkers recently developed a "water-in-salt" electrolyte for LIBs that exhibits a potential window of ≈ 3 V, improving upon the 1.23 V potential window for water electrolysis but still well below the potential window of alkyl carbonate solvents

(≈4.5 V).[39] Although the small potential window yields low energy densities, several other LIB electrolyte requirements (nonflammable, $\sigma \approx 10$ mS cm^{-1}, cycle life ≈ 1,000, economical) are met. Water-in-salt electrolytes could be useful for large-scale, stationary applications in which safety is paramount but energy density requirements are less stringent.

Electrolyte safety remains at the forefront of battery research. Approaches range from incorporating fluorinated[40] and phosphate[41] flame-retardant additives into alkyl carbonate electrolytes to replacing the electrolyte entirely with nonvolatile polymer electrolytes or room-temperature ionic liquids (RTILs).[25,42–44] A brief review regarding additives and replacement electrolytes is included below.

1.6.1 Electrolyte Additives

Zhang et.al. provided a thorough review of electrolyte additives to improve LIB performance via interphase formation, salt stabilization, and flammability reduction.[45] Briefly, researchers have explored flame-retardant additives for alkyl carbonate electrolytes in order to preserve the basic battery chemistries while improving safety. These additives may function in three ways:

i. Char formation, creating an insulating layer between condensed and gas phases to prevent heat transfer and further combustion of the electrolyte.
ii. Radical scavenging, terminating chain reactions contributing to gas-phase combustion.
iii. Inert dilution of flammable components until flash point is eliminated.

Phosphate and phosphazene-based additives typically act as type ii flame retardants. Unfortunately, flame retardance often comes at a cost to other electrolyte performance parameters including reductive stability and ionic conductivity of the electrolyte in phosphorus-containing

systems.[46,47] Fluorine-containing additives have also been studied extensively. These compounds function as type iii additives, and flash-point elimination is only observed when the fluorinated compound is the major component.[48] Again, the fluorinated additive tends to reduce ionic conductivity of the electrolyte, resulting in a trade-off between flammability and cell performance.[49]

1.6.2 Room-Temperature Ionic Liquids (RTILs)

Ionic liquids are a liquid mixture of anions and cations (Figure 1.13) in the absence of a molecular solvent—simply, they are molten salts. RTILs, which typically contain quaternary ammonium cations, are a specific class of ionic liquids that have melting temperatures below room temperature.[50] Li^+-containing ionic liquids often have significantly high melting temperatures because of the small ionic radius of Li^+. For this reason, a majority of electrolytes consist of non-lithium-containing RTILs mixed with lithium salts rather than lithium-based ILs.

RTILs are considered nonflammable due to their negligible vapor pressures.[43] They exhibit ionic conductivities as high as $\approx 10^{-2}$ S cm^{-1} at room temperature and transference numbers as high as ≈0.4.[51] However, there are several drawbacks to using RTILs as LIB electrolytes. Due to their moisture sensitivity and high viscosities (up to 5000 cP),[52] the cost of stringent purification and manufacturing is high. Furthermore, the lack of solvent molecules to act as sacrificial building blocks for electrode-electrolyte interphase formation diminishes the kinetic metastability of RTILs.[24] In fact, RTILs generate more heat in the presence of active electrode materials than small molecule alkyl carbonates despite the ionic liquids' larger thermodynamic electrochemical stability window.[53] These findings led Kang Xu, author of two excellent review articles on nonaqueous electrolytes, to conclude: "there is no reason to be optimistic about the large-scale application of RTIL in commercial LIB in the foreseeable future."[24]

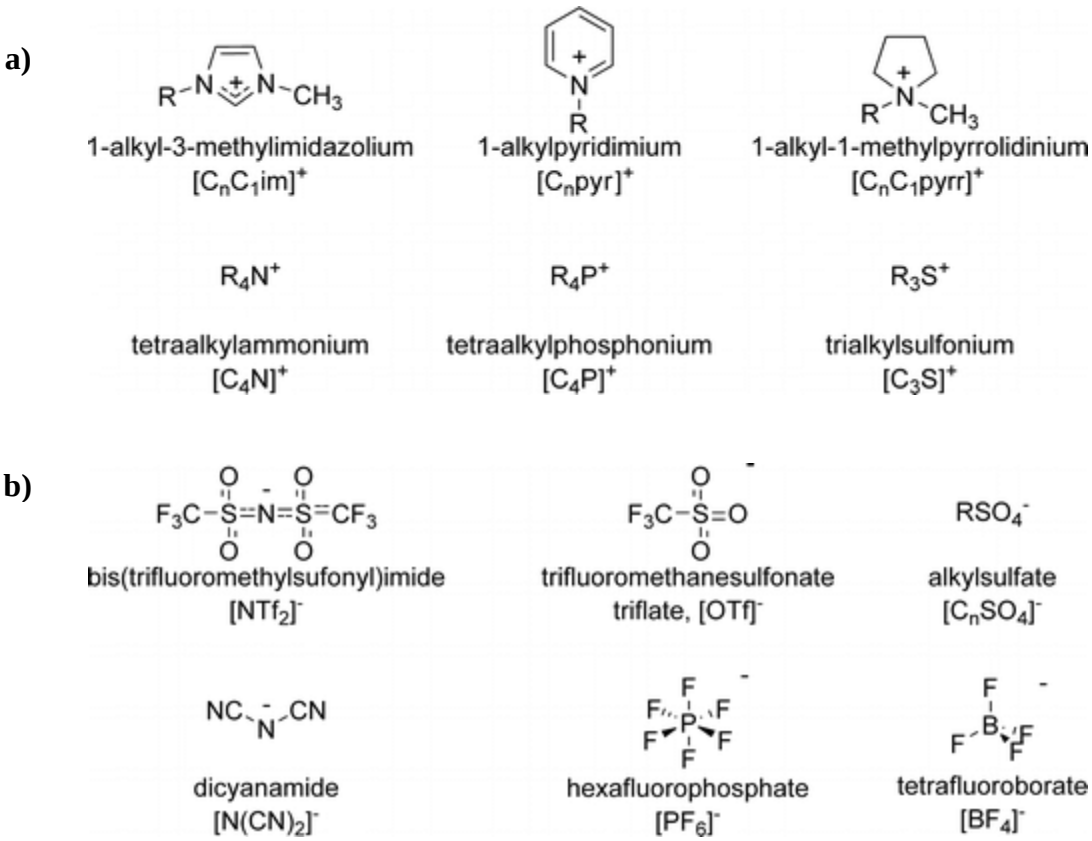

Figure 1.13 Structure of a) cations and b) anions for a set of representative ionic liquids. Reprinted with permission from ref. [50]. Copyright (2011) American Chemical Society.

1.6.3 Polymer Electrolytes

Polymer electrolytes present the intriguing possibility of implementing a thin, flexible membrane to serve as both the conductive medium and the electronic separator between electrode materials in a battery. These materials consist of lithium salts dissolved either in a neat polymer ("solid polymer electrolytes") or in crosslinked polymer networks swollen with plasticizing solvents ("gel polymer electrolytes"). Fenton and coworkers first reported the ability of PEO to dissolve alkali metal salts in 1973, providing the basis for research in polymer electrolytes.[54] Since that time, the field of polymer electrolytes has been largely dominated by studies of PEO and its polyether analogs.

Although PEO exhibits $\sigma > 10^{-4}$ S cm^{-1} above its melting temperature (≈60°C), crystallinity at room temperature hinders segmental motions of polymer chains and impedes ionic conduction.[55] Numerous efforts have been made to mitigate the issue of PEO's crystallinity, including synthesis of copolymers,[56] polymer blends,[57] comblike structures,[58] and polymer brushes.[59] Despite these elegant architectures, ionic conductivities greater than 10^{-3} S cm^{-1} at room temperature are rare in PEO-based electrolytes, and electrode-electrolyte compatibility is often sacrificed.

Single-ion conductors (also referred to as "polyelectrolytes" or "ionomers" in the high- or low-ion content case, respectively) consist of lithium salts in which the anions are covalently attached to a polymer backbone, as shown in Figure 1.14.[60] This effectively immobilizes the anions, enabling transference numbers of unity to be achieved. However, these materials suffer from low lithium salt dissociation[61] and dramatic increases in T_g with increasing ion content along the polymer backbone.[62] For these reasons, ionic conductivities above 10^{-4} S cm^{-1} have not been realized in single-ion conductors.

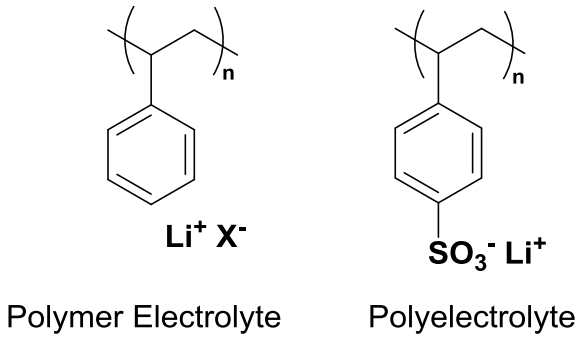

Figure 1.14 Comparison between polymer electrolyte and polyelectrolyte in which the anion is covalently attached to the polymer. Reprinted from ref. [60] with permission from Elsevier.

Gel polymer electrolytes were developed out of necessity in order to achieve sufficient ionic conductivities in polymer electrolytes. Polymer networks plasticized with more than 60% liquid electrolyte generally exhibit ionic conductivities that are only 2-5 times lower than that of the pure liquid electrolyte.[63] Furthermore, the electrochemical and thermal stability of gel polymer

electrolytes is largely determined by the plasticizer molecules. Thus, although ionic conductivities on the order of 10^{-3} S cm^{-1} are achievable, gel polymer electrolytes may still be flammable and have similar electrochemical stability windows to that of neat liquid electrolytes.[64]

1.6.3.1 Ion Solvation

Research in polymer electrolytes has overwhelmingly targeted the lithium ion for solvation. Cation solvation is straightforward and can be accomplished by lone pairs of electrons on heteroatoms. For example, Li^+ is solvated via coordination to 3-7 ether oxygens in the PEO backbone, as shown in Figure 1.15.[65–67] Preferential coordination of heteroatoms to Li^+ hinders its mobility, leading to low t^+ values.[68]

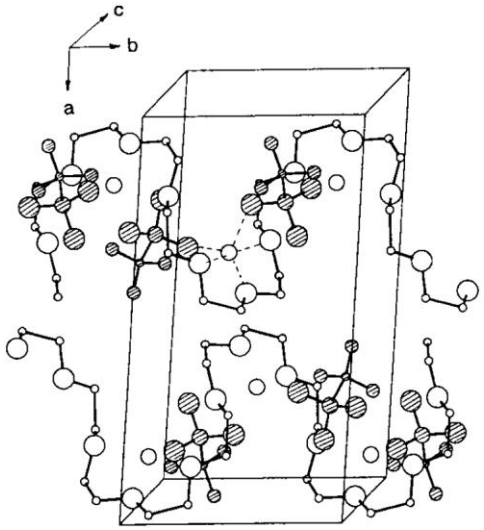

Figure 1.15 Crystal structure of $(PEO)_3LiCF_3SO_3$ with $CF_3SO_3^-$ shaded. Dashed lines show coordination to a lithium ion. From ref. [67]. Reprinted with permission from AAAS.

Very few efforts have been made to preferentially solvate the counterion of lithium salts. Traditionally, anion solvation is achieved via hydrogen bonding. But, polymers that exhibit hydrogen bonding are usually quite stiff and cohesive, hindering the mobility of ions significantly.[69] Lewis acidity is an alternative property that can be utilized to achieve anion solvation. For example, Mehta *et al.* incorporated boron-containing rings into a polyether

backbone, leading to elevated transference numbers ($t^+ \approx 0.75$) but moderate ionic conductivities ($\sigma \approx 10^{-6}$ S cm^{-1}).[70] To our knowledge, boron-containing polymers and additives are the only Lewis-acidic electrolytes that aim to "trap", or solvate, anions.

1.6.3.2 Ion Transport

Ionic conduction in amorphous materials occurs via two mechanisms: vehicular transport and ion hopping.[71] Vehicular transport refers to the co-diffusion of Li^+ within its "vehicle"—the molecules in its solvation shell. Considering that gel polymer electrolytes contain plasticizing solvents, vehicular transport dominates ionic conduction in these materials.[25] In contrast, the vehicular transport phenomenon is negligible in solid polymer electrolytes of high molecular weight because chain entanglements constrain polymer diffusion.[72] Instead, ion hopping dominates Li^+ transport, as shown in Figure 1.16.[73] Above T_g, segmental motions of polymer chains cause the coordination environment of Li^+ to fluctuate away from its most stable conformation, leading the ion to diffuse down the backbone toward lower free energy sites.[74] This repetitive perturbation and diffusion of Li^+ is the driving force for long-range ion transport.

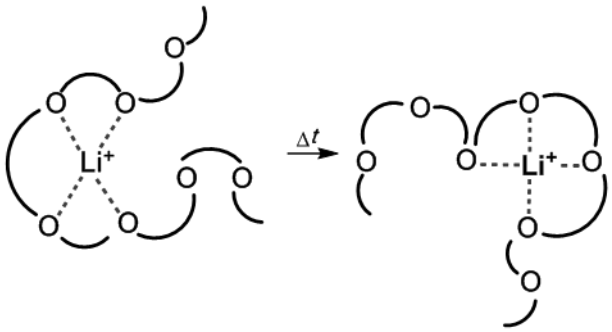

Figure 1.16 Lithium ion hopping facilitated by segmental motions of PEO chains. Adapted with permission from ref. [73]. Copyright (1988) American Chemical Society.

1.6.4 Perfluoropolyether (PFPE) Materials

All perfluoropolyethers (PFPEs) contain C-F, C-C, and C-O bonds that provide this class of materials its unique thermal stability, low volatility, chain flexibility, and extreme chemical resistance.[75,76] PFPEs' chemical stability and large use temperature range make them appealing long-life lubricants in harsh applications such as aerospace, automotive, and industrial manufacturing industries.[77] Crosslinked PFPE networks have also been developed and implemented as surface coatings for marine biofouling applications,[78] microfluidics,[75] and particle replication molds.[79] Coincidentally, PFPE's unique thermal stability, extreme chemical resistance, amorphous nature, and non-polarizability make it an intriguing solvent for LIB electrolytes as well.

1.6.4.1 Commercially Available Perfluoropolyethers

PFPEs may be categorized into four families based on repeat unit structure, as summarized in Table 1.1 below. The PFPEs studied herein belong to the second two product lines, manufactured by Solvay and Exfluor Research Corporation.

Table 1.1 Molecular structures of commercially available PFPEs.

Product Line	Manufacturer	Repeat Unit	Structure
Krytox®	Chemours (DuPont)	Hexafluoropropylene Oxide	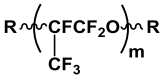
Demnum®	Daikin	Hexafluorooxetane	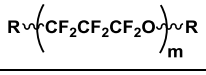
Fomblin/Fluorolink®	Solvay	Tetrafluoroethylene Oxide and Difluoromethylene Oxide	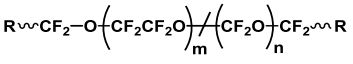
C#G[1]	Exfluor	Tetrafluoroethylene Oxide	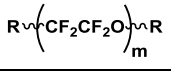

[1] The # in "C#G" refers to the number of carbons in the molecule. For example, Exfluor designates perfluorinated triethylene glycol, which contains six carbons, as "C6G".

Commercial PFPEs are available in a range of molecular weights with various non-functional and functional end groups useful for surface modification. Solvay generally classifies its PFPEs as "Fomblin®" for molecular weights between 2000 and 4000 g/mol and "Fluorolink®" for molecular weights below 2000 g/mol. A representative selection of commercially available PFPE end groups is given in Table 1.2. Although the designations in the table apply to the Fluorolink® product line, the end groups shown are representative of those available in the other product lines. In this work, PFPEs will often be referred to by their trade names, in which the trade name consists of "product line" + "designation" (e.g. Fluorolink® E10 for PFPE with ethoxylated diol end groups).

Table 1.2 Selection of commercially available Fluorolink® end groups.

Designation	End Group	R
D10	Diol	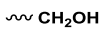
E10	Ethoxylated Diol	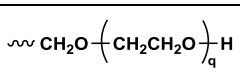
F10	Phosphate	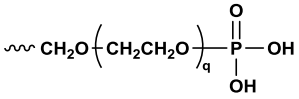
MD700	Methacrylate	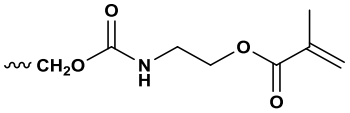

1.6.4.2 Perfluoropolyether Synthesis

Perfluoropolyethers were first synthesized in the way that many great scientific discoveries are made—by mistake. In 1953, Haszeldine reported an oily product when attempting to photopolymerize hexafluoropropylene.[80] He had unknowingly synthesized PFPE following the photooxidation mechanism depicted in Figure 1.17.

Krytox® and Demnum® were the first commercialized PFPE oils. Both are synthesized via anionic ring-opening polymerization of fluorinated monomers. Krytox® is synthesized by the

base-catalyzed homopolymerization of hexafluoropropylene oxide (HFPO) using a fluoride source such as cesium fluoride. The terminal acyl fluoride group is reacted by traditional chemistries to yield functional end groups, or alternatively removed by fluorination to yield inert polyether products ranging anywhere from $n = 2$ to $n = 50$.[81] Control over the polymerization is exerted by solvent and temperature conditions.

Scheme 1.1 Synthesis of Krytox® via anionic ROP of HFPO.

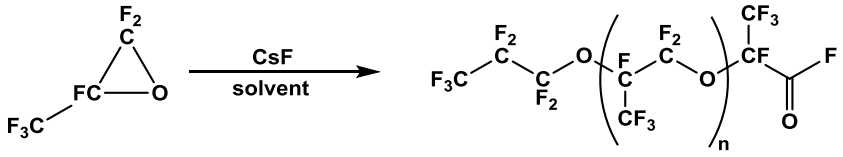

Demnum® is synthesized via an analogous ring-opening polymerization of tetrafluorooxetane.[82] Because the tetrafluorooxetane monomer is only partially fluorinated, the final poly(perfluorotrimethylene oxide) material is obtained only after a subsequent fluorination step and final end group conversion.[83] The subsequent fluorination is carried out by reacting fluorine gas directly with the polymer at 200°C or in the presence of UV irradiation.

Scheme 1.2 Synthesis of Demnum® via anionic ROP of tetrafluorooxetane followed by fluorination (not shown).

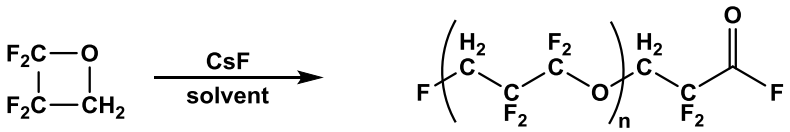

Solvay manufactures its Fomblin/Fluorlink® PFPEs by the photooxidation of fluorinated olefins like tetrafluoroethylene (TFE) or hexafluoropropylene (HFP). Oxygen is added into the liquid monomers at -40°C and irradiated with UV light (λ<300 nm).[83] The mechanism for this polymerization is well-established and was summarized clearly by Bunyard *et al*.[84] Several of the important propagation and termination reactions are shown in Figure 1.17. It should be noted that although the mechanism below corresponds to the photooxidation of HFP, TFE photooxidation

undergoes analagous reactions. The Fluorolink® materials discussed in this dissertation are synthesized by the photooxidation of TFE.

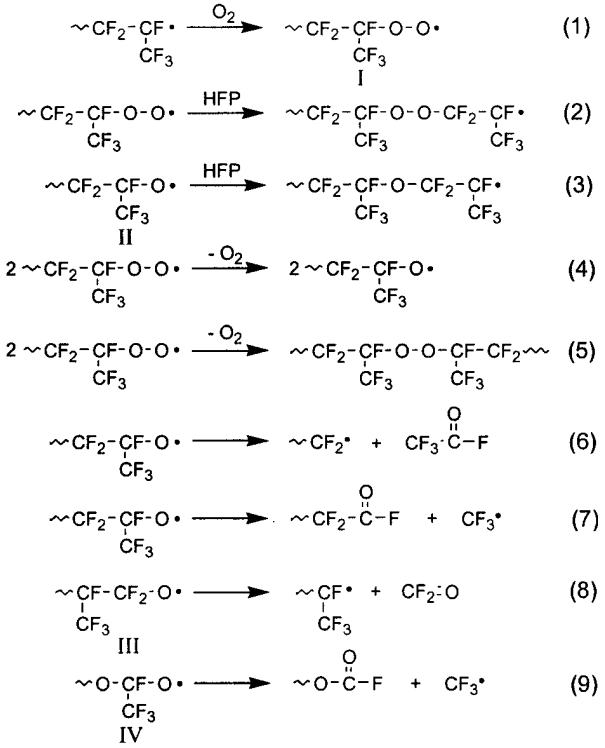

Figure 1.17 Important propagation and termination reactions in the photooxidation of HFP with oxygen. Reprinted with permission from ref. [84]. Copyright (1999) American Chemical Society.

When fluorinated olefins are irradiated, the resulting radical reacts with oxygen at a diffusion-limited rate (reaction 1). Disproportionation of the resulting peroxy radical forms an alkoxy radical (reaction 4), which occurs more quickly than HFP addition to the peroxy radical (reaction 2). Thus, HFP addition to an alkoxy radical is the dominant propagation reaction. Above -50°C, β-scission takes place, forming difluoromethylene radicals (reaction 6). The result is random insertion of difluoromethylene oxide units within the hexafluoropropylene oxide backbone. Temperature, feedstock ratio of reactants, solvent, and monomer concentration can all be adjusted to obtain the desired molecular weight and ratio between hexafluoropropylene oxide and difluoromethylene oxide repeat units.[84]

Finally, direct fluorination may be employed to convert hydrogenated ethers to their perfluorinated derivatives. Three commercially viable methods exist to date: electrochemical fluorination, oxidative fluorination with cobalt trifluoride, and liquid phase fluorination.[85] Each method relies on the same basic mechanism, in which proton abstraction from a carbon yields an alkyl radical, which then reacts with a fluoride source to produce the perfluorinated molecule. However, several direct fluorination methods require the starting material to be soluble in the same medium as the perfluorinated product, which is rare unless the starting material is already partially fluorinated.[86]

Exfluor solved this issue with a method to generate a large excess of fluorine radicals relative to the nonfluorinated substrate under vigorous stirring. The Exfluor-Lagow method involves slow addition of the nonfluorinated substrate and excess fluorine to a halogenated solvent (the DeSimone group has also performed fluorinations in liquid and supercritical CO_2).[87] Benzene is added in small quantities, reacting spontaneously with fluorine to generate high concentrations of fluorine radicals. Though it makes use of toxic, explosive fluorine gas, the Exfluor-Lagow method produces perfluorinated ethers in higher yields and better purities than electrochemical or cobalt trifluoride-based direct fluorinations.[88] The low molecular weight perfluorinated glycols discussed in this work are synthesized by Exfluor's direct fluorination method.

Scheme 1.3 Direct fluorination of a polyether to its perfluorinated PFPE analog.

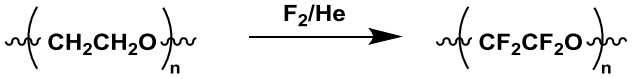

1.6.4.3 Perfluoropolyether Electrolyte Properties

Importantly, Wong *et al.* recently discovered that PFPE oligomers dissolve the commonly studied lithium bis(trifluoromethane)sulfonamide (LiTFSI or $LiN(SO_2CF_3)_2$) salt.[89] PFPE/LiTFSI

electrolytes exhibit ionic conductivity $\sigma \approx 10^{-6}$ S cm^{-1} at room temperature with near-unity transference numbers ($t^+ \geq 0.91$), the highest known t^+ values reported for a polymer electrolyte in which lithium salt is dissolved in a polymer solvent (Figure 1.18). It was proposed that the perfluorinated polymer backbone solvates the highly fluorinated $TFSI^-$ anion, freeing Li^+ for higher mobility.

If correct, this feature would be unique from the vast majority of polymer electrolytes that coordinate to Li^+. Anion solvation may occur via the "fluorous effect," the tendency of perfluoroalkyl chains to segregate in order to minimize energetically unfavorable interactions of the highly nonpolarizable fluorine atoms with other elements.[90] This fluorous effect has been used as an alternative to covalent immobilization in applications such as microarrays,[91] mass spectrometry,[92] and fluorous solid-phase extraction.[93]

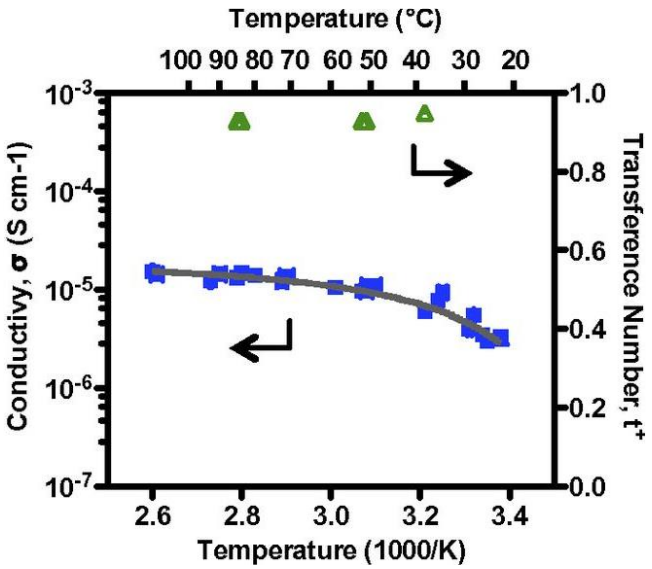

Figure 1.18 Temperature dependence of ionic conductivity and transference number of PFPE electrolyte with 9.1 wt.% LiTFSI. Reprinted with permission from ref. [89].

Wong and coworkers studied $LiN(SO_2CF_3)_2$ solubility in PFPEs of varying molecular weight with diol and methyl carbonate end groups. This maximum salt concentration was expressed as the molar ratio of lithium ions to perfluoroether repeat units (r_{max}).

$$r_{max} = \frac{[Li^+]}{[CF_2CF_2O] + [CF_2O]} \tag{1.9}$$

PEO electrolyte salt concentrations are often expressed as r_{max} (defined as $[Li^+]/[ether]$) because the ether oxygen atom is known to be responsible for solvating lithium. Therefore, r_{max} is constant for PEO of varying molecular weight. In contrast, r_{max} decreases exponentially with increasing PFPE molecular weight (Figure 1.19a).

Because PFPE-DMC dissolves significantly more salt than PFPE-Diol, it was proposed that end groups play an important role in dissolving lithium salts. The LiTFSI solubility was normalized as the ratio of lithium ions per end group (R_{max}), where the end group is either hydroxyl or methyl carbonate (Figure 1.19b). R_{max} was consistent over a range of molecular weights, indicating that end groups do contribute to lithium salt solvation in PFPE electrolytes.

$$R_{max} = \frac{[Li^+]}{[-OH]} \text{ or } \frac{[Li^+]}{[-OCO_2Me]} \tag{1.10}$$

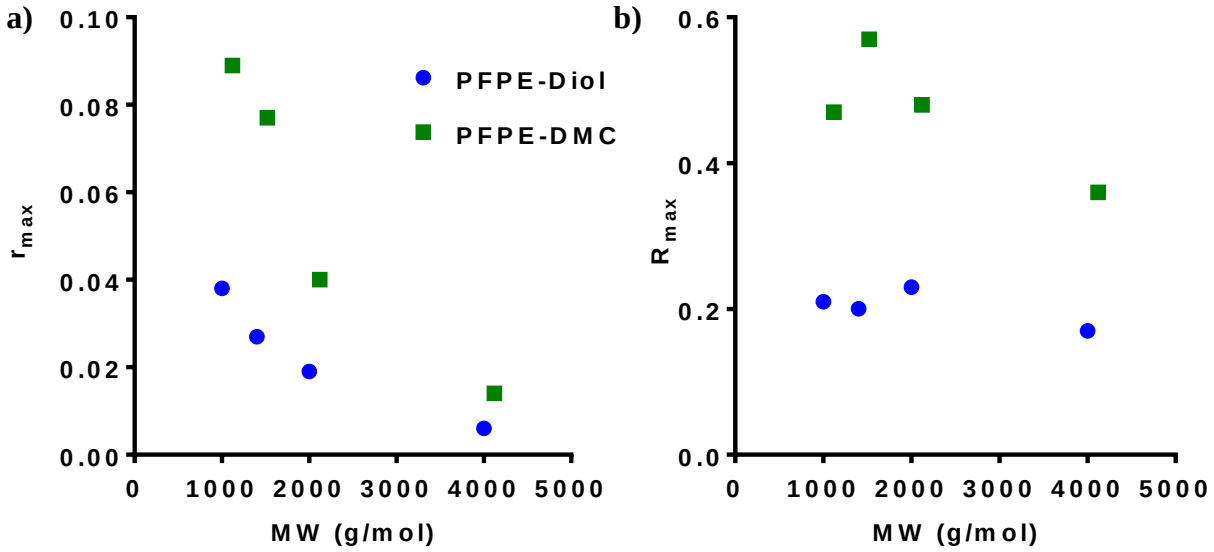

Figure 1.19 Solubility limit of $LiN(SO_2CF_3)_2$ in Fluorolink D10-Diol and D10-DMC as a function of PFPE molecular weight, expressed as a) r_{max} and b) R_{max}. Reprinted with permission from ref. [89].

PFPE was found to form miscible blends with low molecular weight PEO up to a composition of about 30 wt.% PEO, as shown in Figure 1.20.[94] Wong *et al.* prepared electrolytes based on physical blends of PFPE and PEO mixed with LiTFSI salt, and the complex ternary phase interactions altered the miscibility between PFPE and PEO.[95] As shown in Figure 1.21, the ionic conductivity exhibited by PFPE/PEO blends reached ≈ 10^{-4} S cm^{-1} at room temperature, although the transference number was significantly reduced to ≈ 0.3.[95] PEO dramatically affected the conductive behavior of the electrolyte: oligoether coordination to Li^+ resulted in higher lithium salt solubility and conductivity but lower t^+.

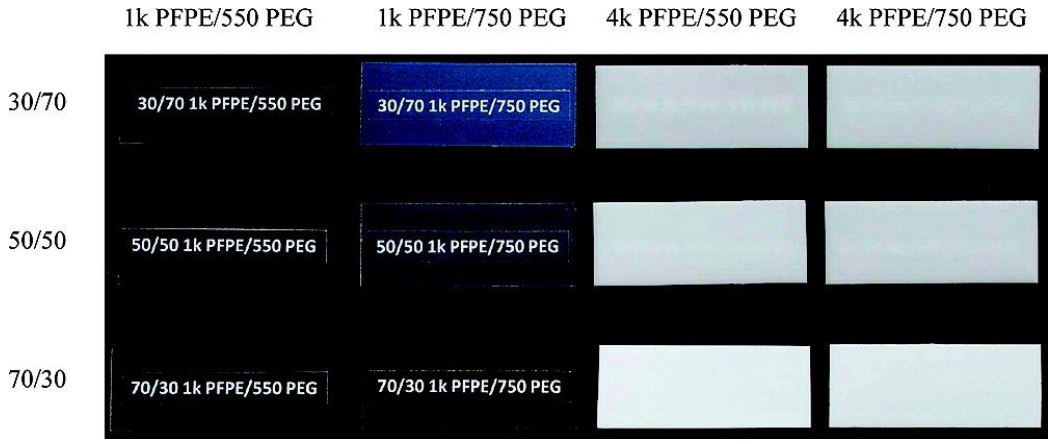

Figure 1.20 Photographs of fully cured PFPE/PEG films. Labels are readable for optically transparent or hazy samples only (vertical label: mass ratio PFPE/PEG). Reprinted with permission from ref. [94]. Copyright (2008) American Chemical Society.

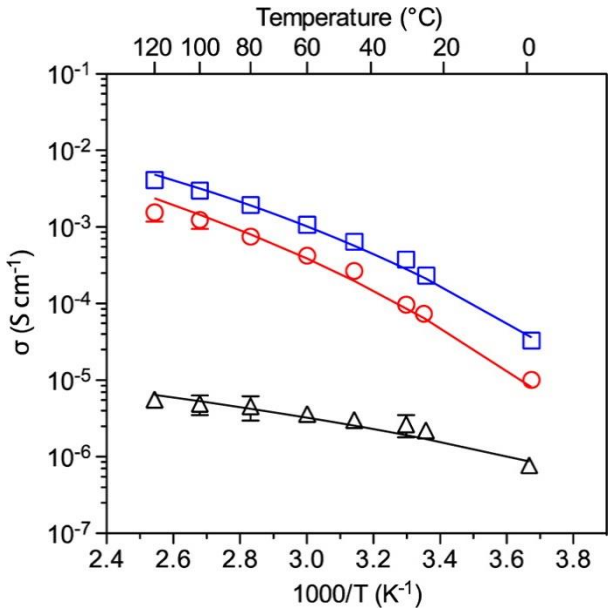

Figure 1.21 Ionic conductivity of PFPE (black), PFPE/PEG (red), and PEG (blue) electrolytes at $LiN(SO_2CF_3)_2$ concentration r=0.026. Reprinted with permission from ref. [95]. Copyright (2015) American Chemical Society.

REFERENCES

(1) Intergovernmental Panel on Climate Change. Fifth Assessment Report on Climate Change. **2014**.

(2) Oreskes, N. The Scientific Consensus on Climate Change. *Science.*. **2004**, *306* (5702).

(3) U.S. Energy Information Administration. Monthly Energy Review https://www.eia.gov/energyexplained/?page=us_energy_home (accessed Jul 6, 2017).

(4) Department of Energy. Achieving 30% Renewable Electricity Use by 2025 https://energy.gov/eere/femp/achieving-30-renewable-electricity-use-2025 (accessed Jul 6, 2017).

(5) Dunn, B.; Kamath, H.; Tarascon, J.-M. Electrical Energy Storage for the Grid: A Battery of Choices. *Science* **2011**, *334* (6058).

(6) Tarascon, J. M.; Armand, M. Issues and Challenges Facing Rechargeable Lithium Batteries. *Nature* **2001**, *414* (6861), 359–367.

(7) Whittingham, M. S. Electrical Energy Storage and Intercalation Chemistry. *Science* **1976**, *192* (4244), 1126–1127.

(8) Mizushima, K.; Jones, P. C.; Wiseman, P. J.; Goodenough, J. B. LixCoO2: A New Cathode Material for Batteries of High Energy Density. *Mater. Res. Bull.* **1980**, *15* (6), 783–789.

(9) Mohri, M.; Yanagisawa, N.; Tajima, Y.; Tanaka, H.; Mitate, T.; Nakajima, S.; Yoshida, M.; Yoshimoto, Y.; Suzuki, T.; Wada, H. Rechargeable Lithium Battery Based on Pyrolytic Carbon as a Negative Electrode. *J. Power Sources* **1989**, *26* (3–4), 545–551.

(10) Goodenough, J. B.; Park, K.-S. The Li-Ion Rechargeable Battery: A Perspective. *J. Am. Chem. Soc.* **2013**, *135* (4), 1167–1176.

(11) Transparency Market Research. Lithium-ion Battery Market- Global Industry Analysis, Size, Share, Growth, Trends, and Forecast 2016-2024 http://www.transparencymarketresearch.com/lithium-ion-battery-market.html (accessed Jul 6, 2017).

(12) Manthiram, A. Materials Challenges and Opportunities of Lithium Ion Batteries. *J. Phys. Chem. Lett.* **2011**, *2* (3), 176–184.

(13) Xu, K. Nonaqueous Liquid Electrolytes for Lithium-Based Rechargeable Batteries. *Chem. Rev.* **2004**, *104* (10), 4303–4418.

(14) Shkrob, I. A.; Zhu, Y.; Marin, T. W.; Abraham, D. Reduction of Carbonate Electrolytes and the Formation of Solid-Electrolyte Interface (SEI) in Lithium-Ion Batteries. 1. Spectroscopic Observations of Radical Intermediates Generated in One-Electron Reduction of Carbonates. *J. Phys. Chem. C* **2013**, *117* (38), 19255–19269.

(15) Vogdanis, L.; Martens, B.; Uchtmann, H.; Hensel, F.; Heitz, W. Synthetic and Thermodynamic Investigations in the Polymerization of Ethylene Carbonate. *Die Makromol. Chemie* **1990**, *191* (3), 465–472.

(16) Doughty, D. H.; Pesaran, A. A. Vehicle Battery Safety Roadmap Guidance. *Natl. Renew. Energy Lab.* **2012**.

(17) Tennessen, P. T.; Weintraub, J. C.; Hermann, W. A. Extruded and Ribbed Thermal Interface for Use with a Battery Cooling System. US20110212356, 2011.

(18) Hellmann, J. V.; Zhu, J. Battery Having an Integral Cooling System. US 6,512,347, 2001.

(19) Peter Dore Rawlinson. Vehicle Battery Pack Ballistic Shield. 8,286,743, 2012.

(20) Egbue, O.; Long, S. Barriers to Widespread Adoption of Electric Vehicles: An Analysis of Consumer Attitudes and Perceptions. *Energy Policy* **2012**, *48*, 717–729.

(21) Wang, Q.; Ping, P.; Zhao, X.; Chu, G.; Sun, J.; Chen, C. Thermal Runaway Caused Fire and Explosion of Lithium Ion Battery. *J. Power Sources* **2012**, *208*, 210–224.

(22) Robinson, A. L.; Whittingham, M. S. Pushing the Frontiers of Lithium-Ion Batteries Raises Safety Questions. *MRS Bull.* **2016**, *41* (3), 188–189.

(23) Stephan, K. Exploding Galaxies: How to Do Recalls Right. *IEEE Consum. Electron. Mag.* **2017**, *6* (2), 99–100.

(24) Xu, K. Electrolytes and Interphases in Li-Ion Batteries and Beyond. *Chem. Rev.* **2014**, *114* (23), 11503–11618.

(25) Meyer, W. H. Polymer Electrolytes for Lithium-Ion Batteries. *Adv. Mater.* **1998**, *10* (6), 439–448.

(26) Guyomard, D.; Tarascon, J. M. High Voltage Stable Liquid Electrolytes for Li1+xMn2O4/carbon Rocking-Chair Lithium Batteries. *J. Power Sources* **1995**, *54* (1), 92–98.

(27) Xu, K.; Ding, M. S.; Richard Jow, T. A Better Quantification of Electrochemical Stability Limits for Electrolytes in Double Layer Capacitors. *Electrochim. Acta* **2001**, *46* (12), 1823–1827.

(28) Cycling Performance http://batteryuniversity.com/learn/article/battery_performance_as_a_function_of_cycling (accessed Jul 11, 2017).

(29) Yoshio, M.; Brodd, R. J.; Kozawa, A. *Lithium-Ion Batteries*; Springer, 2009.

(30) Basics of Electrochemical Impedance Spectroscopy https://www.gamry.com/application-notes/EIS/basics-of-electrochemical-impedance-spectroscopy/ (accessed Jul 11, 2017).

(31) Zugmann, S.; Gores, H. J. Transference Numbers of Ions in Electrolytes. In *Encyclopedia of Applied Electrochemistry*; Springer New York: New York, NY, 2014; pp 2086–2091.

(32) Fernández-Prini, R.; Spiro, M. Conductance and Transference Numbers. In *Physical Chemistry of Organic Solvent Systems*; Springer US: Boston, MA, 1973; pp 525–680.

(33) Doyle, M.; Fuller, T. F.; Newman, J. The Importance of the Lithium Ion Transference Number in Lithium/polymer Cells. *Electrochim. Acta* **1994**, *39* (13), 2073–2081.

(34) Evans, J.; Vincent, C. A.; Bruce, P. G. Electrochemical Measurement of Transference Numbers in Polymer Electrolytes. *Polymer (Guildf).* **1987**, *28* (13), 2324–2328.

(35) Zugmann, S.; Fleischmann, M.; Amereller, M.; Gschwind, R. M.; Wiemhöfer, H. D.; Gores, H. J. Measurement of Transference Numbers for Lithium Ion Electrolytes via Four Different Methods, a Comparative Study. *Electrochim. Acta* **2011**, *56* (11), 3926–3933.

(36) Price, W. S. Pulsed-Field Gradient Nuclear Magnetic Resonance as a Tool for Studying Translational Diffusion: Part 1. Basic Theory. *Concepts Magn. Reson.* **1997**, *9* (5), 299–336.

(37) Diffusion NMR http://chem.ch.huji.ac.il/nmr/techniques/other/diff/diff.html (accessed Jul 13, 2017).

(38) Wu, D. H.; Chen, A. D.; Johnson, C. S. An Improved Diffusion-Ordered Spectroscopy Experiment Incorporating Bipolar-Gradient Pulses. *J. Magn. Reson. Ser. A* **1995**, *115* (2), 260–264.

(39) Suo, L.; Borodin, O.; Gao, T.; Olguin, M.; Ho, J.; Fan, X.; Luo, C.; Wang, C.; Xu, K. "Water-in-Salt" Electrolyte Enables High-Voltage Aqueous Lithium-Ion Chemistries. *Science* **2015**, *350* (6263), 938–943.

(40) Yamaki, J.-I.; Yamazaki, I.; Egashira, M.; Okada, S. Thermal Studies of Fluorinated Ester as a Novel Candidate for Electrolyte Solvent of Lithium Metal Anode Rechargeable Cells. *J. Power Sources* **2001**, *102* (1), 288–293.

(41) Yao, X. L.; Xie, S.; Chen, C. H.; Wang, Q. S.; Sun, J. H.; Li, Y. L.; Lu, S. X. Comparative Study of Trimethyl Phosphite and Trimethyl Phosphate as Electrolyte Additives in Lithium Ion Batteries. *J. Power Sources* **2005**, *144* (1), 170–175.

(42) Galiński, M.; Lewandowski, A.; Stępniak, I. Ionic Liquids as Electrolytes. *Electrochim. Acta* **2006**, *51* (26), 5567–5580.

(43) Lewandowski, A.; Świderska-Mocek, A. Ionic Liquids as Electrolytes for Li-Ion batteries—An Overview of Electrochemical Studies. *J. Power Sources* **2009**, *194* (2), 601–609.

(44) Cameron, G. G.; Ingram, M. D. Liquid Polymer Electrolytes. In *Polymer Electrolyte Reviews*; MacCallum, J. R., Vincent, C. A., Eds.; Elsevier applied science; Springer, 1989.

(45) Zhang, S. S. A Review on Electrolyte Additives for Lithium-Ion Batteries. *J. Power Sources* **2006**, *162* (2), 1379–1394.

(46) Xu, K.; Ding, M. S.; Zhang, S.; Allen, J. L.; Jow, T. R. An Attempt to Formulate Nonflammable Lithium Ion Electrolytes with Alkyl Phosphates and Phosphazenes. *J. Electrochem. Soc.* **2002**, *149* (5), A622.

(47) Wang, X.; Yasukawa, E.; Kasuya, S. Nonflammable Trimethyl Phosphate Solvent-Containing Electrolytes for Lithium-Ion Batteries: II. The Use of an Amorphous Carbon Anode. *J. Electrochem. Soc.* **2001**, *148* (10), A1066.

(48) Arai, J. A Novel Non-Flammable Electrolyte Containing Methyl Nonafluorobutyl Ether for Lithium Secondary Batteries.

(49) Arai, J. Nonflammable Methyl Nonafluorobutyl Ether for Electrolyte Used in Lithium Secondary Batteries. *J. Electrochem. Soc.* **2003**, *150* (2), A219.

(50) Hallett, J.P.; Welton, T. Room-Temperature Ionic Liquids: Solvents for Synthesis and Catalysis. *Chem Rev.* **2011**, *111* (5), 3508-3576.

(51) Frömling, T.; Kunze, M.; Schönhoff, M.; Sundermeyer, J.; Roling, B. Enhanced Lithium Transference Numbers in Ionic Liquid Electrolytes. *J. Phys. Chem. B* **2008**, *112* (41), 12985–12990.

(52) Yu, G.; Zhao, D.; Wen, L.; Yang, S.; Chen, X. Viscosity of Ionic Liquids: Database, Observation, and Quantitative Structure-Property Relationship Analysis. *AIChE J.* **2012**, *58* (9), 2885–2899.

(53) Wang, Y.; Zaghib, K.; Guerfi, A.; Bazito, F. F. C.; Torresi, R. M.; Dahn, J. R. Accelerating Rate Calorimetry Studies of the Reactions between Ionic Liquids and Charged Lithium Ion Battery Electrode Materials. *Electrochim. Acta* **2007**, *52* (22), 6346–6352.

(54) Fenton, D. E.; Parker, J. M.; Wright, P. V. Complexes of Alkali Metal Ions with Poly(ethylene Oxide). *Polymer (Guildf).* **1973**, *14* (11), 589.

(55) Berthier, C.; Gorecki, W.; Minier, M.; Armand, M. B.; Chabagno, J. M.; Rigaud, P. Microscopic Investigation of Ionic Conductivity in Alkali Metal Salts-Poly(ethylene Oxide) Adducts. *Solid State Ionics* **1983**, *11* (1), 91–95.

(56) Wieczorek, W.; Stevens, J. R. Impedance Spectroscopy and Phase Structure of Polyether−Poly(methyl methacrylate)−LiCF 3 SO 3 Blend-Based Electrolytes. *J. Phys. Chem. B* **1997**, *101* (9), 1529–1534.

(57) Quartarone, E.; Mustarelli, P.; Magistris, A. PEO-Based Composite Polymer Electrolytes. *Solid State Ionics* **1998**, *110* (1–2), 1–14.

(58) Booth, C.; Nicholas, C. V.; Wilson, D. J. *Polymer Electrolyte Reviews*, 2nd ed.; McCallum, J. R., Vincent, C. A., Eds.; Elsevier: London, 1989.

(59) Zhang, Y.; Costantini, N.; Mierzwa, M.; Pakula, T.; Neugebauer, D.; Matyjaszewski, K. Super Soft Elastomers as Ionic Conductors. *Polymer (Guildf).* **2004**, *45* (18), 6333–6339.

(60) Song, J. Y.; Wang, Y. Y.; Wan, C. C. Review of Gel-Type Polymer Electrolytes for Lithium-Ion Batteries. *J. Power Sources* **1999**, *77* (2), 183–197.

(61) Watanabe, M.; Suzuki, Y.; Nishimoto, A. Single Ion Conduction in Polyether Electrolytes Alloyed with Lithium Salt of a Perfluorinated Polyimide. *Electrochim. Acta* **2000**, *45* (8–9), 1187–1192.

(62) Liang, S.; Choi, U. H.; Liu, W.; Runt, J.; Colby, R. H. Synthesis and Lithium Ion Conduction of Polysiloxane Single-Ion Conductors Containing Novel Weak-Binding Borates. *Chem. Mater.* **2012**, *24* (12), 2316–2323.

(63) Stallworth, P. .; Fontanella, J. .; Wintersgill, M. .; Scheidler, C. D.; Immel, J. J.; Greenbaum, S. .; Gozdz, A. . NMR, DSC and High Pressure Electrical Conductivity Studies of Liquid and Hybrid Electrolytes. *J. Power Sources* **1999**, *81–82*, 739–747.

(64) Walter van Schalkwijk; Bruno Scrosati. *Advances in Lithium-Ion Batteries*; Kluwer Academic Publishers: Hingham, 2002.

(65) MacGlashan, G. S.; Andreev, Y. G. Structure of the Polymer Electrolyte Poly (Ethylene Oxide) 6: LiAsF6. *Nature* **1999**, *398* (April), 792–794.

(66) Andreev, Y. G.; Lightfoot, P.; Bruce, P. G. Structure of the Polymer Electrolyte Poly(ethylene oxide)$_3$: $LiN(SO_2CF_3)_2$ Determined by Powder Diffraction Using a Powerful Monte Carlo Approach. *Chem. Commun.* **1996**, No. 18, 2169.

(67) Lightfoot, P.; Mehta, M. A.; Bruce, P. G. Crystal Structure of the Polymer Electrolyte Poly(ethylene oxide)$_3$:$LiCF_3SO_3$. *Science* **1993**, *262* (5135), 883–885.

(68) Ghosh, A.; Wang, C.; Kofinas, P. Block Copolymer Solid Battery Electrolyte with High Li-Ion Transference Number. *J. Electrochem. Soc.* **2010**, *157* (7), A846.

(69) Armand, M. B. Polymer Electrolytes. *Annu. Rev. Mater. Sci.* **1986**, *16* (1), 245–261.

(70) Mehta, M. .; Fujinami, T. Novel Inorganic–organic Polymer Electrolytes – Preparation and Properties. *Solid State Ionics* **1998**, *113*, 187–192.

(71) Nitzan, A.; Ratner ', M. A. Conduction in Polymers: Dynamic Disorder Transport. *J. Phys. Chem* **1994**, *98*, 1765–1775.

(72) Borodin, O.; Smith, G. D. Mechanism of Ion Transport in Amorphous Poly(ethylene oxide)/LiTFSI from Molecular Dynamics Simulations. *Macromolecules* **2006**, *39* (4), 1620–1629.

(73) Ratner, M. A.; Shriver, D. F. Ion Transport in Solvent-Free Polymers. *Chem. Rev.* **1988**, *88* (1), 109–124.

(74) Hallinan Jr., D. T.; Balsara, N. P. Polymer Electrolytes. *Annu. Rev. Mater. Res.* **2013**, *43*, 503–525.

(75) Rolland, J. P.; Van Dam, R. M.; Schorzman, D. A.; Quake, S. R.; DeSimone, J. M. Solvent-Resistant Photocurable Liquid Fluoropolymers for Microfluidic Device Fabrication [Corrected]. *J. Am. Chem. Soc.* **2004**, *126* (8), 2322–2323.

(76) Yamashita, H.; Forster, E. O.; Pompili, M. Streamer Formation in Perfluoropolyether under Impulse Conditions. *IEEE Trans. Electr. Insul.* **1993**, *28* (3), 324.

(77) Sianesi, D.; Marchionni, G.; De Pasquale, R. J. Perfluoropolyethers (PFPEs) from Perfluoroolefin Photooxidation. In *Organofluorine Chemistry*; Springer US: Boston, MA, 1994; pp 431–461.

(78) Hu, Z.; Finlay, J. A.; Chen, L.; Betts, D. E.; Hillmyer, M. A.; Callow, M. E.; Callow, J. A.; DeSimone, J. M. Photochemically Cross-Linked Perfluoropolyether-Based Elastomers: Synthesis, Physical Characterization, and Biofouling Evaluation. *Macromolecules* **2009**, *42* (18), 6999–7007.

(79) Jason P. Rolland, †; Benjamin W. Maynor, †; Larken E. Euliss, †; Ansley E. Exner, †; Ginger M. Denison, † and; Joseph M. DeSimone*, †,‡. Direct Fabrication and Harvesting of Monodisperse, Shape-Specific Nanobiomaterials. **2005**.

(80) Haszeldine, R. N. The Addition of Free Radicals to Unsaturated Systems. Part IV. The Direction of Radical Addition to Hexafluoropropene. *J. Chem. Soc.* **1953**, 3559.

(81) Hill, J. T. Polymers from Hexafluoropropylene Oxide (HFPO). *J. Macromol. Sci. Part A - Chem.* **1974**, *8* (3), 499–520.

(82) Yohnosuke Ohsaka; Takashi Tohzuka; Shoji Takaki. Halogen-Containing Polyether. US4845268, 1989.

(83) Marchionni, G.; Ajroldi, G.; Pezzin, G. Structure–Property Relationships in Perfluoropolyethers: A Family of Polymeric Oils. In *Comprehensive Polymer Science and Supplements*; 1989; pp 347–388.

(84) Bunyard, W. C.; Romack, T. J.; Desimone, J. M. Perfluoropolyether Synthesis in Liquid Carbon Dioxide by Hexafluoropropylene Photooxidation. *Macromolecules* **1999**, *32* (24), 8224–8226.

(85) Chambers, R. D. Preparation of Highly Fluorinated Compounds. In *Fluorine in Organic Chemistry*; Blackwell Publishing Ltd.: Oxford, UK; pp 23–46.

(86) Chambers, R. D.; Joel, A. K.; Rees, A. J. Elemental Fluorine: Part 11. Fluorination of Modified Ethers and Polyethers. *J. Fluor. Chem.* **2000**, *101* (1), 97–105.

(87) DeSimone, J. M.; Wei, H.-C.; Romack, T. J. Fluorination in Liquid or Supercritical Carbon Dioxide. WO2000068170 A1, 2000.

(88) Thomas R. Bierschenk; Timothy J. Juhlke; Hajimu Kawa; Richard J. Lagow. Liquid-Phase Fluorination. US 5753776, 1998.

(89) Wong, D. H. C.; Thelen, J. L.; Fu, Y.; Devaux, D.; Pandya, A. a; Battaglia, V. S.; Balsara, N. P.; DeSimone, J. M. Nonflammable Perfluoropolyether-Based Electrolytes for Lithium Batteries. *Proc. Natl. Acad. Sci. U. S. A.* **2014**, *111* (9), 3327–3331.

(90) Cametti, M.; Crousse, B.; Metrangolo, P.; Milani, R.; Resnati, G. The Fluorous Effect in Biomolecular Applications. *Chem. Soc. Rev. Chem. Soc. Rev* **2012**, *41* (41), 31–42.

(91) Kwang-Seuk Ko; Firoz A. Jaipuri, A.; Pohl, N. L. Fluorous-Based Carbohydrate Microarrays. *J. Am. Chem. Soc.* **2005**, *127* (38), 13162–13163.

(92) Northen, T. R.; Yanes, O.; Northen, M. T.; Marrinucci, D.; Uritboonthai, W.; Apon, J.; Golledge, S. L.; Nordström, A.; Siuzdak, G. Clathrate Nanostructures for Mass Spectrometry. *Nature* **2007**, *449* (7165), 1033–1036.

(93) Curran, D. P.; Sabine Hadida; He, M. Thermal Allylations of Aldehydes with a Fluorous Allylstannane. Separation of Organic and Fluorous Products by Solid Phase Extraction with Fluorous Reverse Phase Silica Gel. *J. Org. Chem.* **1997**, *62* (20), 6714–6715.

(94) Hu, Z.; Chen, L.; Betts, D. E.; Pandya, A.; Hillmyer, M. A.; DeSimone, J. M. Optically Transparent, Amphiphilic Networks Based on Blends of Perfluoropolyethers and Poly(ethylene Glycol). *J. Am. Chem. Soc.* **2008**, *130* (43), 14244–14252.

(95) Wong, D. H. C.; Vitale, A.; Devaux, D.; Taylor, A.; Pandya, A. A.; Hallinan, D. T.; Thelen, J. L.; Mecham, S. J.; Lux, S. F.; Lapides, A. M.; et al. Phase Behavior and Electrochemical Characterization of Blends of Perfluoropolyether, Poly(ethylene Glycol), and a Lithium Salt. *Chem. Mater.* **2015**, *27* (2), 597–603.

Chapter 2: Perfluoropolyether Electrolytes with Oligoether End Groups[2]

2.1 Introduction

Rechargeable batteries are crucial for accommodating growing energy needs in our society.[1,2] State-of-the-art lithium-ion (Li-ion) batteries are not only incorporated into portable consumer electronic devices and zero-emission vehicles, but also are of interest for electricity storage in smart grid applications.[3] Large-scale use of these batteries has been hindered by the flammability of the electrolyte, which consists of small molecule alkyl carbonates mixed with a lithium salt.[4] Numerous efforts have been made to address this safety concern, including the implementation of cooling systems, external circuitry for disconnecting the battery at high potentials caused by overcharging, and "redox shuttle" molecules for dissipating charge and eliminating thermal runaway.[5,6] However, continual reports of catastrophic battery failures highlight the need for an intrinsically nonflammable Li-ion battery.

Perfluorinated small molecules have been investigated as nonflammable electrolyte alternatives to enhance the safety of Li-ion batteries for potential large-scale applications, but they often exhibit low ionic conductivities due to low lithium salt solubility in the solvent.[7] Therefore, similar to phosphate-based additives, fluorinated small molecules have commonly been explored as flame-retardant additives for conventional alkyl carbonate solvents rather than as neat electrolyte solvents.[8] Although safety characteristics are enhanced with these additives, the

[2] This chapter previously appeared as an article in *Polymer*. The original citation is as follows: Olson K, Wong DHC, Chintapalli M, Timachova K, Janusziewicz R, Daniel W, Mecham S, Sheiko S, Balsara NP, DeSimone JM. (2016). Liquid perfluoropolyether electrolytes with enhanced ionic conductivity for lithium battery applications. Polymer. 100(25):126-133.

fluorinated solvent often must be the major component in order to observe nonflammability.[9,10] Furthermore, electrolyte-electrode interfacial performance is sacrificed in some cases.[11]

Polymer electrolytes have also been investigated as nonflammable electrolytes for Li-ion batteries. Poly(ethylene oxide) (PEO) is by far the most studied polymer electrolyte due to its ability to solvate lithium salts via coordination of ether oxygens to the lithium cation.[12–14] PEO is nonflammable and exhibits high ionic conductivity at elevated temperatures, but it is crystalline at room temperature (melting temperature ≈60°C).[15] Ion transport occurs via a hopping mechanism in polymer electrolytes, which is closely coupled to segmental motions of the polymer chain. Thus, PEO exhibits room-temperature ionic conductivities that are far below the levels necessary for practical use.[15] In addition, PEO exhibits poor oxidative stability and low Li-ion mobility due to the cation's coordination to backbone oxygens.[16,17]

We recently reported that perfluoropolyether (PFPE), a perfluorinated analog of PEO, dissolves the commonly studied salt lithium bis(trifluoromethane)sulfonamide (LiTFSI) and enables the transport of lithium ions.[18] PFPEs are a unique class of fluoropolymers that remain liquids over a wide temperature range [glass transition temperature (T_g) <–80°C], are nonflammable, and can be chemically tailored to enhance lithium salt solubility.

In addition to the safety enhancement provided by polymer electrolytes and fluorinated solvents, we have proposed that the highly fluorinated PFPE backbone solvates the fluorinated anion of lithium salts, a feature that is distinctive from other polymer and small molecule electrolytes that primarily interact with the lithium cation.[8,19–21] Perfluoroalkyl chains tend to segregate in order to minimize energetically unfavorable interactions between highly nonpolarizable fluorine atoms and other elements.[22] This "fluorous effect" is a powerful tool for molecular adsorption and aggregation in applications such as fluorous solid phase extraction,[23]

immobilization of biomolecules on microarrays,[24] and peptide self-association,[25,26] among others. We propose that this fluorous effect causes the PFPE backbone and the highly fluorinated anion of lithium salts to interact significantly.

High transference numbers are achievable in electrolytes that solvate the fluorinated anion of lithium salts, hindering its mobility (rather than that of the Li-ion). Indeed, we previously measured near-unity transference numbers in PFPE/LiTFSI electrolytes, providing evidence that the PFPE backbone solvates the fluorinated anion.[18] However, the conductivity (σ) of the electrolyte—approximately 2.5×10^{-6} S cm^{-1} at 30°C—must be improved for practical applications, and efforts to accomplish this require establishing the underpinnings of ion transport in the PFPE electrolyte system.

Quantifying the factors that govern ion transport in liquid mixtures is challenging due to the interplay of many factors such as ion solvation, electrostatic coupling, local dynamics in the vicinity of ions, and the glass transition temperature.[27–29] Herein, we report on the synthesis and characterization of a new series of ethoxylated PFPE electrolytes. We elucidate the effect of molecular structure, viscosity, and glass transition temperature on ionic conductivity within the PFPE electrolyte platform.

2.2 Materials and Sample Preparation

Perfluoropolyether Fluorolink E10 was obtained from Solvay-Solexis. Lithium bis(trifluoromethane)sulfonamide (LiTFSI), triethylamine, and methyl chloroformate were obtained from Sigma-Aldrich. 1,1,1,3,3-pentafluorobutane was obtained from MicroCare Corporation. PFPE and LiTFSI were dried at 90°C under vacuum for at least 24 hours prior to use. PFPE and LiTFSI were mixed together and stirred at room temperature for at least 24 hours. Salt solubility limits were determined as the point at which the solution visibly changed from

transparent to translucent, which has been shown to agree with quantitative measurements (inductively coupled plasma mass spectrometry) for these systems.[18]

2.3 Experimental

2.3.1 Synthesis of DMC-terminated PFPE

Fluorolink E10 (30 g, 0.025 mol) and triethylamine (7 mL, 0.05 mol) were dissolved in 300 mL 1,1,1,3,3-pentafluorobutane at 0°C under stirring conditions and nitrogen atmosphere. Methyl chloroformate (3.9 mL, 0.05 mol) was added dropwise over 3 minutes, after which the mixture was heated to 20°C and stirred for 18 hours. The resulting mixture was gravity filtered, washed with water 3x, and washed with brine once. The organic layer was isolated, dried using magnesium sulfate, gravity filtered, and evaporated under reduced pressure. The product was filtered again using a 0.45 micron syringe filter, yielding the final $PFPE_{E10}$-DMC product as a faint yellow, transparent liquid. Yield: 85%. ^{1}H NMR (600 MHz, 25°C, $(CD_3)_2CO$): 3.54-4.31 ppm (m, 22H). IR (neat): 2885 (C-H), 1751 (C=O), 1183 (C-H), 1067cm^{-1} (C-O).

2.3.2 Polymer Characterization

Gel permeation chromatography (GPC) measurements were performed on an Agilent Technologies 1260 Infinity LC system equipped with a DAWN HELEOS II multi-angle static light-scattering detector and OptiLab T-rEX refractometer from Wyatt Technologies. The sample (~30 mg/mL in tetrahydrofuran) was eluted through a 3 micron MIXED-E PLgel column (300 mm x 7.5 mm) at 1 mL/min for 60 minutes. A monodisperse 18 kDa polystyrene sample and monodisperse poly(ethylene glycol) samples of varying molecular weight were used as standards.

A 600 MHz Ultra-Shield Bruker NMR instrument was used for NMR analysis. Quantitative ^{13}C NMRs were obtained by increasing the d1 relaxation delay time until the relative intensity of all peaks remained constant, indicating full relaxation of all carbons. The $^{13}C\{^{1}H, ^{19}F\}$

NMR was obtained at a frequency of 150.9028 MHz with relaxation delay d1 = 50 seconds, 512 scans, ^{1}H decoupling offset = 4 ppm, and ^{19}F decoupling offset = -86 ppm.

2.3.3 Electrolyte Physical Properties Characterization.

Differential scanning calorimetry (DSC) thermograms were recorded using a TA Instruments DSC Q200 on samples that were prepared in air with a temperature range from -150°C to 100°C using a heat/cool/heat method at a heating rate of 10°C/min and cooling rate of 5°C/min. Glass transition temperatures (T_gs) were determined using the average from the midpoint method on the cooling cycle and second heating cycle thermogram. Thermogravimetric analysis (TGA) was run using a Perkin Elmer Pyris 1 TGA apparatus under nitrogen from 25°C to 550°C with a heating rate of 10°C/minute.

An ARES-G2 Rheometer (TA Instruments), equipped with a cone plate (50 mm diameter; 0.0202 radian cone angle), was used to measure viscosity at 25°C as a function of shear rate, which was ramped from $5x10^{-5}$ to 50 s^{-1}. The viscosity was modeled using Bingham analysis, which is commonly used to describe viscoplastic materials that exhibit a nonzero shear stress at zero shear rate.[30]

2.3.4 Characterization of Ion Transport

Electrolyte conductivity was measured in a stainless steel liquid cell using AC impedance spectroscopy. Impedance measurements were performed using a Bio-Logic VMP3 potentiostat, with 20 mV as the input signal amplitude, and 1 to 10^6 Hz as the frequency range. The minimum in a Nyquist plot of the impedance was used to determine the bulk resistance of the electrolyte, and the geometric factor of the liquid cell, described elsewhere, was used to calculate the conductivity.[31] The temperature of the electrolyte was controlled using a home-built heating

chamber. All conductivity measurements were performed in an argon glove box, as the liquid cell was not hermetically sealed.

2.4 Results and Discussion

PFPE is a random copolymer of tetrafluoroethylene oxide and difluoromethylene oxide. Dihydroxyl-terminated Fluorolink D10 (herein, "$PFPE_{D10}$-Diol"), and its ethoxylated Fluorolink E10 analog (herein "$PFPE_{E10}$-Diol") are shown in Figure 2.1. Here, $2q$ is the total number of EO repeat units in a single $PFPE_{E10}$ chain, m is the number of tetrafluoroethylene oxide repeat units, and n is the number of difluoromethylene oxide repeat units.

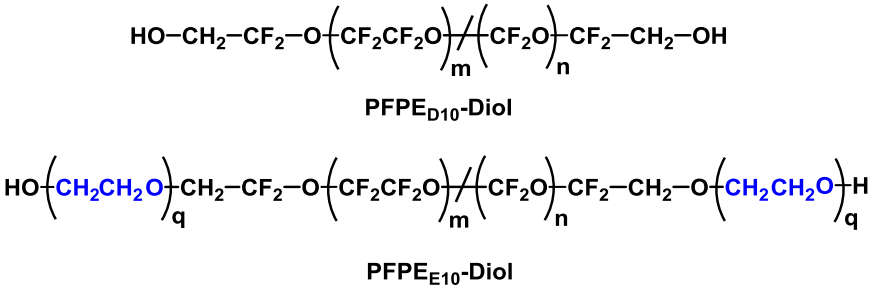

Figure 2.1 Structure of $PFPE_{D10}$-Diol compared to its ethoxylated $PFPE_{E10}$-Diol analog. The slash between perfluoroether repeat units denotes that it is a random copolymer.

Mass spectrometry indicates that on average, the number of repeat units in a single $PFPE_{E10}$ chain are q=2, m=5, and n=4, whereas m and n were previously reported as 7 and 3, respectively, for $PFPE_{D10}$.[18] We attribute the difference between the m and n values of $PFPE_{E10}$ and $PFPE_{D10}$ to batch-to-batch variation in the industrial synthesis rather than a systematic change between the two analogs.

To our knowledge, there is no precedent for studying a material with perfluoroether, ethylene oxide (EO), and methyl carbonate moieties covalently bound in a single polymer chain. Incorporating all of these functionalities into a pure electrolyte is appealing because EO and methyl carbonate contribute to lithium salt solvation and enhance conductivity,[32] while perfluoroether

provides thermal stability and high transference of Li-ions.[18] As shown in Figure 2.2, $PFPE_{E10}$-Diol (Structure **1**) was functionalized with methyl carbonate end groups to form DMC-terminated PFPE (herein, "$PFPE_{E10}$-DMC", Structure **2**) in order to enhance electrode-electrolyte compatibility and lithium salt solubility in the polymer. This reaction is analogous to our previously reported functionalization of $PFPE_{D10}$ with DMC end groups.[18]

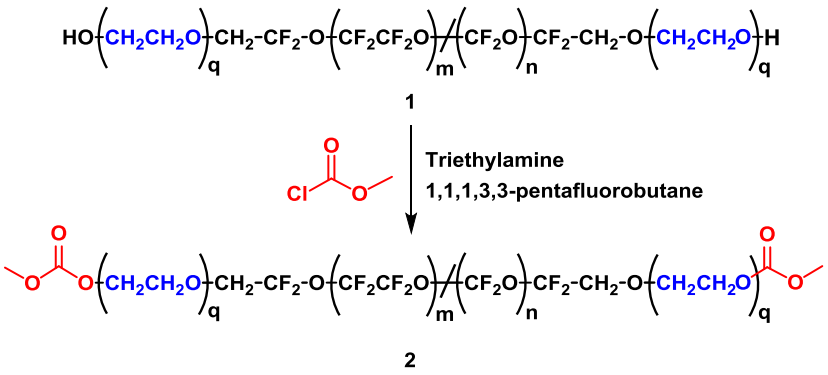

Figure 2.2. Synthesis of DMC-terminated $PFPE_{E10}$.

Chain coupling was unexpectedly observed during the synthesis of $PFPE_{E10}$-DMC from $PFPE_{E10}$-Diol that was not seen with the analogous $PFPE_{D10}$ system. Figure 2.3 shows the molecular weight distribution of the PFPE samples, measured using gel permeation chromatography (GPC) in tetrahydrofuran (THF). Each subsequent peak's number-average molecular weight (M_n) was measured to be slightly less than a multiple of the M_n of the first peak, which is consistent with the expected loss of end groups during chain coupling (peaks at elution time t=13.3, 13.6, 14.2, and 15.2 min corresponding to M_n=1.46, 2.60, 3.80, and 5.10 kDa, respectively, for $PFPE_{E10}$-DMC). Coupling in $PFPE_{E10}$-Diol itself was observed to a lesser extent, while no coupling was observed in $PFPE_{D10}$-Diol and $PFPE_{D10}$-DMC. Therefore, a small degree of coupling occurs during the industrial synthesis of $PFPE_{E10}$-Diol. To our knowledge, this coupling phenomenon in the PFPE Fluorolink E10 has not previously been reported in the literature.

During the addition of DMC end groups to $PFPE_{E10}$-Diol, we hypothesize that chain coupling increases significantly through the formation of carbonate linkages, as in structures **2-5** of Figure 2.4. To reject the possibility that ether linkages are formed under our reaction conditions, triethylamine was added to the $PFPE_{E10}$-Diol in the absence of methyl chloroformate. No chain coupling was observed, providing support for the proposed carbonate linkages.

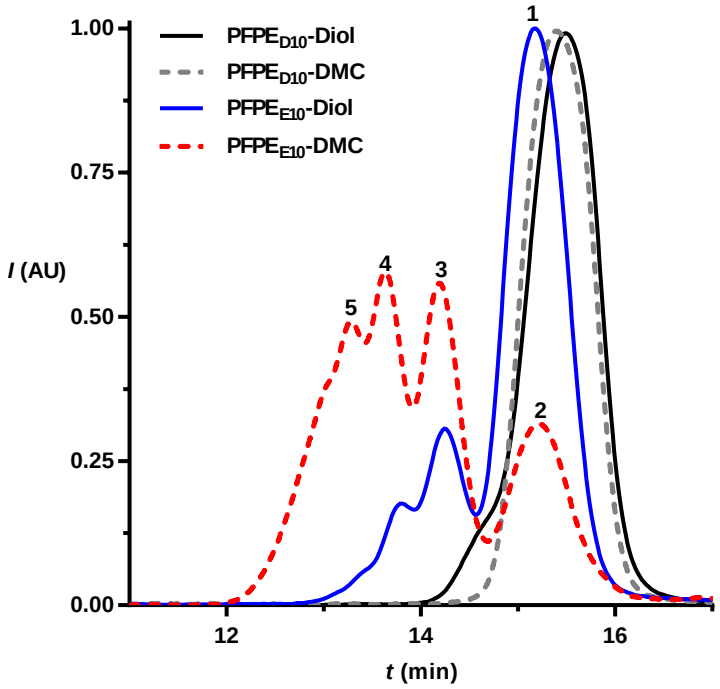

Figure 2.3 Comparative GPC chromatograms (light scattering intensity *I* vs. elution time *t*) of $PFPE_{E10}$ and $PFPE_{D10}$ oligomers, demonstrating coupling in the E10 derivatives only. The numbers above each peak correspond to the numbered structures shown in Figure 2.4.

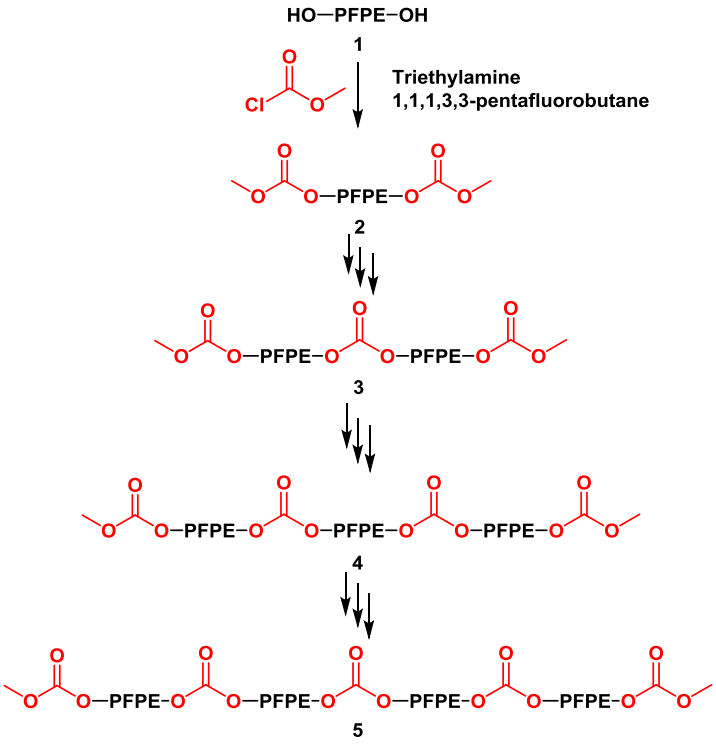

Figure 2.4 Proposed structures of coupled products with carbonate linkages. Elution peaks for each numbered compound are shown in Figure 2.3.

To support this hypothesis, we used the relative abundance—determined by GPC—of products **2-5** and the corresponding number of carbons in each coupled product (assuming carbonate linkages, see Table 2.1) to calculate the theoretical number of carbons in an average polymer chain. We then used quantitative ^{13}C NMR spectroscopy and integration methods to determine the relative ratios of terminal methoxy (OCH_3) to carbonyl (C=O) carbons in an average $PFPE_{E10}$-DMC chain. This ratio, as shown in Figure 2.5, was determined by NMR to be 2.0 : 2.9, which is in good agreement with the theoretical integration ratio of 2.0 : 2.7 based on the GPC results and proposed structures. There are more than two carbonyl carbons per chain, supporting the presence of carbonate linkages. If chain coupling did not occur through carbonate linkages, the only carbonyl groups in the polymer would be end groups, and the aforementioned ratio would be exactly 2.0 : 2.0.

Table 2.1 Abundance and structural differences between coupled products of Figure 2.4.

Structure	# of Terminal Methoxy (OCH_3) C's per Chain	# of Carbonyl (C=O) C's per Chain	Relative Abundance (weight fraction)
2	2	2	0.43
3	2	3	0.25
4	2	4	0.05
5	2	5	0.27

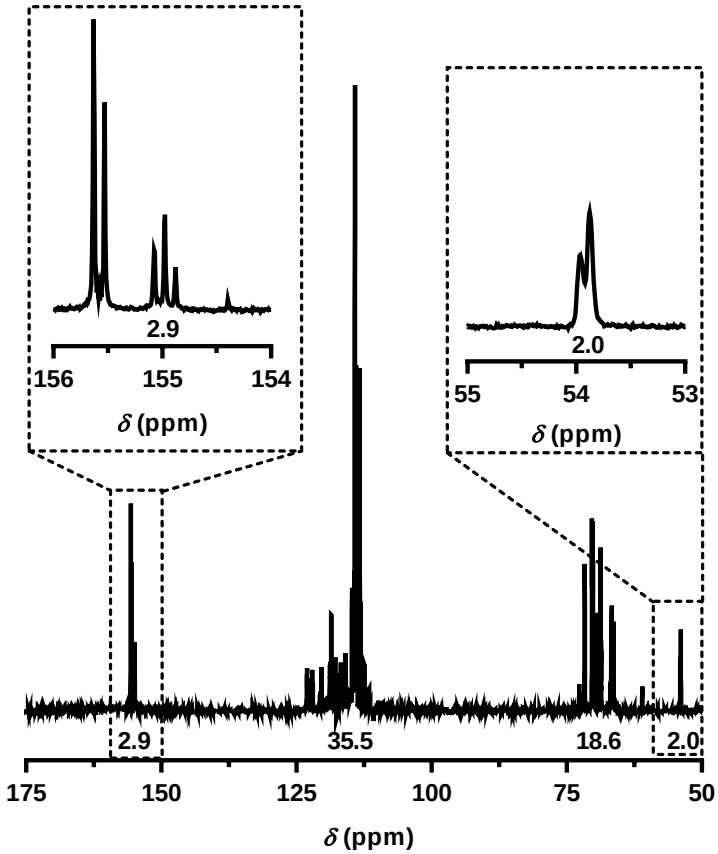

Figure 2.5 Quantitative ^{13}C NMR of $PFPE_{E10}$-DMC with corresponding integrations. Inset: carbonyl (δ=155 ppm) and terminal methoxy (δ=54 ppm) regions.

Electrolytes consisting of a mixture of distinct molecular weight (MW) polymer chains are rare in the literature, despite Preechatiwong's and Schultz's previous findings that blends of three MWs of poly(ethylene oxide) (PEO) resulted in higher conductivity than a single MW or a blend of two MWs.[33] Very low MW polymer chains remain unentangled and have low viscosities, which

enhances conductivity. However, they are too short to behave as random coils and generate significant free volume, which is necessary for ion transport from site to site in amorphous polymer electrolytes.[34] Relatively higher MW polymers (≥5000 g/mol) not only create free volume but also have been proposed by many to allow conducting tunnels to form in PEO.[35,36] Although many polymer electrolytes in the literature are polydisperse, few meet the criterion of containing MWs both above and below the threshold for entanglements, which can potentially provide diverse benefits in an electrolyte. For this reason, we were interested in further investigating our electrolyte composed of a variety of distinct MW PFPE chains.

The physical properties of the PFPE oligomers are compared in Table 2.2. Thermogravimetric analysis was used to analyze the decomposition temperature of the polymers, represented by the temperature at which 5 wt.% of the sample decomposed ($T_{d\ (5\%)}$), as shown in Figure 2.6. The evaporation profile of dimethyl carbonate (DMC) is included for reference. T_gs of the polymers were determined using differential scanning calorimetry (DSC). The $PFPE_{E10}$ polymers are thermally stable ($T_{d\ (5\%)}$>180°C) amorphous liquids over a broad temperature range (T_g<-90°C). In addition, we found that the presence of lithium salt did not systematically affect the degradation temperature of the PFPE materials.

Table 2.2 Physical properties of PFPE polymers.

Electrolyte	$T_{d\ (5\%)}$	T_g	Maximum [LiTFSI]		
	(°C)	*(°C)*	*(wt. %)*	*(mol L^{-1})*	*(r)*
$PFPE_{D10}$-Diol	210	–89	11%	0.76	0.04
$PFPE_{D10}$-DMC	212	–95	19%	1.45	0.09
$PFPE_{E10}$-Diol	181	–93	30%	2.57	0.14
$PFPE_{E10}$-DMC	194	–92	31%	2.70	0.16

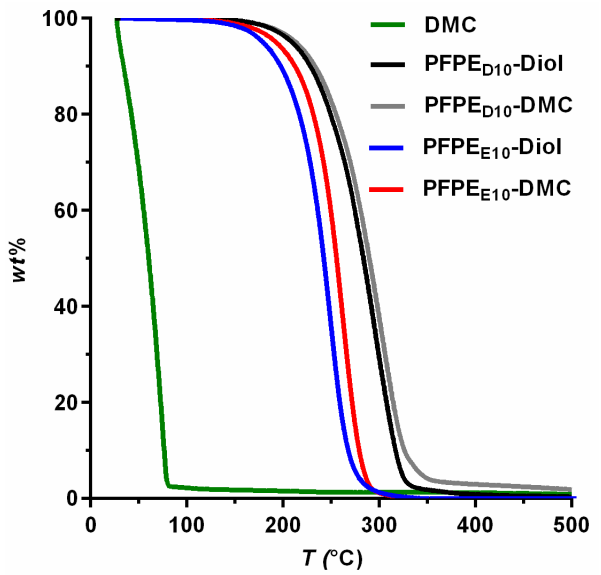

Figure 2.6 Thermogravimetric analysis of dimethyl carbonate and PFPE polymers.

As shown in Table 2.2, increased intermolecular interactions through hydrogen bonding cause PFPE$_{D10}$-Diol to exhibit a higher T_g than PFPE$_{D10}$-DMC. Interestingly, there is little difference in the T_gs of PFPE$_{E10}$-DMC and PFPE$_{E10}$-Diol. Chain coupling in the PFPE$_{E10}$-DMC product, resulting in higher average molecular weight, likely has a competing effect with the reduction in hydrogen bonding on the T_g.[37] The polymers exhibit a similar trend in viscosity (Figure 2.7A): in the absence of salt (r=0), hydrogen bonding in PFPE$_{D10}$-Diol leads to higher viscosity than PFPE$_{D10}$-DMC, while chain coupling negates this effect in the PFPE$_{E10}$ polymers.

LiTFSI salt was dissolved in the PFPE polymers to form an electrolyte. The maximum lithium salt-loading in the PFPE$_{E10}$ polymers was significantly higher than in the PFPE$_{D10}$ polymers (Table 2.2; r is herein defined as $[Li^+]/[m+n+q]$). This enhanced solubility indicates strong contributions from the EO portions of the backbone to lithium salt solvation, as expected.[32,38] Accordingly, the addition of methyl carbonate end groups only marginally enhanced lithium salt solubility in the polymer. The lithium salt solubility in PFPE was lower than in PEO (approximately 81 wt.% LiTFSI),[32] but comparable to the salt concentrations in commercial alkyl carbonate electrolytes (near 1.0 M).[39] It should be noted that the concentration of dissolved lithium

salt in PFPE electrolytes is not directly equivalent to the concentration of charge carriers. Ion pairing occurs in weak, concentrated electrolytes, including polymer electrolytes, and is likely prevalent in this system as well.[40] Ion pair formation results in the presence of uncharged species, reducing the effective concentration of charge carriers contributing to ionic conductivity.

Figure 2.7 A,B shows the viscosity (η) and T_g of the electrolytes at various salt concentrations. Addition of LiTFSI significantly increased the viscosity and T_g of the $PFPE_{E10}$ electrolytes. This is unsurprising, as complexation with lithium ions forms transient ionic crosslinks, which reduces chain mobility and thus raises viscosity and T_g.[41] It follows that the $PFPE_{D10}$ system experienced only moderate increases in viscosity and T_g because the electron-withdrawing fluorine groups reduce the strength of physical crosslinks between Li-ions and oxygen atoms in the polymer backbone.

In contrast to viscosity and T_g, conductivity at 28°C in the $PFPE_{E10}$ electrolytes was a non-monotonic function of lithium salt concentration, reaching a maximum at r=0.03 (Figure 2.7C). Previous studies have reported the LiTFSI concentration at which PEO electrolytes reach a maximum in conductivity at r=0.085.[32] In the dilute regime of polymer electrolytes, conductivity increases upon addition of lithium salt due to elevations in the number of available charge carriers. At higher salt concentrations, addition of lithium salt causes conductivity to decrease because any increase in the number of charge carriers is more than offset by the elevations in T_g and viscosity induced by transient ionic crosslinks, which reduce ion mobility.[42] The behavior of $PFPE_{E10}$ electrolytes spanned both of these regimes. In contrast, conductivity in the $PFPE_{D10}$ electrolytes increased monotonically with salt concentration. We propose that LiTFSI reaches its solubility limit in the $PFPE_{D10}$ polymers before entering the second regime.

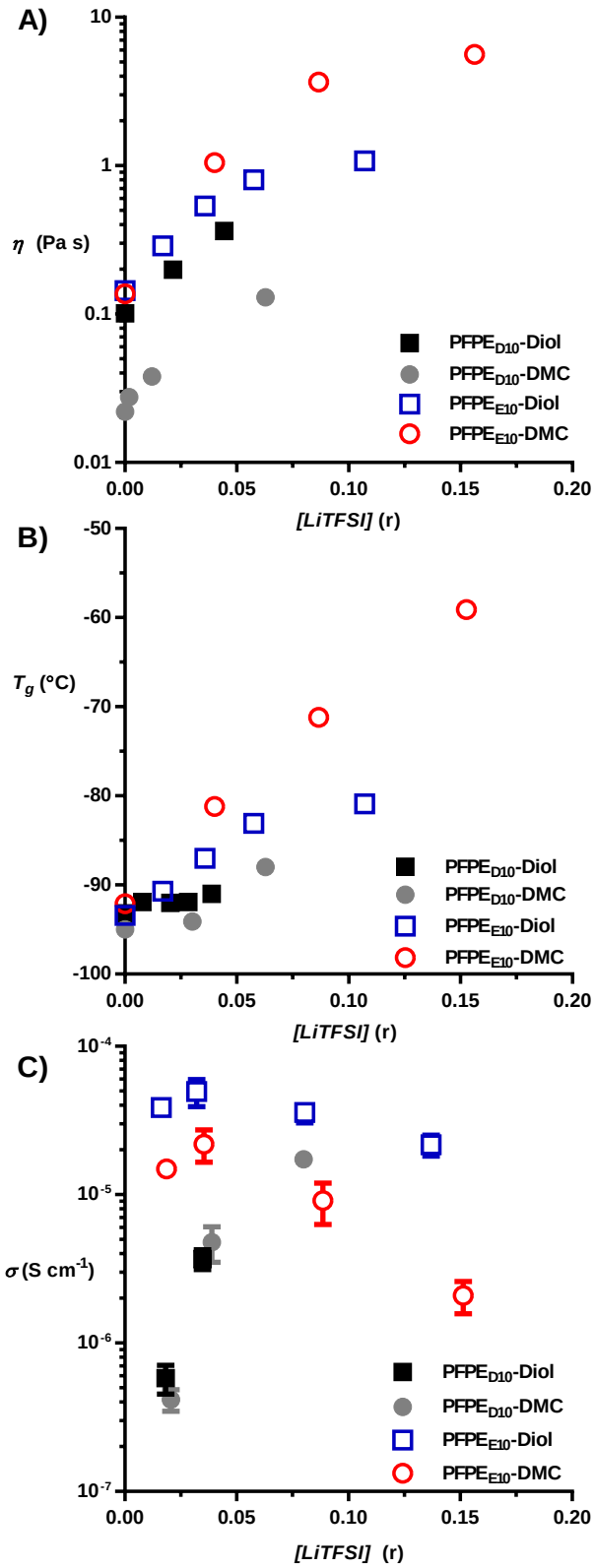

Figure 2.7 Effect of LiTFSI salt-loading on A) viscosity at 28°C, B) glass transition temperature, and C) conductivity at 28°C.

Conductivity was about an order of magnitude higher in the $PFPE_{E10}$ electrolyte than in its $PFPE_{D10}$ analog at 9.1 wt.% LiTFSI ($\sigma \approx 5x10^{-5}$ S cm^{-1} and $\sigma \approx 5x10^{-6}$ S cm^{-1}, respectively), despite the elevated viscosity in the former. This observation was unexpected. Considering that transport of ionic species in polymer electrolytes is generally accepted to be closely coupled to segmental motions of polymer chains,[43] conductivity typically decreases with increasing viscosity. To further analyze this observation, Figure 2.8 shows temperature-dependent conductivity measurements of the PFPE systems at 9.1 wt.% LiTFSI.

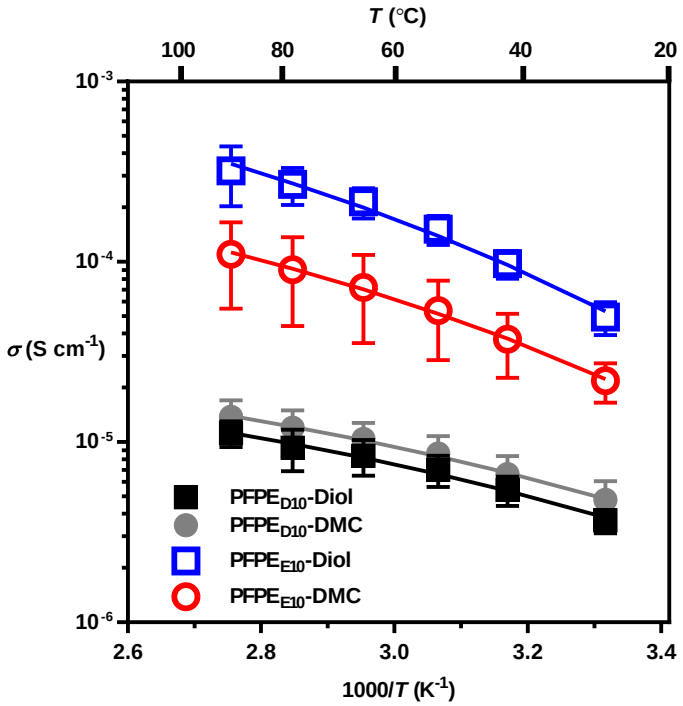

Figure 2.8 Conductivity of PFPE electrolytes at 9.1 wt% LiTFSI.

The temperature dependence of the ionic conductivity in the PFPE electrolytes was found to be well described by the Vogel-Fulcher-Tamman (VFT) equation:[44–46]

$$\sigma(T) = \frac{A}{\sqrt{T}} \exp\left[\frac{-B}{R(T - T_0)}\right] \tag{2.1}$$

where σ is the ionic conductivity, *A* is a constant proportional to the number of charge carriers, *B* is equivalent to the activation energy for ion transport, *R* is the gas constant, *T* is the experimental temperature, and T_0 is an empirical reference temperature (chosen here as T_g–50K).[47] Fits to this equation are shown as solid lines in Figure 2.8, and the parameters are listed in Table 2.3.

Table 2.3 VFT fit parameters for PFPE electrolytes at 9.1 wt.% LiTFSI.

Electrolyte	A *(S cm^{-1} K$^{1/2}$)*	B *(kJ mol^{-1})*	T_0 *(K)*
$PFPE_{D10}$-Diol	$5.3x10^{-3} \pm 1.7x10^{-3}$	6.0 ± 0.5	134
$PFPE_{D10}$-DMC	$3.7x10^{-3} \pm 1.3x10^{-3}$	5.2 ± 0.1	132
$PFPE_{E10}$-Diol	1.5 ± 0.9	10.0 ± 0.6	135
$PFPE_{E10}$-DMC	$1.2x10^{-1} \pm 0.6x10^{-1}$	7.4 ± 0.3	140

From the VFT fit parameters, it is clear that in spite of higher activation energies for ion motion, the conductivity of $PFPE_{E10}$ electrolytes is high due to an elevated number of charge carriers (i.e., significantly higher *A* values in $PFPE_{E10}$ electrolytes). This is consistent with our previous findings that electrolytes based on physical blends of $PFPE_{D10}$/PEG contain significantly more free charge carriers than electrolytes based on $PFPE_{D10}$ alone.[48] Even at the same concentration of dissolved lithium salt (a macroscopic property), the number of mobile charge carriers in $PFPE_{E10}$ electrolytes (a microscopic property) is higher. We attribute this primarily to strong interactions between Li-ions and EO, resulting in enhanced ion solvation. It is also this strong interaction between EO and Li-ions that hinders ion mobility at high salt concentrations in the $PFPE_{E10}$ polymers to a greater extent than in the $PFPE_{D10}$ polymers.

In addition, it has been reported that the dielectric constant of PFPE (without ethylene oxide moieties) ranges between 2.0-2.9, while PEO exhibits a dielectric constant approximately double

that ($\varepsilon \approx 5$).[49,50] The presence of hydrogenated ethers likely modestly increases the dielectric constant of $PFPE_{E10}$ compared to $PFPE_{D10}$ and contributes to ion dissociation, although we believe the factors discussed previously—ion solvation and segmental mobility—are primarily responsible for the observed results.

Comparisons between the behavior of $PFPE_{E10}$ and $PFPE_{D10}$/PEG blends demonstrate that unique properties are introduced into the electrolytes by covalently attaching EO to PFPE rather than physically blending the two together. Covalently bonding EO to PFPE eliminates the complex phase interactions between PFPE and PEG in the presence of LiTFSI.[48] It should be noted that the EO content (33 mol% for PFPE/PEG blends and 30 mol% for $PFPE_{E10}$) and lithium salt concentration (r=0.026 for PFPE/PEG and r=0.032 for $PFPE_{E10}$) of both of the investigated electrolytes was comparable.

As we have previously shown,[18] the end group of the $PFPE_{D10}$ electrolytes did not significantly affect conductivity at a given salt concentration. In contrast, the conductivity of the $PFPE_{E10}$-DMC was appreciably lower than that of $PFPE_{E10}$-Diol. We attribute this to chain coupling in the former, which causes increases in molecular weight along with viscosity and T_g. However, coupling of PFPE chains links EO blocks together, which may introduce a competing effect with viscosity by allowing these salt-loaded blocks to segregate and create conductive channels as has previously been reported for PEO block copolymer-based electrolytes.[36]

In short, high charge carrier concentrations in $PFPE_{E10}$ electrolytes overcome the effects of higher glass transition temperatures (compared to $PFPE_{D10}$ electrolytes) on ionic conductivity. Full characterization of the ionic species and concentrations in a weak, concentrated electrolyte system is non-trivial, as many-body ion interactions may be present.[51] Further investigation of ion pairing, including quantitative determination of charge carrier concentrations in PFPE electrolytes, is

currently underway. We thoroughly discuss the complex connection between continuum transport properties (e.g., conductivity and transference number) and microscopic transport properties (e.g., ion dissociation and self-diffusivity) in PFPE electrolytes elsewhere.[52]

2.5 Conclusion

We have prepared novel liquid perfluoropolyether polymer electrolytes with EO and methyl carbonate functionalities. We discovered unexpected chain coupling in the commercial $PFPE_{E10}$ material that was augmented by our subsequent functionalization of the chains with methyl carbonate end groups, resulting in carbonate linkages. PFPE electrolytes are thermally stable and exist as liquids at a broad range of temperatures, affording a wide temperature window of operation. Despite significant increases in T_g and viscosity upon salt-loading, the $PFPE_{E10}$ electrolytes exhibit ionic conductivities that are an order of magnitude higher than that of their lower viscosity $PFPE_{D10}$-based analogs at 9.1 wt.% LiTFSI.

Commercial alkyl carbonate electrolytes exhibit $\sigma \approx 10^{-2}$ S/cm at room temperature.[8] Although the lower conductivity of this class of PFPE electrolytes ($5x10^{-5}$ S/cm at room temperature) compared to commercial electrolytes is a disadvantage, the improved safety properties and highly unique anion solvation make them worthy of further investigation. We have established a set of structure-property relationships that we will continue to systematically manipulate to further enhance ion transport in this unique electrolyte platform.

REFERENCES

(1) Tarascon, J. M.; Armand, M. Issues and Challenges Facing Rechargeable Lithium Batteries. *Nature* **2001**, *414* (6861), 359–367.

(2) Goodenough, J. B.; Park, K.-S. The Li-Ion Rechargeable Battery: A Perspective. *J. Am. Chem. Soc.* **2013**, *135* (4), 1167–1176.

(3) Cheng, F.; Liang, J.; Tao, Z.; Chen, J. Functional Materials for Rechargeable Batteries. *Adv. Mater.* **2011**, *23* (15), 1695–1715.

(4) Mandal, B. K.; Padhi, A. K.; Shi, Z.; Chakraborty, S.; Filler, R. Thermal Runaway Inhibitors for Lithium Battery Electrolytes. *J. Power Sources* **2006**, *161* (2), 1341–1345.

(5) Berdichevsky, E.; Kohn, S.; Lyons, D. Battery Pack and Method for Protecting Batteries. US7671565 B2, March 2, 2010.

(6) Chen, Z.; Qin, Y.; Amine, K. Redox Shuttles for Safer Lithium-Ion Batteries. *Electrochim. Acta* **2009**, *54* (24), 5605–5613.

(7) Ue, M.; Sasaki, Y.; Tanaka, Y.; Morita, M. Nonaqueous Electrolytes with Advances in Solvents; Springer New York, 2014; pp 93–165.

(8) Xu, K. Nonaqueous Liquid Electrolytes for Lithium-Based Rechargeable Batteries. *Chem. Rev.* **2004**, *104* (10), 4303–4418.

(9) Arai, J. No-Flash-Point Electrolytes Applied to Amorphous carbon/Li1+xMn2O4 Cells for EV Use. *J. Power Sources* **2003**, *119*, 388–392.

(10) Sato, K.; Yamazaki, I.; Okada, S.; Yamaki, J. Mixed Solvent Electrolytes Containing Fluorinated Carboxylic Acid Esters to Improve the Thermal Stability of Lithium Metal Anode Cells. *Solid State Ionics* **2002**, *148* (3), 463–466.

(11) Ihara, M.; Hang, B. T.; Sato, K.; Egashira, M.; Okada, S.; Yamaki, J.-I. Properties of Carbon Anodes and Thermal Stability in LiPF6 /Methyl Difluoroacetate Electrolyte. *J. Electrochem. Soc.* **2003**, *150* (11), A1476–A1483.

(12) MacGlashan, G. S.; Andreev, Y. G. Structure of the Polymer Electrolyte Poly (Ethylene Oxide) 6: LiAsF6. *Nature* **1999**, *398* (April), 792–794.

(13) Lightfoot, P.; Mehta, M. A.; Bruce, P. G. Crystal Structure of the Polymer Electrolyte Poly(ethylene oxide)$_3$:$LiCF_3SO_3$. *Science* **1993**, *262* (5135), 883–885.

(14) Andreev, Y. G.; Lightfoot, P.; Bruce, P. G. Structure of the Polymer Electrolyte Poly(ethylene oxide)$_3$: $LiN(SO_2CF_3)_2$ Determined by Powder Diffraction Using a Powerful Monte Carlo Approach. *Chem. Commun.* **1996**, No. 18, 2169.

(15) Berthier, C.; Gorecki, W.; Minier, M.; Armand, M. B.; Chabagno, J. M.; Rigaud, P. Microscopic Investigation of Ionic Conductivity in Alkali Metal Salts-Poly(ethylene Oxide) Adducts. *Solid State Ionics* **1983**, *11* (1), 91–95.

(16) Watanabe, M.; Nishimoto, A. Effects of Network Structures and Incorporated Salt Species on Electrochemical Properties of Polyether-Based Polymer Electrolytes. *Solid State Ionics* **1995**, *79*, 306–312.

(17) Evans, J.; Vincent, C. A.; Bruce, P. G. Electrochemical Measurement of Transference Numbers in Polymer Electrolytes. *Polymer (Guildf).* **1987**, *28* (13), 2324–2328.

(18) Wong, D. H. C.; Thelen, J. L.; Fu, Y.; Devaux, D.; Pandya, A. a; Battaglia, V. S.; Balsara, N. P.; DeSimone, J. M. Nonflammable Perfluoropolyether-Based Electrolytes for Lithium Batteries. *Proc. Natl. Acad. Sci. U. S. A.* **2014**, *111* (9), 3327–3331.

(19) Armand, M. B. Polymer Electrolytes. *Annu. Rev. Mater. Sci.* **1986**, *16* (1), 245–261.

(20) Blint, R. J. Binding of Ether and Carbonyl Oxygens to Lithium Ion. *J. Electrochem. Soc.* **1995**, *142* (3), 696.

(21) Matsuda, Y.; Fukushima, T.; Hashimoto, H.; Arakawa, R. Solvation of Lithium Ions in Mixed Organic Electrolyte Solutions by Electrospray Ionization Mass Spectroscopy. *J. Electrochem. Soc.* **2002**, *149* (8), A1045.

(22) Cametti, M.; Crousse, B.; Metrangolo, P.; Milani, R.; Resnati, G. The Fluorous Effect in Biomolecular Applications. *Chem. Soc. Rev. Chem. Soc. Rev* **2012**, *41* (41), 31–42.

(23) Zhang, W.; Curran, D. P. Synthetic Applications of Fluorous Solid-Phase Extraction (F-SPE). *Tetrahedron* **2006**, *62* (51), 11837–11865.

(24) Kwang-Seuk Ko; Firoz A. Jaipuri, A.; Pohl, N. L. Fluorous-Based Carbohydrate Microarrays. *J. Am. Chem. Soc.* **2005**, *127* (38), 13162–13163.

(25) Buer, B. C.; Salud-Bea, R. de la; Hashimi, H. M. Al; Marsh, E. N. G. Engineering Protein Stability and Specificity Using Fluorous Amino Acids: The Importance of Packing Effects. *Biochemistry* **2009**, *48* (45), 10810–10817.

(26) Lee, H.-Y.; Lee, K.-H.; Hashim M. Al-Hashimi, A.; E. Neil G. Marsh. Modulating Protein Structure with Fluorous Amino Acids: Increased Stability and Native-like Structure Conferred on a 4-Helix Bundle Protein by Hexafluoroleucine. *J. Am. Chem. Soc.* **2006**, *128* (1), 337–343.

(27) Seo, D. M.; Borodin, O.; Balogh, D.; O'Connell, M.; Ly, Q.; Han, S.-D.; Passerini, S.; Henderson, W. A. Electrolyte Solvation and Ionic Association III. Acetonitrile-Lithium Salt Mixtures-Transport Properties. *J. Electrochem. Soc.* **2013**, *160* (8), A1061–A1070.

(28) Kunze, M.; Karatas, Y.; Wiemhöfer, H.-D.; Eckert, H.; Schönhoff, M. Activation of Transport and Local Dynamics in Polysiloxane-Based Salt-in-Polymer Electrolytes: A Multinuclear NMR Study. *Phys. Chem. Chem. Phys.* **2010**, *12* (25), 6844–6851.

(29) Stolwijk, N. A.; Heddier, C.; Reschke, M.; Wiencierz, M.; Bokeloh, J.; Wilde, G. Salt-Concentration Dependence of the Glass Transition Temperature in PEO–NaI and PEO–LiTFSI Polymer Electrolytes. *Macromolecules* **2013**, *46* (21), 8580–8588.

(30) Pehlivan, İ. B.; Marsal, R.; Niklasson, G. A.; Granqvist, C. G.; Georén, P. PEI–LiTFSI Electrolytes for Electrochromic Devices: Characterization by Differential Scanning Calorimetry and Viscosity Measurements. *Sol. Energy Mater. Sol. Cells* **2010**, *94* (12), 2399–2404.

(31) Teran, A. A.; Tang, M. H.; Mullin, S. A.; Balsara, N. P. Effect of Molecular Weight on Conductivity of Polymer Electrolytes. *Solid State Ionics* **2011**, *203* (1), 18–21.

(32) Lascaud, S.; Perrier, M.; Vallee, A.; Besner, S.; Prud'homme, J.; Armand, M. Phase Diagrams and Conductivity Behavior of Poly(ethylene Oxide)-Molten Salt Rubbery Electrolytes. *Macromolecules* **1994**, *27* (25), 7469–7477.

(33) Preechatiwong, W.; Schultz, J. M. Electrical Conductivity of Poly(ethylene Oxide)—alkali Metal Salt Systems and Effects of Mixed Salts and Mixed Molecular Weights. *Polymer (Guildf).* **1996**, *37* (23), 5109–5116.

(34) Lundberg, R. D.; Bailey, F. E.; Callard, R. W. Interactions of Inorganic Salts with Poly(ethylene Oxide). *J. Polym. Sci. Part A-1 Polym. Chem.* **1966**, *4* (6), 1563–1577.

(35) Tsuchida, E.; Ohno, H.; Tsunemi, K.; Kobayashi, N. Lithium Ionic Conduction in Poly (Methacrylic Acid)-Poly (Ethylene Oxide) Complex Containing Lithium Perchlorate. *Solid State Ionics* **1983**, *11* (3), 227–233.

(36) Yuan, R.; Teran, A. A.; Gurevitch, I.; Mullin, S. A.; Wanakule, N. S.; Balsara, N. P. Ionic Conductivity of Low Molecular Weight Block Copolymer Electrolytes. *Macromolecules* **2013**, *46* (3), 914–921.

(37) Fox, T. G.; Flory, P. J. Second-Order Transition Temperatures and Related Properties of Polystyrene. I. Influence of Molecular Weight. *J. Appl. Phys.* **1950**, *21* (6), 581.

(38) Gandini, A.; Le Nest, J.-F. Solid Polymer Electrolytes (Preparation, Characterization, Properties). *Polymeric Materials Encyclopedia, Vol 10*; CRC Press, 1996; p 7814.

(39) Xu, K. Electrolytes and Interphases in Li-Ion Batteries and Beyond. *Chem. Rev.* **2014**, *114* (23), 11503–11618.

(40) Dupon, R.; Papke, B. L.; Ratner, M. A.; Whitmore, D. H.; Shriver, D. F. Influence of Ion Pairing on Cation Transport in the Polymer Electrolytes Formed by Poly(ethylene Oxide) with Sodium Tetrafluoroborate and Sodium Tetrahydroborate. *J. Am. Chem. Soc.* **1982**, *104* (23), 6247–6251.

(41) Sun, J.; Stone, G. M.; Balsara, N. P.; Zuckermann, R. N. Structure–Conductivity Relationship for Peptoid-Based PEO–Mimetic Polymer Electrolytes. *Macromolecules* **2012**, *45* (12), 5151–5156.

(42) Cameron, G. G.; Ingram, M. D. Liquid Polymer Electrolytes. In *Polymer Electrolyte Reviews*; MacCallum, J. R., Vincent, C. A., Eds.; Elsevier applied science; Springer, 1989.

(43) Marzantowicz, M.; Dygas, J. R.; Krok, F.; Florjańczyk, Z.; Zygadło-Monikowska, E. Influence of Crystalline Complexes on Electrical Properties of PEO:LiTFSI Electrolyte. *Electrochim. Acta* **2007**, *53* (4), 1518–1526.

(44) Vogel, H. The Law of the Relation between the Viscosity of Liquids and the Temperature. *Phys. Zeitschrift* **1921**, *22*, 645–646.

(45) Fulcher, G. S. Analysis of Recent Measurements of the Viscosity of Glasses. *J. Am. Ceram. Soc.* **1925**, *8* (6), 339–355.

(46) Tammann, G.; Hesse, W. Die Abhangigkeit Der Viscositat von Der Temperatur Bie Unterkuhlten Flussigkeiten. *Zeitschrift fur Anorg. und Allg. Chemie* **1926**, *156* (1), 245–257.

(47) Barteau, K. P.; Wolffs, M.; Lynd, N. A.; Fredrickson, G. H.; Kramer, E. J.; Hawker, C. J. Allyl Glycidyl Ether-Based Polymer Electrolytes for Room Temperature Lithium Batteries. *Macromolecules* **2013**, *46* (22), 8988–8994.

(48) Wong, D. H. C.; Vitale, A.; Devaux, D.; Taylor, A.; Pandya, A. A.; Hallinan, D. T.; Thelen, J. L.; Mecham, S. J.; Lux, S. F.; Lapides, A. M.; et al. Phase Behavior and Electrochemical Characterization of Blends of Perfluoropolyether, Poly(ethylene Glycol), and a Lithium Salt. *Chem. Mater.* **2015**, *27* (2), 597–603.

(49) Marchionni, G.; Ajroldi, G.; Pezzin, G. Structure–Property Relationships in Perfluoropolyethers: A Family of Polymeric Oils. In *Comprehensive Polymer Science and Supplements*; 1989; pp 347–388.

(50) Tonelli, C.; Gavezotti, P.; Strepparola, E. Linear Perfluoropolyether Difunctional Oligomers: Chemistry, Properties and Applications. *J. Fluor. Chem.* **1999**, *95* (1), 51–70.

(51) Wieczorek, W.; Raducha, D.; Zalewska, A.; Stevens, J. R. Effect of Salt Concentration on the Conductivity of PEO-Based Composite Polymeric Electrolytes. *J. Phys. Chem. B* **1998**, *102* (44), 8725–8731.

(52) Chintapalli, M.; Timachova, K.; Olson, K. R.; Mecham, S. J.; Devaux, D.; DeSimone, J. M.; Balsara, N. P. Relationship between Conductivity, Ion Diffusion, and Transference Number in Perfluoropolyether Electrolytes. *Macromolecules* **2016**, *49* (9), 3508–3515.

Chapter 3: Effects of PFPE End Group Polarity on Ion Solvation and Transport[3]

3.1 Background on Ion Solvation and Dissociation

The primary factor that determines a solvent's ability to dissolve lithium salts is still under investigation.[1,2] The dielectric constant ε, or relative permittivity, of a solvent is a measure of its ability to isolate charges from one another, where higher ε indicates better charge screening. The donor number (DN), or "donicity", is a measure of a solvent's Lewis basicity, its ability to donate an electron pair to a Lewis acid.[1] A solvent's DN is defined by the amount of heat released when it is mixed with $SbCl_5$ (an arbitrarily selected standard Lewis acid) in dichloroethane, a non-coordinating solvent.[3]

Scheme 3.1 Schematic representation of two-step salt dissolution process, where S = solvent, A = anion, and C = cation. Adapted with permission from ref. [3]. Copyright (1978) American Chemical Society.

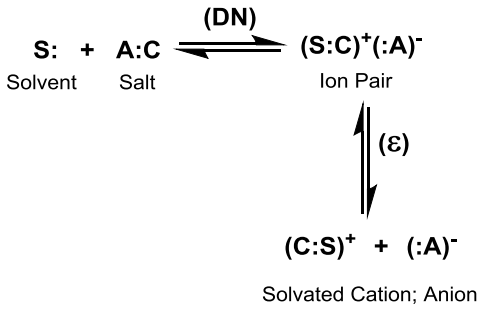

In his review of Lewis acids and bases, Jensen described salt dissolution as a two-step process, shown in Scheme 3.1.[3] First, the solvent displaces the anion to form a solvated ion pair. Second, the solvent separates the ion pair to yield a solvated cation and an anion. The first step is

[3] The characterization of ion transport summarized briefly in Sections 3.2.1 and 3.2.2 , important to the scope of this work, was completed at the University of California, Berkeley by Dr. Mahati Chintapalli and Ksenia Timachova under the guidance of Dr. Nitash Balsara. The work described in Section 3.3 was accomplished by the author under the training of Dr. Dominica Wong.

primarily determined by the solvent DN, the second step is largely determined by the solvent ε, and the degree of ionization is determined by a combination of the two factors. In short, a solvent's donor number determines its ability to *solvate* ions, while its dielectric constant determines its ability to *dissociate* ion pairs. In PFPE electrolytes, a third interaction must be accounted for—the interaction between the fluorinated backbone and the fluorinated anion. Thus, Scheme 3.1 should be considered a helpful, but oversimplified, framework for understanding ion solvation in PFPE electrolytes.

Because DN values are rarely measured for polymer solvents, they are often estimated under the assumption that the DN of a polymer is proportional to that of an organic solvent containing the same functional groups.[2] Dimethyl carbonate has a dielectric constant of 3 and a donor number of 15.1,[4] and glyme has a dielectric constant of 7.5 and a donor number of 24.[2] In this work, parameters of the low molecular weight analogs are used to estimate end group contributions rather than to directly infer bulk solvent values.

This chapter is split into three main sections, with each assessing the importance of end group polarity in PFPE electrolytes contextualized in Jensen's framework for ion solvation. Section 3.2 briefly summarizes advanced ion transport characterization carried about by our collaborators at the University of California, Berkeley on PFPE-DMC ($PFPE_{D10}$-DMC) and PFPE-EO ($PFPE_{E10}$-Diol) electrolytes. This work builds directly on the studies reported in Chapter 2 and provides necessary insights for understanding ion solvation and transport in PFPE electrolytes. Section 3.3 discusses the effects of modulating end group polarity on lithium ion transport and solvation in PFPE-EO systems. Finally, Section 3.4 explores the effects of modulating PFPE end group polarity in the absence of backbone ether units.

3.2 Part 1: Dependence of Ion Solvation and Transport on PFPE End Group

End groups play a crucial role in lithium salt solvation in PFPE solvents. As discussed in Chapter 1 and previously by Wong *et al.*,[5] lithium salt solubility normalized to end group concentration is consistent across a range of PFPE molecular weights. Furthermore, lithium salt solubility at a given PFPE molecular weight can be altered by simple end group substitution, as shown in Figure 3.1. It should be noted that R_{max} for PFPE-EO is defined as [Li^+]/[EO repeat unit] rather than simply [Li^+]/[end group], as there are 2 repeat units of EO per end group on average.

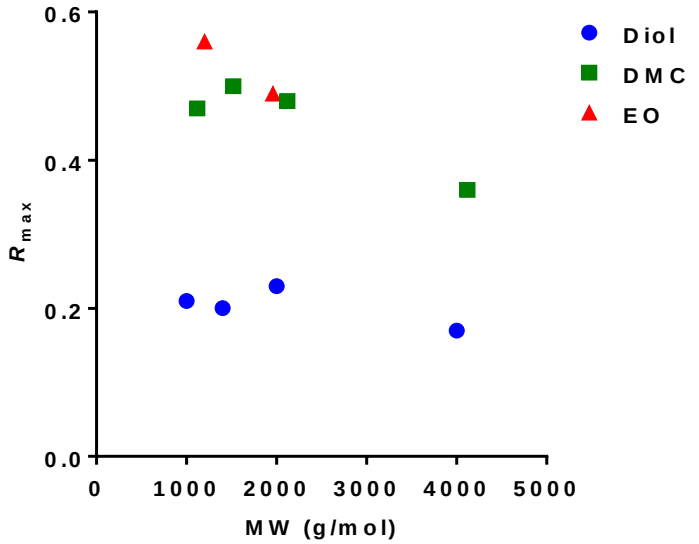

Figure 3.1 Maximum lithium salt solubility normalized to end group concentration (R_{max} = Li^+ / end group); blue: hydroxyl, green: methyl carbonate, red: ethylene oxide. Diol and DMC data were obtained from ref. [5].

DMC and EO units are capable of solvating a similar number of Li^+ ions, determined by the macroscopic salt solubility normalized by molar concentration (Figure 3.1, $R_{max} \approx 0.5$). But PFPE-DMC electrolyte performance varies significantly from PFPE-EO electrolyte performance. At low salt concentrations, PFPE-EO exhibits ionic conductivity that is approximately two orders of magnitude above that of PFPE-DMC. At high salt concentrations, PFPE-EO exhibits ionic conductivity that is only double that of PFPE-DMC (see Chapter 2).[6] Considering the similarity in

macroscopic lithium salt solubility but the stark difference in conductive properties, it seems that unique molecular underpinnings govern ion solvation and transport in PFPEs with end groups of differing polarity. It is important to establish these molecular underpinnings in order to design better-performing electrolytes based on the PFPE platform.

3.2.1 Ionic Conductivity

Ac impedance spectroscopy was previously used to directly measure the ionic conductivity of the PFPE electrolytes (as reported in Chapter 2).[6] Here, ion diffusion coefficients were measured by pfg-NMR, and the Nernst-Einstein equation (Eqn. 3.1)[7,8] was applied to each electrolyte in order to calculate the theoretical ionic conductivity:

$$\sigma_{NMR} = \frac{F^2 c}{RT}(D_{Li} + D_{TFSI}) \qquad (3.1)$$

where σ_{NMR} is the calculated ionic conductivity, F is Faraday's constant, c is the molar salt concentration, R is the gas constant, T is temperature, D_{Li} is the self-diffusion of dissociated lithium, and D_{TFSI} is the self-diffusion of its dissociated anion. Equation 3.1 is valid for dilute solutions with complete ion dissociation.[7] However, pfg-NMR measures the diffusion of *nuclei*, averaging the diffusivity of dissociated ions with that of neutral ion pairs and higher-order ion aggregates.

Comparison of the measured ionic conductivity by ac impedance spectroscopy (σ_{AC}) with that calculated based on ion diffusivities from pfg-NMR (σ_{NMR}) provides insight into the nature of ion dissociation and transport in electrolytes. The dimensionless parameter β, sometimes referred to as the "ionicity", is the ratio between the measured and calculated ionic conductivity.[7–10] β is unity for an electrolyte with fully dissociated ions that follows Nernst-Einstein behavior. The presence of ion aggregation typically decreases β because ion pair formation reduces the number

of free charge-carriers (reducing σ_{AC}), but the nuclear diffusivities measured by NMR remain fairly constant (σ_{NMR} is relatively unaffected).

$$\beta = \frac{\sigma_{AC}}{\sigma_{NMR}} = \frac{\sigma_{AC}}{\frac{F^2 c}{RT}(D_{Li} + D_{TFSI})} \tag{3.2}$$

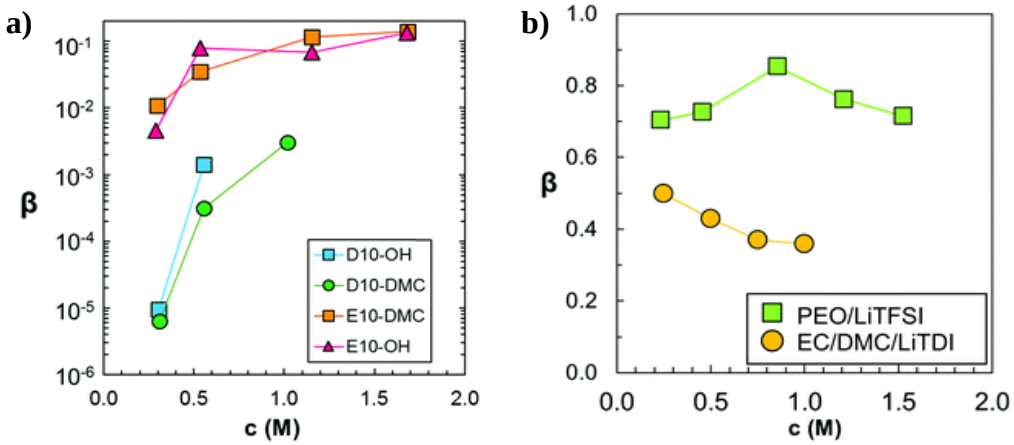

Figure 3.2 Dependence of β on salt concentration in a) PEO, carbonate electrolytes and b) PFPE electrolytes. Reproduced from ref. [8] with permission from the Royal Society of Chemistry.

As seen in Figure 3.2a, PFPE materials exhibit very low β values (~10^{-5}), indicating that ion pairs and higher-order aggregates are present in the system.[8] Interestingly, β increases by more than two orders of magnitude with increasing salt concentration in Fluorolink D10 electrolytes. This is unusual: ion aggregation usually increases at high salt concentrations, and therefore β typically decreases or remains constant with increasing salt concentration for the reasons described above. This behavior is observed in PEO- and alkyl carbonate-based electrolytes (Figure 3.2b).[8,11–13] But in PFPE electrolytes, ion transport begins to follow Nernst-Einstein behavior more closely at higher salt concentrations.

This led us to propose that inter-cluster hopping is the main mechanism for ion transport in $PFPE_{D10}$ electrolytes. At low salt concentrations, ion clusters are too far separated for ion hopping to occur efficiently, and therefore significant deviation from Nernst-Einstein behavior

occurs. At high salt concentrations, ion clusters are closely spaced, allowing ions to hop from one cluster to the next. Through this mechanism, the number of active charge carriers actually increases with increasing salt concentration because a new conduction pathway is "switched on".

Comparatively, Fluorolink E10 exhibits moderate β values (0.01) and only modest increases in β with increasing salt concentration. Its behavior is intermediate between $PFPE_{D10}$ electrolytes and PEO-based electrolytes. Therefore, inter-cluster hopping may contribute to ionic conduction, though the major conduction mechanism is proposed to be ion hopping along the polymer chain as typically observed in PEO.[14]

3.2.2 Transference Number

The transference number of PFPE electrolytes with various end groups was determined from the potentiostatic polarization method and from ion diffusion coefficients measured by pfg-NMR.[15] A brief review of these methods for transference number determination is given in Section 1.5.5. Because pfg-NMR is unable to differentiate the diffusion of associated and dissociated ions, the potentiostatic polarization method is generally considered more accurate for the determination of transference number in electrolytes that exhibit incomplete ion dissociation.[16] The two methods will produce similar values for dilute, ideal electrolytes in which ions are fully dissociated. Disagreement between the two methods is indicative of incomplete ion dissociation.[17] Figure 3.3 compares the t^+ values obtained using each method for PFPEs with varying end group.[15]

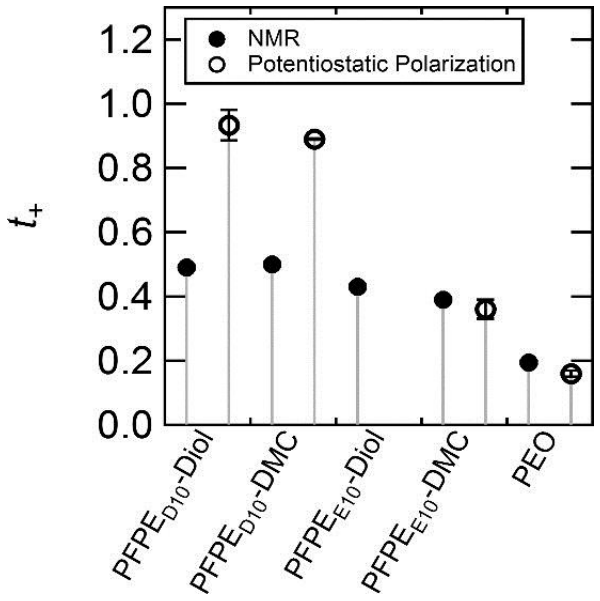

Figure 3.3 Transference number of PFPE and PEO (M_v≈5000 kg mol^{-1}) electrolytes, measured by potentiostatic polarization (open circles) and pfg-NMR (filled circles). Reprinted with permission from ref. [15]. Copyright (2016) American Chemical Society.

For an electrolyte with weak ion dissociation, the nuclear diffusion coefficients measured by NMR will be dominated by the diffusion of ion pairs D^i, and $t^+ = \frac{D^+}{D^+ + D^-} = \frac{D^i}{D^i + D^i} = \frac{1}{2}$ by NMR. In contrast, the t^+ measured by potentiostatic polarization depends on the mobility of charged ions and is therefore unaffected by motion of neutral ion pairs. For both PEO and PFPE-EO electrolytes, t^+ measured by potentiostic polarization and pfg-NMR are consistent with each other. But the two methods produce strikingly different t^+ values for PFPE$_{D10}$ electrolytes. The discrepancy between the t^+ values measured by NMR and potentiostatic polarization indicates there is significant ion pairing in PFPE$_{D10}$ electrolytes, while PFPE-EO and PEO-based electrolytes exhibit much less ion pairing. The apparent difference in ion pairing between PFPE$_{D10}$-DMC and PFPE-EO electrolytes is, at first, surprising considering the similar solvating ability of -DMC and -EO end groups (evidenced by the similar R_{max} values in Figure 3.1).

By the potentiostatic polarization method, PFPE-EO electrolytes exhibit $t^+ \approx 0.36$ and PFPE-DMC electrolytes exhibit $t^+ \approx 0.9$.[15] PFPE-DMC's high t^+ is consistent with the findings of Bogle and coworkers, who discovered a loose but prevalent association between Li^+ and DMC.[18] They rationalized that DMC's high DN makes its electrons highly available to Li^+, but the solvent's low ε causes weak binding strength. This weak DMC-Li^+ association enables lithium to travel more freely through PFPE-DMC electrolytes. In contrast, glyme-based solvents are known to coordinate strongly to Li^+ due to a combination of its high donor number, high dielectric constant, and ideal spacing between oxygens for Li^+ solvation.[19,20] Thus, PFPE-EO hinders the mobility of Li^+ to a greater extent than PFPE-DMC.

Consistent with the observed discrepancy in t^+ values and deviation from Nernst-Einstein behavior, we propose that significant ion pairing occurs in PFPE-DMC because of the low solvent ε. PFPE electrolytes with CF_3 end groups have a dielectric constant of about 2.[21] Addition of DMC end groups to PFPE is not expected to significantly change the dielectric constant (DMC $\varepsilon \approx 3$). In contrast, EO end groups should increase the dielectric constant of PFPEs appreciably (glyme $\varepsilon \approx 7$). PFPE-EO electrolytes exhibit less ion pairing than PFPE-DMC electrolytes based on the similar t^+ measurements, supporting this hypothesis. Again, ion pairs are solvated with similar efficiency in each electrolyte (step 1 of Scheme 3.1), yielding similar macroscopic salt solubility. But $PFPE_{E10}$ separates those ion pairs more efficiently (step 2 of Scheme 3.1), yielding a significantly higher concentration of free charge-carriers in solution. These striking differences between $PFPE_{D10}$ and $PFPE_{E10}$ materials led us to investigate a series of PFPEs with systematically increasing end group polarity so that we might better understand the molecular phenomena that govern ion solvation and transport in PFPE-based materials.

3.3 Part 2: Systematic Exploration of End Group Polarity in PFPE-EO Electrolytes

It is well established that organic carbonates dissolve lithium salts due to coordination between Li^+ and carbonyl oxygen atoms.[22–24] The coordination number of Li^+ in organic carbonates ranges from 2 to 6, with the majority of studies indicating the coordination number is either 4 or 6.[18,25–29] The optimized structure based on DFT calculations for the tetrahedral coordination of carbonyl oxygen atoms around Li^+ in ethylene carbonate solvent is shown in Figure 3.4.[30]

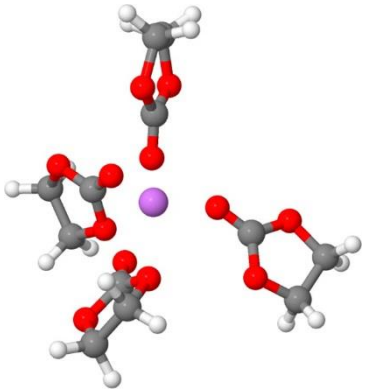

Figure 3.4 Structure of the optimized $Li(EC)_4^+$ cluster. Reprinted with permission from ref. [30]. Copyright (2015) American Chemical Society.

We have probed the interactions between Li^+ and a series of PFPE carbonate end groups by systematically tuning the electron density of the terminal carbonyl oxygen atom. To this end, we functionalized Fluorolink E10 (PFPE-EO, "$PFPE_{E10}$") with propargyl carbonate (DPC), allyl carbonate (DAC), and methyl carbonate (DMC) end groups, as shown in Scheme 3.2. The methyl group in methyl carbonate is slightly electron donating, increasing the electron density of the carbonyl and potentially enhancing the carbonate-Li^+ interaction. Allyl and propargyl groups, on the other hand, are electron withdrawing and therefore should weaken the carbonate-Li^+ interaction. By tuning this interaction, we aimed to change the number of dissociated ions, along with those charge carriers' mobilities, in PFPE electrolytes.

Scheme 3.2 Functionalization of PFPE-EO with end groups of varying polarity.

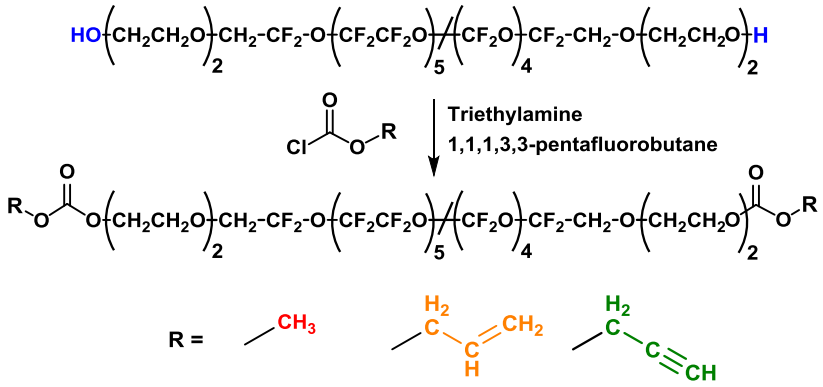

3.3.1 Materials

Fluorolink E10 ("PFPE-EO", 1200 g/mol) was purchased from Solvay Solexis and used as received. 1,1,1,3,3-pentafluorobutane ("Solkane 365mfc") was purchased from MicroCare Corporation and was dried over molecular sieves. Lithium bis(trifluoromethane)sulfonamide (LiTFSI), triethylamine (TEA), methyl chloroformate (99%), allyl chloroformate (97%), and propargyl chloroformate (96%) were purchased from Sigma Aldrich and used as received.

3.3.2 Experimental

3.3.2.1 General Synthesis of $PFPE_{E10}$-Carbonates

Fluorolink E10 (5 g, 4.2 mmol) and 2 mol eq. TEA relative to the OH groups (2.3 mL, 16.8 mmol) were dissolved in 1,1,1,3,3-pentafluorobutane (approximately 100 mL) at 0 °C in an ice bath with magnetic stirring under a nitrogen atmosphere (N_2). "R" chloroformate (16.8 mmol, where "R" = methyl, allyl, or propargyl) was then added dropwise over approximately one minute, after which the mixture was allowed to return to ambient temperature (approximately 25°C) and stirred for 18 h. The resulting mixture was gravity filtered to remove TEA HCl salt, then the filtrate was washed with water three times and brine once in a separatory funnel. The bottom layer was isolated and the solvent was removed on a rotary evaporator under reduced pressure. The remaining liquid product was then filtered using a 0.45 μm syringe filter, giving the product as a pale yellow, transparent liquid.

PFPE$_{E10}$-Dimethyl Carbonate (PFPE$_{E10}$-DMC)

(Quantitative conversion; 81% isolated yield) IR (neat): 2886 cm^{-1} (C-H), 1752 cm^{-1} (C=O), 1184 cm^{-1} (C-H), 1085 cm^{-1} (C-O). ^{1}H NMR ((CD$_3$)$_2$CO): 4.26-4.31 ppm (m, 3H), 4.10 ppm (m, 4H) 3.54-4.01 ppm (m, 14H).

PFPE$_{E10}$-Diallyl Carbonate (PFPE$_{E10}$-DAC)

(Quantitative conversion; 85% isolated yield) IR (neat): 2885 cm^{-1} (C-H), 1751 cm^{-1} (C=O), 1653 cm^{-1} (C=C), 1183 cm^{-1} (C-H), 1067 cm^{-1} (C-O). ^{1}H NMR ((CD$_3$)$_2$CO): 3.55-4.00 ppm (m, 14H), 4.10 ppm (m, 4H), 4.63 ppm (m, 2H), 5.25 ppm (d, 1H), 5.36 ppm (d, 1H), 5.98 ppm (m, 1H).

PFPE$_{E10}$-Dipropargyl Carbonate (PFPE$_{E10}$-DPC)

(Quantitative conversion; 94 % isolated yield) IR (neat): 3318 cm^{-1} (C-H), 2843 cm^{-1} (C-H), 2125 cm^{-1} (C≡C), 1755 cm^{-1} (C=O), 1185 cm^{-1} (C-H), 1085 cm^{-1} (C-O). ^{1}H NMR ((CD$_3$)$_2$CO): 3.16 ppm (d, 2 H), 3.55-4.35ppm (m, 36H), 4.81ppm (d, 4H).

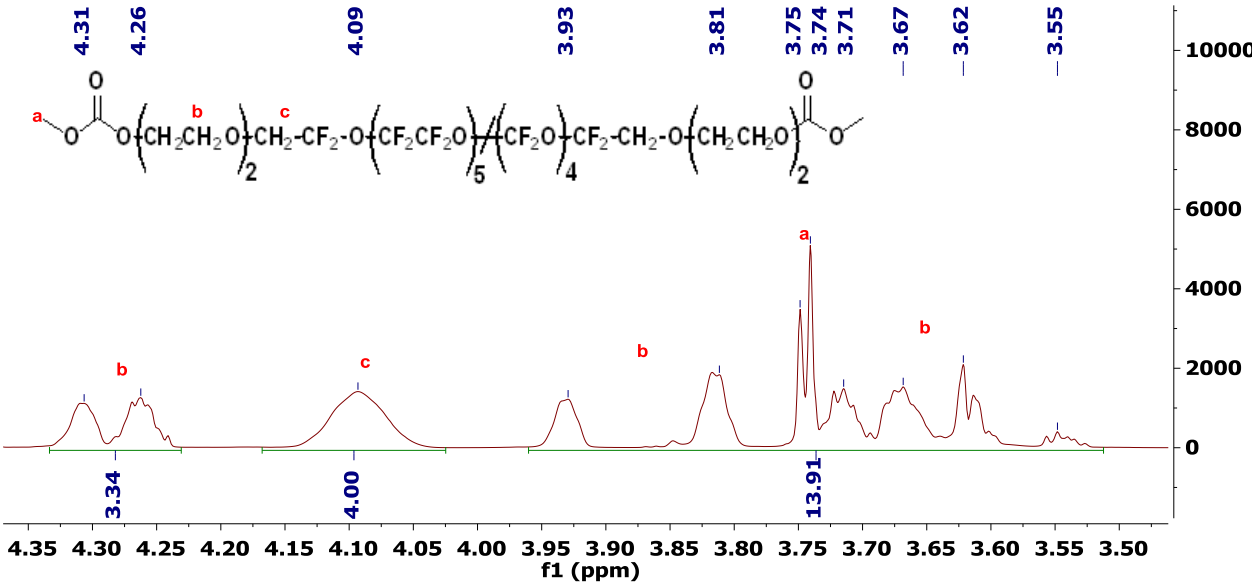

Figure 3.5 Representative ^{1}H NMR of PFPE$_{E10}$ carbonates (PFPE$_{E10}$DMC shown in spectrum above). Ether protons appear across a broad range of the spectrum, caused by the polydispersity of oligoether units along with the chain coupling discussed in Chapter 2. ^{13}C NMR, as shown and discussed in Chapter 2, provides cleaner spectra that prove more useful in product characterization.

3.3.2.2 Physical Characterization of PFPE-EO Electrolytes

The chemical structures of the functionalized PFPE products were confirmed using ^{19}F, ^{13}C, and ^{1}H nuclear magnetic resonance spectroscopy (NMR). NMR samples were prepared in deuterated acetone at a concentration of approximately 100 mg/mL. A 600 MHz Ultra-Shield Bruker NMR instrument was used for NMR analysis. Size exclusion chromatography (SEC) was used to analyze the molecular weight distribution of the products. SEC measurements were performed on an Agilent Technologies 1260 Infinity LC system equipped with a DAWN HELEOS II multi-angle static light-scattering detector and OptiLab T-rEX refractometer from Wyatt Technologies. The sample (~30 mg/mL in tetrahydrofuran) was eluted through a 3 micron MIXED-E PLgel column (300 mm x 7.5 mm) at 1 mL/min for 60 minutes. A monodisperse 18 kDa polystyrene sample and monodisperse poly(ethylene glycol) samples of varying molecular weight were used as standards. Fourier transform infrared spectroscopy (FTIR) was performed using a Bruker ALPHA FTIR instrument under ambient conditions using an attenuated total reflectance (ATR) attachment (from 500 to 4000 cm^{-1} at 2 cm^{-1} resolution).

Differential scanning calorimetry (DSC) thermograms were recorded using a TA Instruments DSC Q200 on samples which were prepared in air over the temperature range from -130 °C to 100 °C using a heat/cool/heat method at a heating and cooling rate of 10 °C and 5 °C/minute respectively. Glass transition temperatures (T_g's) were determined using the midpoint method on the second heating cycle thermogram.

A TA Instruments ARES-G2 Rheometer, equipped with a cone plate (50 mm diameter; 0.0202 radian cone angle), was used to obtain all rheological measurements. Viscosity, η, was measured as a function of shear rate, which was ramped from 5 x 10^{-5} to 50 s^{-1}. All measurements were performed at 25 °C. The viscosity was determined using a Bingham analysis, which is used

to describe viscoplastic materials (materials that behave as a rigid body at low stress but flow as viscous fluids at high stress).

3.3.3 Results

$PFPE_{E10}$-Diol was functionalized with a series of carbonate end groups of varying polarity. SEC (Figure 3.6) shows that the products consist of a mixture of oligomers—macromonomers joined by carbonate linkages, analogous to the phenomenon discussed in Chapter 2. This chain coupling proceeds via a transesterification reaction between PFPE-carbonate and PFPE-hydroxyl. The degree of chain coupling is similar for each of the carbonate-functionalized materials.

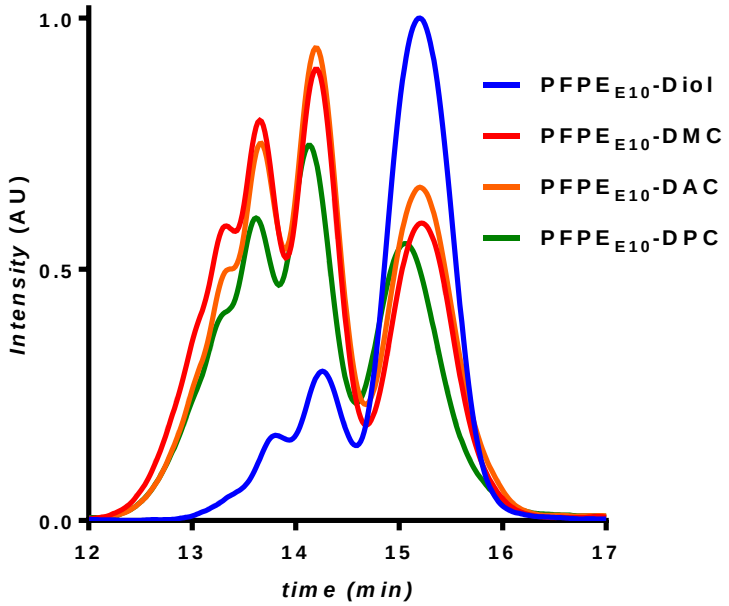

Figure 3.6 SEC chromatogram of $PFPE_{E10}$ oligomers. Chain coupling is evident in all carbonate products.

The fully dried $PFPE_{E10}$ materials were then stirred with lithium bis(trifluoromethane)sulfonamide (LiTFSI) salt under nitrogen atmosphere. LiTFSI was added in small aliquots until the solubility limit was reached. The LiTFSI solubility limit for each product was determined visually, as salt precipitation leads to heterogeneous, opaque mixtures above the salt solubility limit in PFPE systems.[5] Initially heterogeneous solutions were stirred for at least 24 hours to confirm insolubility, after which PFPE was added in small quantities to the solution until

it became transparent once again. The solution was then vacuum-dried at 50°C for 48 hours to confirm that the solution remained transparent and that water did not confound our characterization. The LiTFSI solubility limit for each product is shown in Figure 3.7. Surprisingly, there was no systematic relationship between lithium salt solubility and end group polarity in $PFPE_{E10}$ electrolytes. This was unexpected, considering attachment of progressively polar end groups to PFPE (e.g. DMC, EO) typically increases lithium salt solubility, as seen in the first three entries of Figure 3.7.

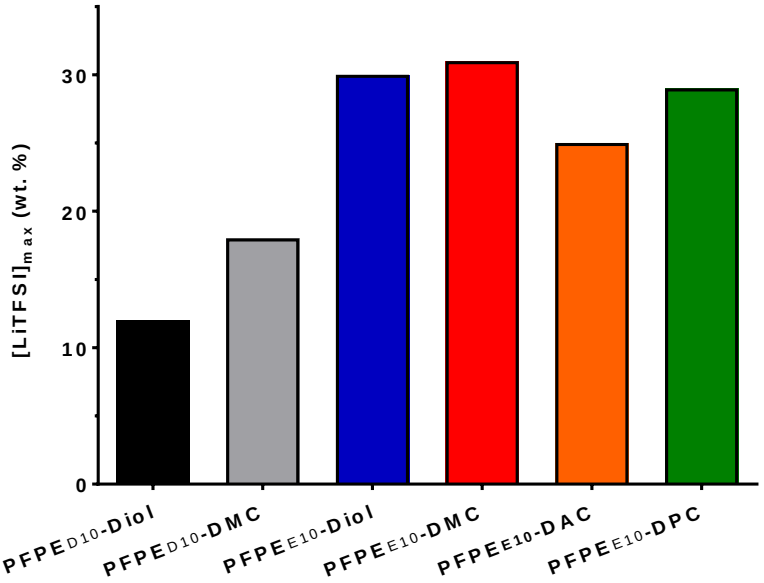

Figure 3.7 Maximum LiTFSI solubility in PFPEs with varying end group polarity.

IR spectroscopy was used to probe the interaction between Li^+ and carbonyl oxygen atoms as a function of carbonate end group polarity. Several previous studies have employed IR spectroscopy on lithium salt-in-solvent electrolytes to i) confirm interaction between a particular functional group and Li^+ and ii) quantify the extent of ion dissociation based on differences in the vibrational frequency of a functional group interacting with Li^+ compared to a functional group interacting with ion aggregates.[31–40] The relative ratio of transmittance intensity for each species enables quantification of ion dissociation in the system.

As shown in Figure 3.8, the C=O stretch of the neat $PFPE_{E10}$-carbonate materials appears at 1754 cm^{-1}. For the saturated electrolytes (~30 wt.% LiTFSI), the C=O stretch shifts to lower energies by about 20 cm^{-1}, providing evidence for the persistent interaction between Li^+ and carbonate end groups. Yet there is no significant difference in the frequency shift of the C=O stretch among DMC (21 cm^{-1}), DAC (21 cm^{-1}), and DPC (19 cm^{-1}) electrolytes considering the 2 cm^{-1} resolution of the instrument. We were unsuccessful in appreciably tuning the carbonate-Li^+ interaction by inductive effects in PFPE-EO materials.

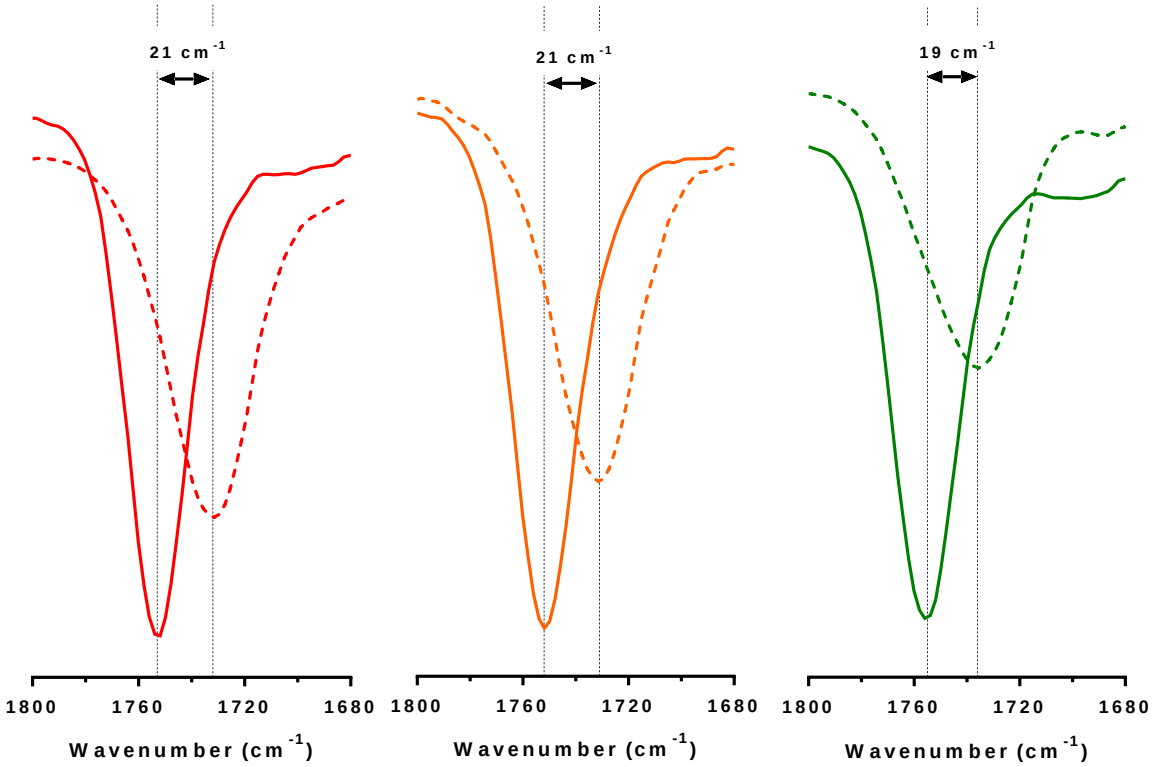

Figure 3.8 IR spectra of PFPE-carbonates in region of carbonyl stretch. Red: DMC, Orange: DAC, Green: DPC). Solid lines: neat PFPE materials; Dashed lines: LiTFSI-saturated PFPE materials.

In the $PFPE_{E10}$ system, perfluoroether, hydrogenated ether, and carbonate moieties are all present. Fish and Smid previously studied an electrolyte consisting of a mixture of propylene carbonate and tetraethylene glycol dimethyl ether. They found that even in electrolytes consisting of up to 90 mol% propylene carbonate, the majority of lithium ions remain bound to ether units.[41]

Similarly, ether oxygen atoms in $PFPE_{E10}$ dominate the Li^+-polymer interaction, mitigating our ability to tune ion interactions by varying the polarity of the carbonate end group. We propose that carbonate end groups maintain weak but persistent interactions with Li^+, forming its secondary solvation shell as is well established in mixtures of linear and cyclic carbonates.[18,42]

Measuring the rate of increase of T_g as a function of lithium salt concentration provides insights into the interaction of the polymer with lithium salts. The increase in T_g is attributed to physical, ionic crosslinks that form among polymer chains and lithium ions.[43] Generally, a larger slope of the T_g vs. [LiTFSI] plot indicates stronger or longer-lived polymer-Li^+ interactions. Figure 3.9a and b show the dependence of T_g and viscosity η on salt concentration, where the lithium salt concentration is normalized as R = [Li^+] / [end group].

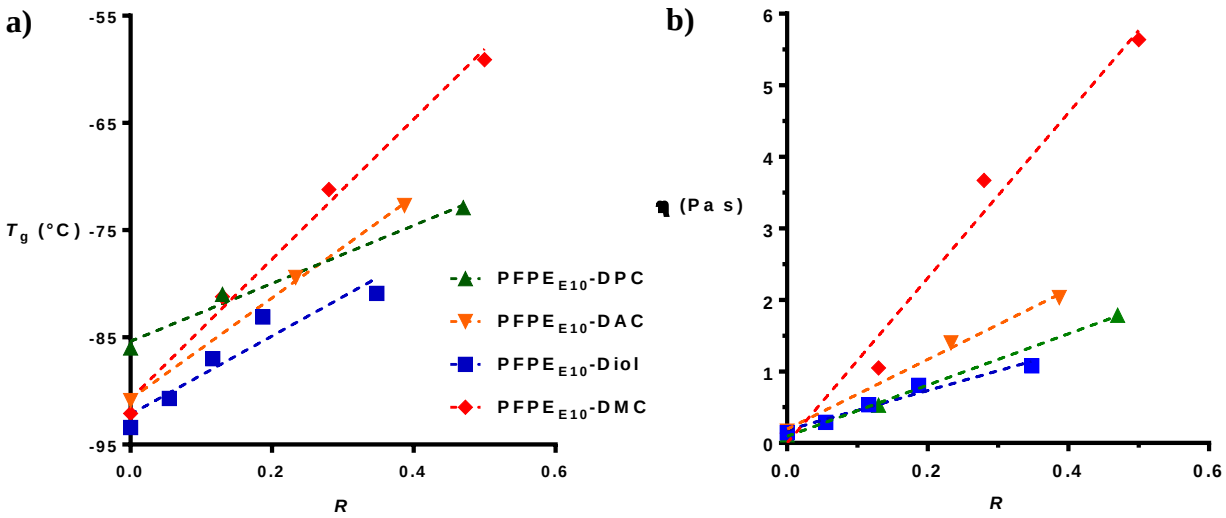

Figure 3.9 Dependence of a) glass transition temperature and b) viscosity on LiTFSI salt content in $PFPE_{E10}$ electrolytes. Dashed lines show linear fits of the data.

In contrast to lithium salt solubility and IR frequency shifts, the rise in T_g followed the expected dependence on end group polarity. Table 3.1 quantifies the rate of T_g increase with increasing salt concentration by measuring the slope of the curves in Figure 3.9a. PFPEs with the highest end group polarity exhibited the highest T_g increases with increasing salt content, while

PFPEs with the lowest end group polarity exhibited the lowest T_g increases (rate of increase: DMC > DAC > DPC). The viscosity data showed similar trends.

Table 3.1 Rate of increase in T_g and η as a function of salt concentration in $PFPE_{E10}$ electrolytes.

End Group	Slope, T_g vs. R (°C)	Slope, η vs. R (Pa s)
Diol	36.5 ± 6.7	2.76 ± 0.30
DPC	27.1 ± 3.2	3.58 ± 0.11
DAC	47.2 ± 1.6	4.87 ± 0.32
DMC	65.3 ± 4.5	11.5 ± 1.2

To summarize, the T_g and η data appear at first to be inconsistent with the lithium salt solubility and FT-IR data. Lithium salt solubility does not systematically increase with increasing polarity of the carbonate end group, and IR spectroscopy indicates that the strength of interaction between Li^+ and the carbonyl oxygen atom does not change as a function of end group polarity. Yet PFPEs with more polar carbonate end groups experience greater increases in T_g and η as a function of salt concentration, generally indicative of stronger Li^+-polymer interactions.

Once again, we propose that Jensen's model of ion solvation provides a useful framework to reconcile this apparent inconsistency. As discussed above, carbonates are relatively poor cation chelating agents compared to ethers. Increases in the carbonate DN—caused by electron inductive effects—are offset by ether's strong chelating ability due to a combination of its high DN, ε, and optimal spacing among oxygens for Li^+ coordination.[20] This accounts for the lack of correlation among carbonate polarity, lithium salt solubility, and C=O—Li^+ interaction strength in ether-containing PFPE systems.

On the other hand, T_g and η increase more rapidly as a function of salt concentration in $PFPE_{E10}$ systems with more electron-rich carbonate end groups (DMC > DAC > DPC). We propose that the changing polarity of the end group may alter the solvent ε, facilitating ion

dissociation in PFPEs with more polar carbonate end groups. At the same salt concentration, more free ions are dissociated in $PFPE_{E10}$-DMC than in $PFPE_{E10}$-DPC, for example, and therefore a greater number of ionic crosslinks are distributed among the ether units in $PFPE_{E10}$-DMC. In the $PFPE_{E10}$-carbonate systems, differences in the slope of the T_g vs. [LiTFSI] curve are attributed to differences in the *number* of ionic crosslinks present in a given system rather than differences in the *strength* of the Li^+-polymer interactions.

3.4 Part 3: Systematic Exploration of End Group Polarity in $PFPE_{D10H}$ Electrolytes

Considering the overwhelming effects of ether groups on PFPE electrolyte performance, we concluded that a controlled study on the effects of electron withdrawing and donating groups on the overall electrolyte properties must be carried out in the $PFPE_{D10H}$ system. By eliminating the presence of the ether, we aimed to gain a better understanding of how making systematic changes to PFPE end group polarity affects ion transport and solvation in the bulk electrolyte. To this end, Fluorolink D10H-Diol (referred to as "$PFPE_{D10H}$-Diol" or simply "PFPE-Diol" for the remainder of this section) was functionalized with carbonyl-containing end groups of varying polarity. $PFPE_{D10H}$-Diol is a random copolymer of tetrafluoroethylene oxide and difluoromethylene oxide with an average of 9 and 4 repeat units, respectively. Figure 3.10 shows the $PFPE_{D10H}$ end group structures investigated in this work, beginning with the commercially available PFPE-Diol and then listed in order of increasing end group polarity predicted from electron inductive effects.

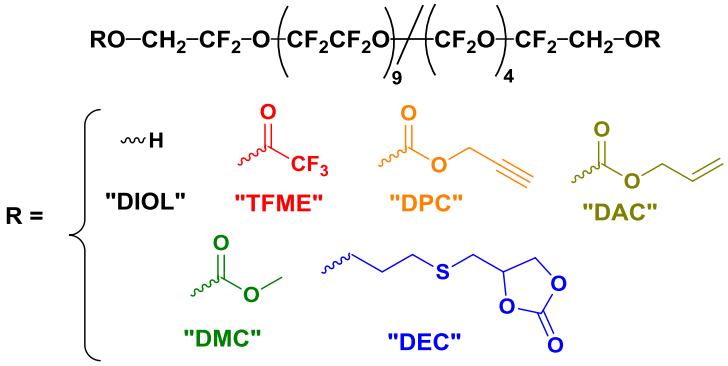

Figure 3.10 $PFPE_{D10H}$ end groups investigated in this work. Abbreviations are as follows: trifluoromethyl ester (TFME), di-propargyl carbonate (DPC), di-allyl carbonate (DAC), di-methyl carbonate (DMC), di-ethylene carbonate (DEC).

3.4.1 Experimental

3.4.1.1 Materials

Fluorolink D10H (Hydroxyl-terminated PFPE, 1480 g/mol, "PFPE-Diol") was purchased from Solvay Solexis and used as received. 1,1,1,3,3-pentafluorobutane ("Solkane 365mfc") was purchased from MicroCare Corporation and was dried over molecular sieves. Lithium bis(trifluoromethane)sulfonamide (LiTFSI), triethylamine (TEA), trifluoroacetic anhydride, methyl chloroformate, allyl chloroformate, propargyl chloroformate, allyl bromide, sodium hydroxide, thioglycerol, and 2,2-dimethoxy-2-phenylacetophenone were purchased from Sigma Aldrich and used as received. Trifluoroethanol (98%) was purchased from Oakwood Chemical and used as received.

3.4.1.2 Synthesis of $PFPE_{D10H}$ –Trifluoromethyl Ester (PFPE-TFME)

Scheme 3.3 Synthesis of $PFPE_{D10H}$-Trifluoromethyl ester using trifluoroacetic anhydride.

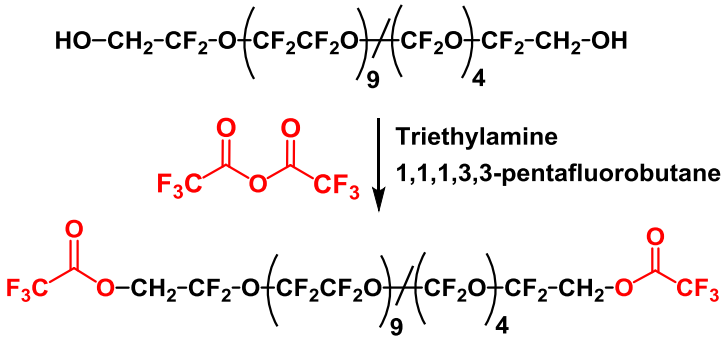

Fluorolink D10H (10 g, 6.6 mmol) and 2 mol eq. (relative to –OH) of TEA (3.6 mL, 26.4 mmol) were dissolved in 1,1,1,3,3-pentafluorobutane (approximately 200 mL) at 0 °C in an ice bath with magnetic stirring under a nitrogen atmosphere (N_2). Trifluoroacetic anhydride (3.6 mL, 26.4 mmol) was then added dropwise over approximately one minute, after which the mixture was allowed to return to ambient temperature (approximately 25°C) and stirred for 18 h. The resulting mixture was gravity filtered, then the filtrate was washed with water three times and brine once in a separatory funnel. The bottom layer was isolated and the solvent was removed on a rotary evaporator under reduced pressure. The remaining liquid product was then filtered using a 0.45 µm syringe filter, giving the product as a pale yellow, transparent liquid.

$PFPE_{D10H}$- Trifluoromethyl Ester (PFPE-TFME)

(Quantitative conversion; 72% isolated yield) IR (neat): 1809 cm^{-1} (C=O), 1179 cm^{-1} (C-H), 1085 cm^{-1} (C-O). ^1H NMR ($(CD_3)_2CO$, ppm): 5.07 (s, 4 H). ^{13}C NMR ($(CD_3)_2CO$, ppm): 155.53 (q), 120.40 (m), 114.19 (q), 111.41 (m), 63.62 (t).

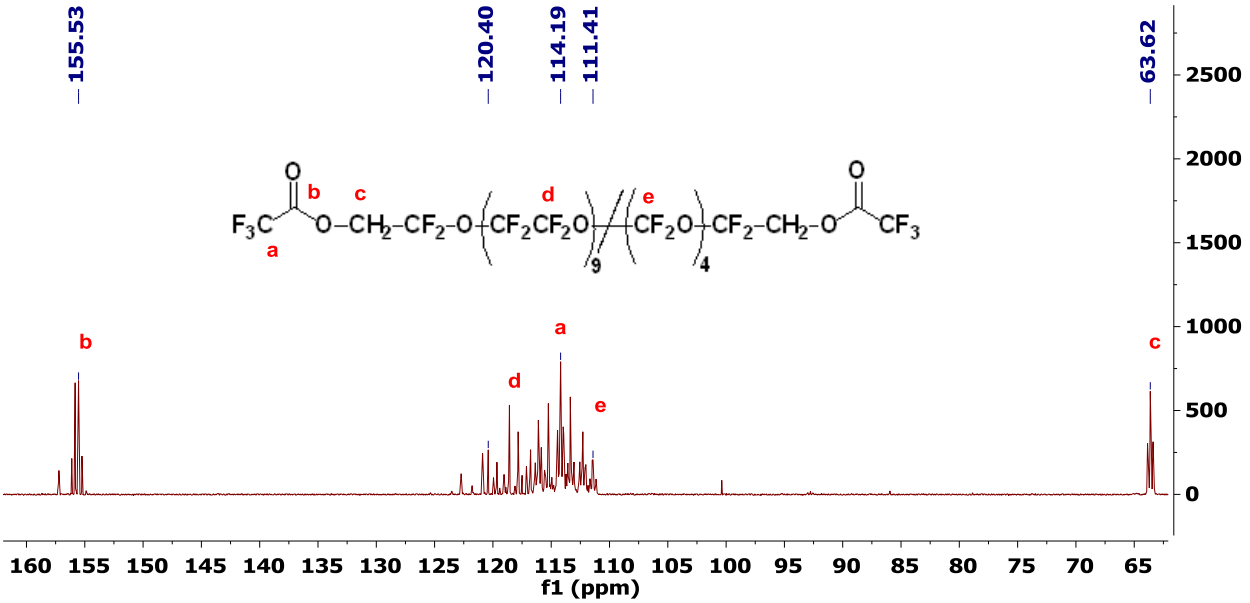

Figure 3.11 ^{13}C NMR spectrum of PFPE-TFME in deuterated acetone. IR spectroscopy also confirms successful product formation (C=O stretch is ~40 cm^{-1} higher than other carbonates).[44]

3.4.1.3 General Synthesis of $PFPE_{D10H}$- Carbonates

Fluorolink D10H (10 g, 6.6 mmol) and 2 mol eq. TEA relative to the –OH groups (3.6 mL, 26.4 mmol) were dissolved in 1,1,1,3,3-pentafluorobutane (approximately 200 mL) at 0 °C with magnetic stirring under N_2. "R" chloroformate (26.4 mmol, where "R" = methyl, allyl, or propargyl) was then added dropwise over approximately one minute, after which the mixture was allowed to return to ambient temperature and stirred for 18 h. The resulting mixture was gravity filtered to remove TEA HCl salt, then the filtrate was washed with water three times and brine once in a separatory funnel. The bottom layer was isolated and the solvent was removed on a rotary evaporator under reduced pressure. The remaining liquid product was then filtered using a 0.45 μm syringe filter, giving the product as a pale yellow, transparent liquid.

<u>$PFPE_{D10H}$-Dipropargyl Carbonate (PFPE-DPC)</u>

(Quantitative conversion; 88% isolated yield) IR (neat): 3320 cm^{-1} (C-H), 1772 cm^{-1} (C=O), 2102 cm^{-1} (C≡C), 1181 cm^{-1} (C-H), 1083 cm^{-1} (C-O). ^1H NMR ($(CD_3)_2CO$): 3.16 ppm (s, 2H), 4.79 ppm (s, 4H), 4.87 ppm (s, 4H).

PFPE$_{D10H}$-Diallyl Carbonate (PFPE-DAC)

(Quantitative conversion; 91 % isolated yield) IR (neat): 2989 cm^{-1} (C-H), 1768 cm^{-1} (C=O), 1654 cm^{-1} (C=C), 1185 cm^{-1} (C-H), 1089 cm^{-1} (C-O). ^{1}H NMR ((CD$_3$)$_2$CO): 4.71 ppm (s, 4 H), 4.78 ppm (s, 4H), 5.28 ppm (d, 2H), 5.38 ppm (d, 2H), 5.97 ppm (p, 2H).

PFPE$_{D10H}$-Dimethyl Carbonate (PFPE-DMC)

(Quantitative conversion; 89 % isolated yield) IR (neat): 1772 cm^{-1} (C=O), 1185 cm^{-1} (C-H), 1089 cm^{-1} (C-O). ^{1}H NMR ((CD$_3$)$_2$CO): 3.83 ppm (s, 6 H), 4.74 ppm (m, 4 H).

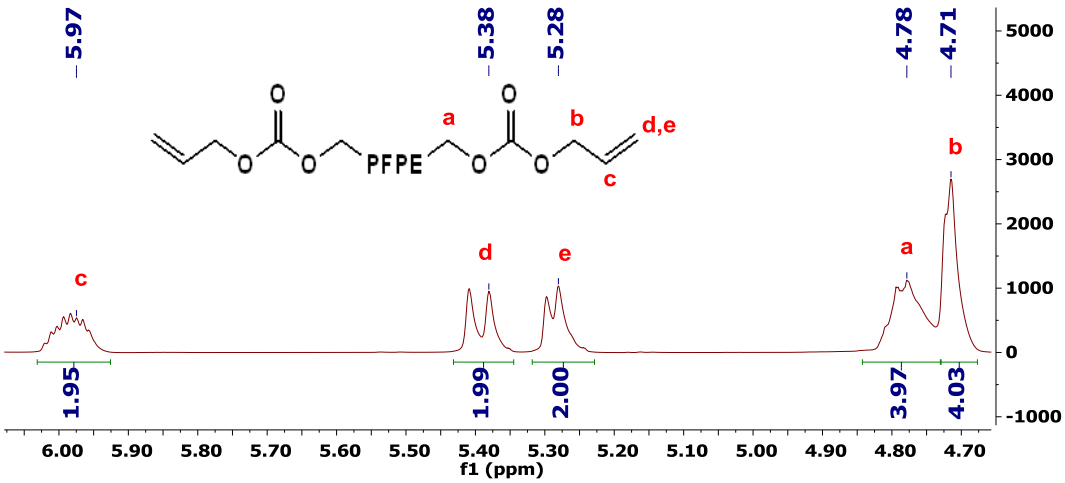

Figure 3.12 Representative ^{1}H spectrum of PFPE-carbonates (PFPE-DAC shown with peak assignments). The perfluoroether backbone (which lacks hydrogens) is abbreviated "PFPE".

3.4.1.4 Synthesis of PFPE$_{D10H}$-Diethylene Carbonate (PFPE-DEC)

Fluorolink D10H (10 g, 6.6 mmol) was transferred to a 2-neck round-bottom flask equipped with a mechanical stirrer. Aqueous sodium hydroxide solution (70 mL, 6.88 M solution) was added along with two drops of phase transfer catalyst Aliquot 336. The immiscible mixture was heated to 40°C and reacted for two hours under rapid stirring. Allyl bromide (24 mL, 138 mmol) was added, and the reaction was carried out at 40°C for an additional 6 hours. 1,1,1,3,3-pentafluorobutane was used to extract the product (4x, 50 mL solvent each). The extracted product was then washed 5x with 50 mL of deionized water to remove excess allyl bromide and residual

sodium hydroxide. The solvent was evaporated, and the product was dried under vacuum at 30°C for 24 hours to obtain the $PFPE_{D10H}$-Diallyl Ether (PFPE-DAE) product as a clear, colorless liquid.

$PFPE_{D10H}$-Diallyl Ether Intermediate (PFPE-DAE)

(Quantitative conversion; 79 % isolated yield) ^{1}H NMR ($(CD_3)_2CO$): 2.84 ppm (m, 4 H), 3.18 ppm (m, 4H), 4.28 ppm (d, 2H), 4.39 ppm (d, 2H), 4.92 ppm (m, 2H). ^{13}C NMR ($(CD_3)_2CO$): 66.90 ppm (t, $CF_2\underline{C}H_2O$). 71.52 ppm (s, $O\underline{C}H_2CH$), 113.30 ppm (m, CF_2CF_2O/ CF_2O), 115.76 ppm (s, $CH=\underline{C}H_2$), 131.83 ppm (s, $\underline{C}H=CH_2$).

PFPE-DAE (8 g, 5.1 mmol) and 2 mol eq. thioglycerol relative to the "ene" (2.2 g, 20.4 mmol) were dissolved in a minimal amount of trifluoroethanol (30 mL) along with 2,2-dimethoxy-2-phenylacetophenone photoinitiator (1 mol% relative to -ene). The thiol-ene click reaction was carried out in a round-bottom flask under rapid stirring while irradiating the solution with a 365 nm UV lamp (positioned above the flask) for 5 minutes. The product was then precipitated into rapidly stirring water using a blender to remove excess thioglycerol and trifluoroethanol solvent. A hydrogel formed upon precipitation. The hydrogel was dried under vacuum at 50°C overnight, resulting in a clear, colorless oil. The oil was dissolved in a minimal amount of acetone and precipitated a second time to remove residual thioglycerol. The hydrogel was dried under vacuum a second time, and the resulting oil was washed with dichloromethane to remove the photoinitiator. The product was isolated as a clear, colorless oil.

$PFPE_{D10H}$-Tetra-ol Intermediate (PFPE-Tetra-ol)

(Quantitative conversion; 68% isolated yield) ^{1}H NMR ($(CD_3)_2CO$): 1.87 ppm (p, 4 H), 2.57 ppm (dd, 2H), 2.65 ppm (t, 4H), 2.68 ppm (dd, 2H), 3.53 ppm (p, 2H), 3.58 ppm (p, 2H), 3.75 ppm (m, 8H), 3.90 (m, 2H), 4.01 (m, 4H). ^{13}C NMR ($(CD_3)_2CO$): 29.34 ppm (s, $SCH_2\underline{C}H_2CH_2$). 30.40 ppm (s, $S\underline{C}H_2CH_2CH_2$), 36.02 ppm (s, $S\underline{C}H_2CH(OH)CH_2$), 65.83 ppm (s,

$SCH_2CH(OH)\underline{C}H_2$), 69.90 ppm (t, $CF_2\underline{C}H_2O$), 71.77 ppm (s, $SCH_2\underline{C}H(OH)CH_2$), 72.50 ppm (s, $SCH_2CH_2\underline{C}H_2$), 115.04 (m, CF_2CF_2O/ CF_2O).

PFPE-Tetra-ol (5 g, 2.8 mmol) and 2 mol eq. TEA relative to the –OH groups (3.1 mL, 22.4 mmol) were dissolved in 1,1,1,3,3-pentafluorobutane (approximately 200 mL) at 0 °C with magnetic stirring under N_2. Methyl chloroformate (22.4 mmol) was then added dropwise over approximately one minute, after which the mixture was allowed to return to ambient temperature and stirred for 18 h. The resulting mixture was gravity filtered to remove TEA HCl salt, then the filtrate was washed with water three times and brine once in a separatory funnel. The bottom layer was isolated and the solvent was removed on a rotary evaporator under reduced pressure. The remaining liquid product was then filtered using a 0.45 μm syringe filter, giving the product as a pale yellow, transparent liquid.

$\underline{PFPE_{D10H}}$-Diethylene carbonate (PFPE-DEC)

(90% isolated yield, 85% desired product) ^{1}H NMR ($(CD_3)_2CO$): 1.90 ppm (p, 4 H), 2.72 ppm (t, 4H), 3.00 ppm (ddd, 4H), 3.75 ppm (m, 4H), 4.02 ppm (m, 4H), 4.31 ppm (t, 2H), 4.66 ppm (t, 2H), 5.03 (p, 2H). ^{13}C NMR ($(CD_3)_2CO$): 30.33 ppm (s, $S\underline{C}H_2CH_2CH_2$). 30.59 ppm (s, $SCH_2\underline{C}H_2CH_2$), 35.01 ppm (s, $S\underline{C}H_2CH(OH)CH_2$), 69.32 ppm (s, $SCH_2CH(OH)\underline{C}H_2$), 69.85 ppm (t, $CF_2\underline{C}H_2O$), 71.50 ppm (s, $SCH_2CH_2\underline{C}H_2$), 76.71 ppm (s, $SCH_2\underline{C}H(O)CH_2$), 115.04 (m, CF_2CF_2O/ CF_2O), 155.42 (s, C=O).

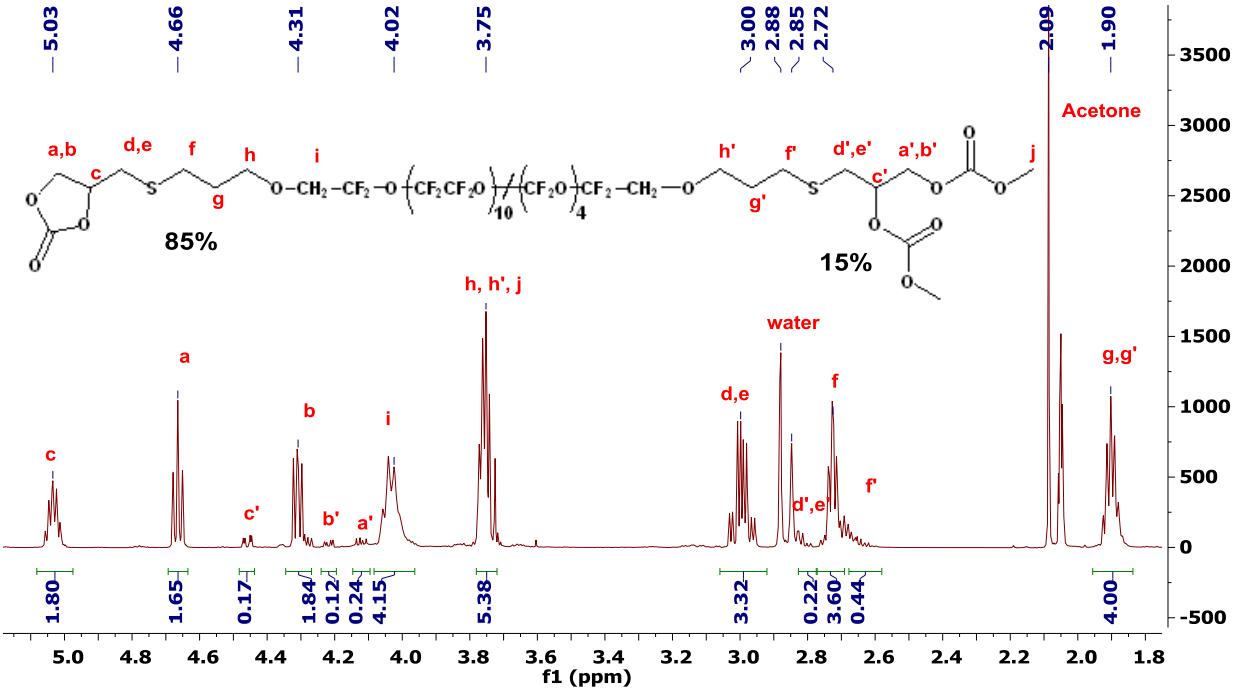

Figure 3.13 ^{1}H NMR spectrum of PFPE-DEC, showing 85% conversion to desired ethylene carbonate end groups (left) and 15% conversion to branched methyl carbonate groups (right).

3.4.1.5 Physical Characterization of PFPE Electrolytes

The chemical structures of the functionalized PFPE products were confirmed using ^{13}C and ^{1}H nuclear magnetic resonance spectroscopy (NMR). Size exclusion chromatography (SEC) was used to analyze the molecular weight distribution of the products. The methods for these experiments are described in the experimental portion of Section 3.3. Fourier transform infrared spectroscopy (FTIR) was performed using a Bruker ALPHA FTIR instrument under ambient conditions using an attenuated total reflectance (ATR) attachment (from 500 to 4000 cm^{-1} at 2 cm^{-1} resolution). Lithium salt solubility was determined after stirring LiTFSI salt with the materials for >48 hours. The solubility limit was determined as the salt concentration at which the solution became visibly cloudy, indicative of salt aggregation.

Differential scanning calorimetry (DSC) thermograms were recorded using a TA Instruments DSC Q200 on samples which were prepared in air over the temperature range

from -130 °C to 100 °C using a heat/cool/heat method at a heating and cooling rate of 10 °C and 5 °C/minute respectively. Glass transition temperatures (T_g's) were determined using the midpoint method on the second heating cycle thermogram.

3.4.2 Results and Discussion

$PFPE_{D10H}$-carbonates were synthesized using a reaction closely analogous to that shown in Scheme 3.2 in which the PFPE-Diol was mixed with chloroformate in the presence of triethylamine to form the carbonate end group. PFPE-TFME was synthesized using a similar strategy, replacing the chloroformate with trifluoroacetic anhydride to convert hydroxyl end groups to trifluoromethyl esters. All products were successfully synthesized at 100% conversion, as confirmed by FT-IR, ^{1}H NMR, and ^{13}C NMR.

A multi-step synthesis was necessary to achieve $PFPE_{D10H}$-diethylene carbonate (PFPE-DEC). Development of the synthetic route will be discussed in further detail in Chapter 4. In short, we targeted reactions with quantitative conversions and easily removable by-products because PFPEs with slightly different end groups are exceedingly difficult to separate by chromatographic methods. Scheme 3.4 shows the synthetic route to achieve PFPE-DEC. The final step of the reaction involves an intramolecular transesterification to form the cyclic carbonate, taking advantage of the same reaction that causes chain coupling in the $PFPE_{E10}$-carbonate systems. This reaction yielded 85% of the desired ethylene carbonate end groups and 15% of the branched methyl carbonate end groups from the simple substitution reaction. Theoretically, the reaction can be pushed to quantitative conversion to ethylene carbonate end groups by infinite dilution and very slow addition of methyl chloroformate, though these efforts are still in progress.

Scheme 3.4 Synthesis of PFPE-DEC from PFPE-Diol. The "PFPE" abbreviation refers to the $PFPE_{D10H}$ core, i.e. $–CH_2CF_2O(CF_2CF_2O)_9/(CF_2O)_4CF_2CH_2$-.

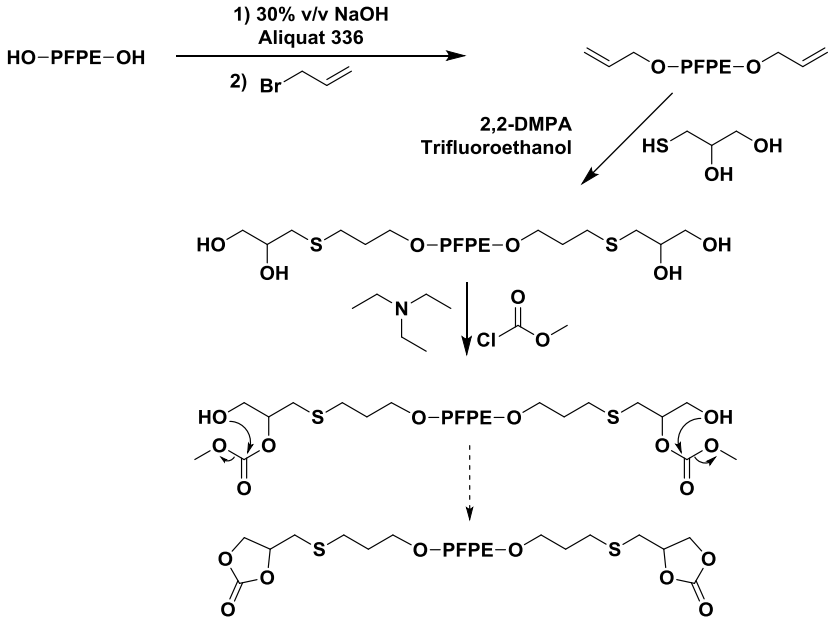

The LiTFSI solubility limit for each product was then determined for each PFPE electrolyte. We normalized the maximum salt solubility as a molar ratio of lithium ions to end groups in order to compare the solvating power of different end groups, expressed as R_{max} = $[Li^+]$/[end group] (Figure 3.14). In contrast to the $PFPE_{E10}$ system, increasing carbonate end group polarity in the $PFPE_{D10H}$ system led to increasing lithium salt solubility. Inductive electron effects change both the carbonate DN and the solvent ε, effectively tuning the Li^+-$PFPE_{D10H}$ interactions. PFPE-DEC is the only exception to the predicted trend: it dissolves approximately the same amount of lithium salt as PFPE-DMC. Although we achieved the closest possible analog to an ethylene carbonate end group, the linkage between PFPE and EC breaks the molecular symmetry, similar to propylene carbonate. The additional methyl group in propylene carbonate lowers the dielectric constant of the molecule (ε = 69 vs. ε = 90 for EC), making propylene carbonate a less

favorable solvent for lithium salts compared to EC.[1,45] We propose that a similar effect occurs in the "DEC"-terminated PFPE system.

PFPE-Trifluoromethyl Ester was unable to dissolve LiTFSI: the solution remained cloudy upon addition of <0.1wt.% lithium salt. A subsequent study on the analogous Fomblin® Z03 (4000 g/mol, -OCF_3 end groups) showed that the trifluoromethyl ether-terminated material was also unable to dissolve lithium salts. It seems that a minimum end group polarity is required for PFPE solvents to dissolve lithium salts. This requirement is met by hydrogenated (but not fluorinated) ether or carbonate end groups. Because of its inability to solvate lithium salts, further characterization of ion solvation and transport was not carried out on the TFME-terminated system.

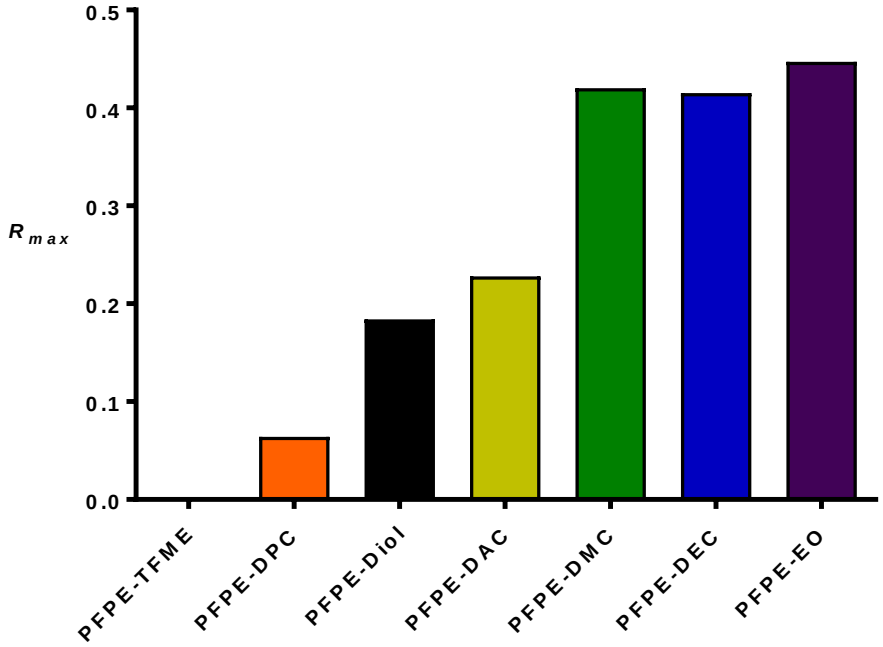

Figure 3.14 Maximum LiTFSI solubility in $PFPE_{D10H}$ materials compared to PFPE-EO ($PFPE_{E10}$-Diol).

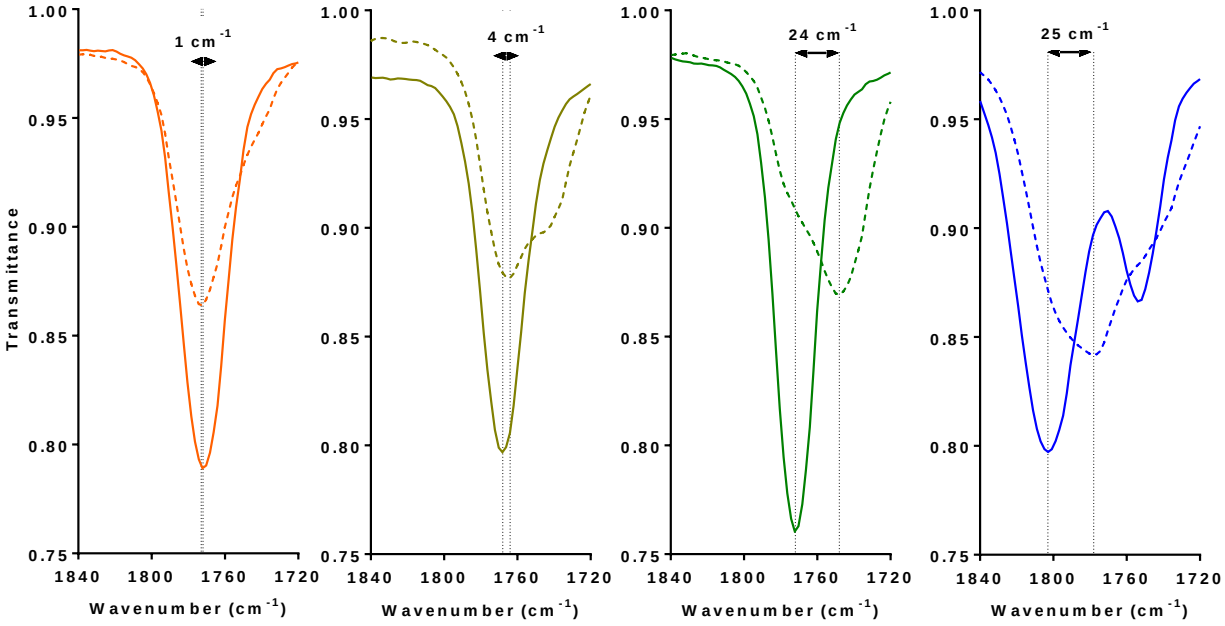

Figure 3.15 IR spectra of PFPE-carbonates in region of carbonyl stretch (orange: DPC, yellow: DAC, green: DMC, blue: DEC). Solid lines: neat PFPE materials; Dashed lines: LiTFSI-saturated PFPE materials.

IR spectroscopy was used to probe the interaction between Li^+ and carbonyl oxygen atoms as a function of carbonate end group polarity, as shown in Figure 3.15. In the $PFPE_{D10H}$ system, the extent of interaction between Li^+ and carbonate end groups followed the expected trend based on end group polarity (DPC < DAC < DMC ≈ DEC), as evidenced by the changing frequency of the strongest C=O transition upon addition of lithium salt. We were successful in changing the interaction between Li^+ and the polymer by systematically tuning the polarity of PFPE end groups.

Interestingly, the carbonyl oxygen atom of PFPE-DPC exhibited no significant interactions with Li^+ according to IR spectroscopy considering the 2 cm^{-1} resolution of the instrument. We propose that the strong electron-withdrawing character of the terminal alkyne reduces the chelating ability of the adjacent carbonate significantly. Salt dissolution is likely enabled in PFPE-DPC by the moderate solvent ε rather than strong Li^+-carbonate interactions. Also of interest are the peak shoulders evident in the saturated PFPE-DAC and PFPE-DMC samples, which we tentatively

attribute to the interaction of the carbonyl with aggregated ion pairs rather than dissociated ions.[33] This highlights the fact that inductive electron withdrawing effects changes both the solvent DN and ε, causing differences in ion pairing among PFPE solvents. Finally, the multiple peaks in the IR spectrum of PFPE-DEC agree with literature reports on overtones of the C=O stretching fundamental in ethylene carbonate's IR spectrum,[46] though it is also possible that the lower frequency peak corresponds to the 15 % methyl carbonate end groups.

The increase in T_g as a function of salt concentration also follows the expected dependence on end group polarity, as shown in Figure 3.16. The slope of the T_g vs. R curve, which provides insight into the strength of interaction between Li^+ and the polymer, is listed for each material in Table 3.2. The DPC-terminated material, which contains the strongest electron-withdrawing group, exhibits the smallest increase in T_g as a function of salt concentration. The DMC- and DEC-terminated materials, which contain electron-donating groups, exhibit the largest increase in T_g as a function of salt concentration.

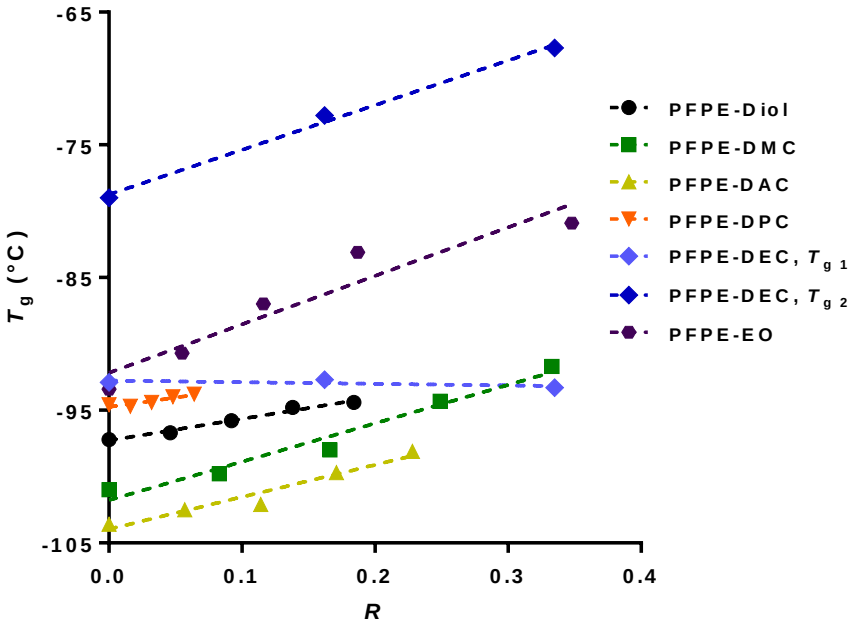

Figure 3.16 Dependence of glass transition temperature on LiTFSI salt content in $PFPE_{D10H}$ electrolytes. Dashed lines show linear fits of the data.

Table 3.2 Rate of increase in Tg as a function of salt concentration in $PFPE_{D10H}$ electrolytes.

PFPE End Group	Slope, T_g vs. R (°C)
DPC	14.4 ± 3.0
Diol	16.3 ± 1.3
DAC	24.2 ± 3.3
DMC	29.0 ± 3.2
DEC (1)	-1.2 ± 1.4
DEC (2)	33.7 ± 2.5
EO	36.5 ± 6.7

Interestingly, PFPE-DEC exhibits two distinct T_g's. A miscible copolymer exhibits a single T_g that is equal to the weighted average of the T_g's of the components according to the Fox equation:[47]

$$\frac{1}{T_g} = \frac{x_1}{T_{g\,1}} + \frac{x_2}{T_{g\,2}} \tag{3.3}$$

where T_g, $T_{g\,1}$, and $T_{g\,2}$ are the glass transition temperatures of the miscible system and each of the pure components, respectively, and X_1 and X_2 are the weight fractions of each respective component. Two distinct T_g's, on the other hand, are indicative of microphase separation in a copolymer system.

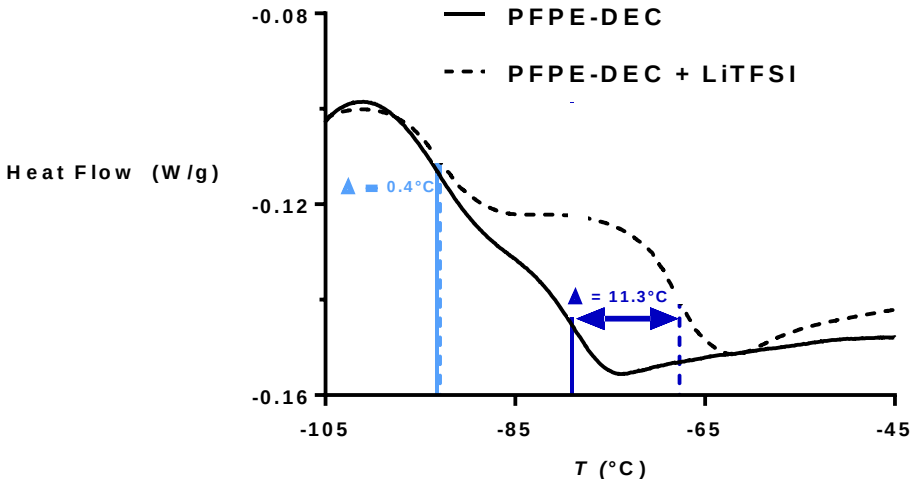

Figure 3.17 DSC thermograms of PFPE-DEC (solid: neat; dashed: + LiTFSI, R = 0.34). Dark blue lines mark the midpoint T_g of the DEC phase, and light blue lines mark the midpoint T_g of the PFPE phase.

The phase behavior of a copolymer is determined by three factors: the overall degree of polymerization *N*, the volume fractions, and the Flory-Huggins interaction parameter χ.[48,49] The first two factors affect the configurational and translational entropy, while χ is largely an enthalpic contribution. Considering the very short chain length of the DEC end groups attached to the PFPE backbone, the enthalpic interaction between PFPE and DEC must be highly disfavored (i.e. high χ values). PFPE-EO, which has only a single T_g by DSC, exhibits incipient microphase separation observable by wide-angle x-ray scattering (WAXS).[50] The χ parameter for the PFPE-EO system is high ($\approx$ 2.5), evidencing energetic repulsion between the PFPE and PEO segments. The Flory-Huggins interaction parameter χ may be even higher in the PFPE-DEC system considering the two distinct T_g's observable by DSC, although this remains to be confirmed by WAXS or small-angle x-ray scattering (SAXS). Addition of lithium salt may further enhance the immiscibility between PFPE and DEC end groups: several studies have reported changes in block copolymer morphology upon addition of lithium salt caused by strong repulsion between polystyrene and PEO-salt complexes, increasing the effective χ parameter of the block polymer.[51–54]

As seen in Figure 3.16 and Figure 3.17, $T_{g\,1}$, the T_g of the perfluoropolyether backbone, remains constant as lithium salt concentration increases. In contrast, $T_{g\,2}$, the T_g of the end group phase, increases significantly with increasing lithium salt concentration. We propose that lithium partitions itself into the highly polar DEC phase. The phase behavior of this system as a function of lithium salt concentration will be probed via WAXS measurements to evaluate this hypothesis. X-ray scattering measurements are also needed to confirm that the observed phenomenon is indeed microphase separation of thiother-DEC end groups from the PFPE backbone. We do not wish to remain bound to the theory that the terminal groups are sufficiently long to form domains with a distinct T_g observable by differential scanning calorimetry.

Finally, the ionic conductivity of the $PFPE_{D10H}$-DEC system was characterized at 9.1 wt.% LiTFSI using the method detailed in Chapter 4. At 30°C, the ionic conductivity of $PFPE_{D10H}$-DEC was determined to be $4x10^{-6}$ S cm^{-1}, approximately an order of magnitude higher than that of $PFPE_{D10H}$-Diol and equal to that of $PFPE_{D10H}$-DMC at the same salt concentration and temperature.[5] Apparently, increases in the charge carrier concentration due to the high polarity of the DEC end groups offsets the high T_g of the salt-loaded electrolyte. Attempts were also made to measure the transference number of the electrolyte using the potentiostatic polarization method, but the current was too low at the low polarization potentials for accurate measurements. The cell geometry is currently being optimized for accurate t^+ measurements. Conductivity and t^+ measurements on the remainder of the $PFPE_{D10H}$-carbonate materials are also underway.

3.4.3 Conclusions

Clearly, end groups play an important role in solvating lithium salts in PFPE solvents. The interaction between Li^+ and end groups can be systematically tuned using electron inductive effects to alter the solvent DN and dielectric constant. This interaction ranges from PFPEs with perfluorinated end groups, which are unable to dissolve lithium salts, to PFPEs with propargyl end groups, which experience negligible Li^+-carbonate interactions but still dissolve lithium salts due to the moderate solvent polarity, to ether end groups, which dissolve and coordinate strongly to lithium salts.

Unfortunately, the above results indicate that there is a fundamental trade-off between charge carrier concentration and mobility. PFPEs with more polar carbonate end groups dissolve a higher concentration of lithium salts, providing a higher concentration of charge carriers in solution. Yet those same PFPEs experience the highest increases in T_g as lithium salt concentration increases. Because lithium ion mobility is closely coupled to the local segmental mobility of

polymer electrolytes,[14] increases in T_g correspond to lower Li^+ mobility. It is possible that the increase in the number of charge carriers more than offsets the reduction in ion mobility, affording higher ionic conductivity in PFPE solvents that contain highly polar end groups. Even in this case, there remains an apparent trade-off between ionic conductivity and t^+ in PFPE electrolytes. Figure 3.18 summarizes the effects of end group polarity on σ and t^+ schematically.

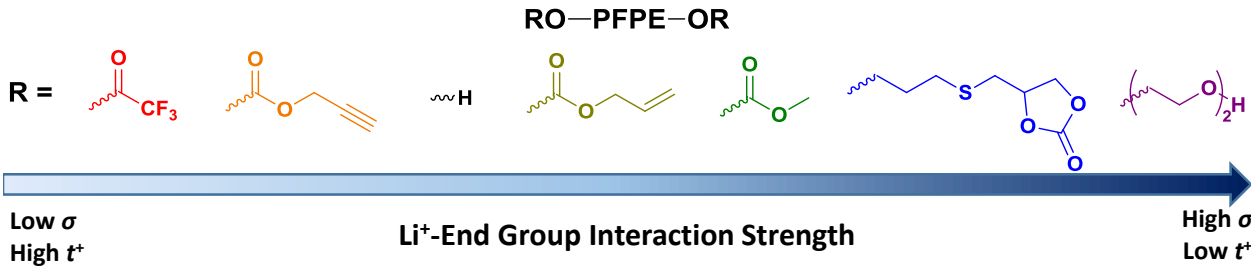

Figure 3.18 Schematic representation of conductivity-transference number trade-off as a function of PFPE end group polarity.

Thankfully, this is far from the end of the story. The strength of end group-Li^+ interactions, while fundamentally important to PFPE electrolyte properties, represent only one tunable parameter. Chapter 4 will discuss how PFPE electrolyte properties are affected by end group concentration and polymer molecular weight. Rather than increasing the *strength* of polymer-ion interactions, which yields higher salt solubility at the cost of lower ion mobility, we aimed to increase the *number* of polymer-ion interactions by changing the concentration of end groups. This provides a potential route to increase salt dissociation without hindering ion mobility, circumventing the apparent conductivity-transference number trade-off in PFPE electrolytes. The importance of the perfluoropolyether backbone in ion solvation will also be highlighted, which will lead into the importance of tuning the perfluoroether-anion interaction in the recommendations for future work in Chapter 5.

REFERENCES

(1) Xu, K. Electrolytes and Interphases in Li-Ion Batteries and Beyond. *Chem. Rev.* **2014**, *114* (23), 11503–11618.

(2) Kim, C. S.; Oh, S. M. Importance of Donor Number in Determining Solvating Ability of Polymers and Transport Properties in Gel-Type Polymer Electrolytes. *Electrochim. Acta* **2000**, *45* (13), 2101–2109.

(3) Jensen, W. B. The Lewis Acid-Base Definitions: A Status Report. *Chem. Rev.* **1978**, *78* (1), 1–22.

(4) Xu, K.; von Cresce, A.; Lee, U.; Ogumi, Z.; Ogumi, Z.; Carter, W. C.; Chiang, Y.-M.; Ogumi, Z.; Ceder, G. Li^+-Solvation/desolvation Dictates Interphasial Processes on Graphitic Anode in Li Ion Cells. *J. Mater. Res.* **2012**, *27* (18), 2327–2341.

(5) Wong, D. H. C.; Thelen, J. L.; Fu, Y.; Devaux, D.; Pandya, A. a; Battaglia, V. S.; Balsara, N. P.; DeSimone, J. M. Nonflammable Perfluoropolyether-Based Electrolytes for Lithium Batteries. *Proc. Natl. Acad. Sci. U. S. A.* **2014**, *111* (9), 3327–3331.

(6) Olson, K. R.; Wong, D. H. C.; Chintapalli, M.; Timachova, K.; Janusziewicz, R.; Daniel, W. F. M.; Mecham, S.; Sheiko, S.; Balsara, N. P.; DeSimone, J. M. Liquid Perfluoropolyether Electrolytes with Enhanced Ionic Conductivity for Lithium Battery Applications. *Polymer (Guildf).* **2016**, *100*, 126–133.

(7) Aihara, Y.; Sugimoto, K.; Price, W. S.; Hayamizu, K. Ionic Conduction and Self-Diffusion near Infinitesimal Concentration in Lithium Salt-Organic Solvent Electrolytes. *J. Chem. Phys.* **2000**, *113*, 1981.

(8) Timachova, K.; Chintapalli, M.; Olson, K. R.; Mecham, S. J.; DeSimone, J. M.; Balsara, N. P. Mechanism of Ion Transport in Perfluoropolyether Electrolytes with a Lithium Salt. *Soft Matter* **2017**, *13*, 5389-5396.

(9) Videa, M.; Xu, W.; Geil, B.; Marzke, R.; Angell, C. A. High Li^+ Self-Diffusivity and Transport Number in Novel Electrolyte Solutions. *J. Electrochem. Soc.* **2001**, *148* (12), A1352.

(10) Gouverneur, M.; Kopp, J.; van Wüllen, L.; Schönhoff, M.; Dvinskikh, S. V.; Kato, T.; Furo, I. Direct Determination of Ionic Transference Numbers in Ionic Liquids by Electrophoretic NMR. *Phys. Chem. Chem. Phys.* **2015**, *17* (45), 30680–30686.

(11) Berhaut, C. L.; Porion, P.; Timperman, L.; Schmidt, G.; Lemordant, D.; Anouti, M. LiTDI as Electrolyte Salt for Li-Ion Batteries: Transport Properties in EC/DMC. *Electrochim. Acta* **2015**, *180*, 778–787.

(12) Timachova, K.; Watanabe, H.; Balsara, N. P. Effect of Molecular Weight and Salt Concentration on Ion Transport and the Transference Number in Polymer Electrolytes. *Macromolecules* **2015**, *48* (21), 7882–7888.

(13) Lascaud, S.; Perrier, M.; Vallee, A.; Besner, S.; Prud'homme, J.; Armand, M. Phase Diagrams and Conductivity Behavior of Poly(ethylene Oxide)-Molten Salt Rubbery Electrolytes. *Macromolecules* **1994**, *27* (25), 7469–7477.

(14) Hallinan Jr., D. T.; Balsara, N. P. Polymer Electrolytes. *Annu. Rev. Mater. Res.* **2013**, *43*, 503–525.

(15) Chintapalli, M.; Timachova, K.; Olson, K. R.; Mecham, S. J.; Devaux, D.; DeSimone, J. M.; Balsara, N. P. Relationship between Conductivity, Ion Diffusion, and Transference Number in Perfluoropolyether Electrolytes. *Macromolecules* **2016**, *49* (9), 3508–3515.

(16) Zugmann, S.; Gores, H. J. Transference Numbers of Ions in Electrolytes. In *Encyclopedia of Applied Electrochemistry*; Springer New York: New York, NY, 2014; pp 2086–2091.

(17) Zugmann, S.; Fleischmann, M.; Amereller, M.; Gschwind, R. M.; Wiemhöfer, H. D.; Gores, H. J. Measurement of Transference Numbers for Lithium Ion Electrolytes via Four Different Methods, a Comparative Study. *Electrochim. Acta* **2011**, *56* (11), 3926–3933.

(18) Bogle, X.; Vazquez, R.; Greenbaum, S.; Cresce, A. von W.; Xu, K. Understanding Li^+ – Solvent Interaction in Nonaqueous Carbonate Electrolytes with ^{17}O NMR. *J. Phys. Chem. Lett.* **2013**, *4* (10), 1664–1668.

(19) Gray, F. M.; Royal Society of Chemistry (Great Britain). *Polymer Electrolytes*; Royal Society of Chemistry, 1997.

(20) Nakajima, T.; Groult, H. *Fluorinated Materials for Energy Conversion*; Elsevier, 2005.

(21) Marchionni, G.; Ajroldi, G.; Pezzin, G. Structure–Property Relationships in Perfluoropolyethers: A Family of Polymeric Oils. In *Comprehensive Polymer Science and Supplements*; 1989; pp 347–388.

(22) Fulfer, K. D.; Kuroda, D. G. Solvation Structure and Dynamics of the Lithium Ion in Organic Carbonate-Based Electrolytes: A Time-Dependent Infrared Spectroscopy Study. *J. Phys. Chem. C* **2016**, *120* (42), 24011–24022.

(23) Deepa, M.; Agnihotry, S. .; Gupta, D.; Chandra, R. Ion-Pairing Effects and Ion–solvent–polymer Interactions in $LiN(CF_3SO_2)_2$–PC–PMMA Electrolytes: A FTIR Study. *Electrochim. Acta* **2004**, *49* (3), 373–383.

(24) Matsubara, K.; Kaneuchi, R.; Maekita, N. 13C NMR Estimation of Preferential Solvation of Lithium Ions in Non-Aqueous Mixed Solvents. *J. Chem. Soc. Faraday Trans.* **1998**, *94* (24), 3601–3605.

(25) Qiao, H.; Fang, X.; Luan, H.; Zhou, Z.; Wu, Y.; Yao, W.; Wang, X.; Li, J.; Chen, C. Vibrational Spectroscopic and Density Functional Studies on Ion Solvation and Ion Association of Lithium Tetrafluoroborate in 4-Methoxymethyl-Ethylene Carbonate. *J. Mol. Liq.* **2008**, *138* (1–3), 69–75.

(26) Tsunekawa, H.; Narumi, A.; Sano, M.; Hiwara, A.; Fujita, M.; Yokoyama, H. Solvation and Ion Association Studies of LiBF4−Propylenecarbonate and LiBF4−Propylenecarbonate−Trimethyl Phosphate Solutions. *J. Phys. Chem. B* **2003**, *107* (39), 10962–10966.

(27) Giorgini, M. G.; Futamatagawa, K.; Torii, H.; Musso, M.; Cerini, S. Solvation Structure around the Li + Ion in Mixed Cyclic/Linear Carbonate Solutions Unveiled by the Raman Noncoincidence Effect. *J. Phys. Chem. Lett.* **2015**, *6* (16), 3296–3302.

(28) Kameda, Y.; Umebayashi, Y.; Takeuchi, M.; Wahab, M. A.; Fukuda, S.; Ishiguro, S.; Sasaki, M.; Amo, Y.; Usuki, T. Solvation Structure of Li^+ in Concentrated LiPF6−Propylene Carbonate Solutions. *J. Phys. Chem. B* **2007**, *111* (22), 6104–6109.

(29) Cazzanelli, E.; Croce, F.; Appetecchi, G. B.; Benevelli, F.; Mustarelli, P. Li^+ Solvation in Ethylene Carbonate–propylene Carbonate Concentrated Solutions: A Comprehensive Model. *J. Chem. Phys.* **1997**, *107*, 5740.

(30) Skarmoutsos, I.; Ponnuchamy, V.; Vetere, V.; Mossa, S. Li + Solvation in Pure, Binary, and Ternary Mixtures of Organic Carbonate Electrolytes. *J. Phys. Chem. C* **2015**, *119* (9), 4502–4515.

(31) Seo, D. M.; Boyle, P. D.; Sommer, R. D.; Daubert, J. S.; Borodin, O.; Henderson, W. A. Solvate Structures and Spectroscopic Characterization of LiTFSI Electrolytes. *J. Phys. Chem. B* **2014**, *118* (47), 13601–13608.

(32) Brouillette, D.; Irish, D. E.; Taylor, N. J.; Perron, G.; Odziemkowski, M.; Desnoyers, J. E. Stable Solvates in Solution of Lithium Bis(trifluoromethylsulfone)imide in Glymes and Other Aprotic Solvents: Phase Diagrams, Crystallography and Raman Spectroscopy. *Phys. Chem. Chem. Phys.* **2002**, *4* (24), 6063–6071.

(33) Wang, Z.; Gao, W.; Huang, X.; Mo, Y.; Chen, L. Spectroscopic Studies on Interactions and Microstructures in Propylene Carbonate-LiTFSI Electrolytes. *J. Raman Spectrosc.* **2001**, *32* (11), 900–905.

(34) Reya, I.; Lassègues, J. C.; Grondin, J.; Servant, L. Infrared and Raman Study of the PEO-LiTFSI Polymer Electrolyte. *Electrochim. Acta* **1998**, *43* (10–11), 1505–1510.

(35) Ferry, A. Ionic Interactions and Transport Properties in Methyl Terminated Poly(propylene glycol)(4000) Complexed with $LiCF_3SO_3$. *J. Phys. Chem. B* **1997**, *101* (2), 150–157.

(36) Huang, W.; Wheeler, R. A.; Frech, R. Vibrational Spectroscopic and Ab Initio Molecular Orbital Studies of the Normal and 13C-Labelled Trifluoromethanesulfonate Anion. *Spectrochim. Acta Part A Mol. Spectrosc.* **1994**, *50* (5), 985–996.

(37) Huang, W.; Frech, R.; Wheeler ', R. A. Molecular Structures and Normal Vibrations of CF3S03-and Its Lithium Ion Pairs and Aggregates. *J. Phys. Chem* **1994**, *98*, 100–101.

(38) Frech, R.; Chintapalli, S.; Bruce, P. G.; Vincent, C. A. Structure of an Amorphous Polymer Electrolyte, Poly(ethylene Oxide) 3 : LiCF 3 SO 3. *Chem. Commun.* **1997**, *0*, 157–158.

(39) Chen, H.-W.; Chang, F.-C. Interaction Mechanism of a Novel Polymer Electrolyte Composed of Poly(acrylonitrile), Lithium Triflate, and Mineral Clay. *J. Polym. Sci. Part B Polym. Phys.* **2001**, *39* (20), 2407–2419.

(40) Burba, C. M.; Frech, R. Spectroscopic Measurements of Ionic Association in Solutions of LiPF6. *J. Phys. Chem. Bournal Phys. Chem.* **2005**, *109* (31), 15161–15164.

(41) Fish, D.; Smid, J. Solvation of Lithium Ions in Mixtures of Tetraethylene Glycol Dimethyl Ether and Propylene Carbonate. *Electrochim. Acta* **1992**, *37* (11), 2043–2049.

(42) von Cresce, A.; Xu, K. Preferential Solvation of Li^+ Directs Formation of Interphase on Graphitic Anode. *Electrochem. Solid-State Lett.* **2011**, *14* (10), A154.

(43) Sun, J.; Stone, G. M.; Balsara, N. P.; Zuckermann, R. N. Structure–Conductivity Relationship for Peptoid-Based PEO–Mimetic Polymer Electrolytes. *Macromolecules* **2012**, *45* (12), 5151–5156.

(44) Radice, S.; Canil, G.; Toniolo, P.; Guarda, P. A.; Petricci, S.; Milani, A.; Tommasini, M.; Castiglioni, C.; Zerbi, G. Infrared Intensity Studies in Fluorinated Macromolecules. *Macromol. Symp.* **2008**, *265* (1), 218–224.

(45) Chen, H. P.; Fergus, J. W.; Jang, B. Z. The Effect of Ethylene Carbonate and Salt Concentration on the Conductivity of Propylene Carbonate Lithium Perchlorate Electrolytes. *J. Electrochem. Soc.* **2000**, *147* (2), 399.

(46) Fortunato, B.; Mirone, P.; Fini, G. Infrared and Raman Spectra and Vibrational Assignment of Ethylene Carbonate. *Spectrochim. Acta Part A Mol. Spectrosc.* **1971**, *27* (9), 1917–1927.

(47) Brostow, W.; Chiu, R.; Kalogeras, I. M.; Vassilikou-Dova, A. Prediction of Glass Transition Temperatures: Binary Blends and Copolymers. *Mater. Lett.* **2008**, *62* (17–18), 3152–3155.

(48) Bates, F. S.; Fredrickson, G. H. Block Copolymer Thermodynamics: Theory and Experiment. *Annu. Rev. Phys. Chern* **1990**, *41*, 525–557.

(49) Rubinstein, M.; Colby, R. H. *Polymer Physics*; Oxford University Press, 2003.

(50) Chintapalli, M.; Timachova, K.; Olson, K. R.; Banaszak, M.; Thelen, J. L.; Mecham, S. J.; DeSimone, J. M.; Balsara, N. P. Incipient Microphase Separation in Short Chain Perfluoropolyether-Block-Poly(ethylene Oxide) Copolymers. *Soft Matter* **2017**, *13* (22), 4047–4056.

(51) Young, W.-S.; Kuan, W.-F.; Epps, T. H. Block Copolymer Electrolytes for Rechargeable Lithium Batteries. *J. Polym. Sci. Part B Polym. Phys.* **2014**, *52* (1), 1–16.

(52) Gomez, E. D.; Panday, A.; Feng, E. H.; Chen, V.; Stone, G. M.; Minor, A. M.; Kisielowski, C.; Downing, K. H.; Borodin, O.; Smith, G. D.; et al. Effect of Ion Distribution on Conductivity of Block Copolymer Electrolytes. *Nano Lett.* **2009**, *9* (3), 1212–1216.

(53) Young, W.-S.; Epps, T. H. Salt Doping in PEO-Containing Block Copolymers: Counterion and Concentration Effects. *Macromolecules* **2009**, *42* (7), 2672–2678.

(54) Gunkel, I.; Thurn-Albrecht, T. Thermodynamic and Structural Changes in Ion-Containing Symmetric Diblock Copolymers: A Small-Angle X-Ray Scattering Study. *Macromolecules* **2012**, *45* (1), 283–291.

Chapter 4: Effects of End Group Concentration and Molecular Weight on PFPE Electrolyte Performance

4.1 Introduction

The effects of molecular weight and end groups on polymer electrolyte performance are rarely discussed in the literature. The reason for this is two-fold: i) the vast majority of solid polymer electrolytes in the literature have degree of polymerization $N >> 20$, and therefore end group contributions are insignificant and ii) typically, end groups are close analogs of the polymer repeat unit itself (e.g. hydroxyl or methoxy end groups in PEO-based electrolytes).[1] The studies that have explored ion diffusivities as a function of N in polymer electrolytes justifiably neglect the effects of N on ion solvation.[2–5]

A few exceptions do exist. Devaux *et al.* studied ion transport in PEO oligomers as a function of both N and end group.[6] Differences in ionic conductivity between hydroxyl- and methoxy-terminated PEO was attributed to changes in the free volume of the electrolyte rather than differences in charge carrier concentrations caused by the changing solvating ability of the polymer end groups. Furthermore, Wong *et al.* studied the solubility of LiTFSI salt as well as ionic conductivity of some commercially available PFPEs of varying molecular weight with hydroxyl and carbonate end groups.[7] We aim to build on this study by evaluating a broad range of molecular weights, along with isolating the effects of end group concentration from molecular weight.

The PFPE electrolytes studied in this work are distinguished from the majority of polymer electrolytes in the literature by a few key factors. First, the PFPEs' degree of polymerization N is ≈ 15, making the concentration of end groups much higher than typical polymer electrolytes with

N >> 20. Furthermore, in contrast to the homogeneity of hydroxyl- or methyl ether-terminated poly(ethylene oxide), PFPE's polar hydrogenated end groups differ significantly from that of the perfluoroether backbone. In perfluoro polymers, hydrogen-containing end groups influence thermal stability, fluidity, electrical conductivity, and crystallization kinetics, to name a few.[1] In PFPE electrolytes, evidence suggests there is a persistent interaction between the perfluorinated backbone and the fluorinated anion of lithium salts. But as discussed in Chapters 2 and 3, the complimentary interaction between hydrogenated end groups and Li^+ is equally important to consider. In short, end group contributions are more significant in PFPE electrolytes than in previously studied polymer electrolytes.

In Chapter 3, we demonstrated that the interaction of end groups with Li^+ can be systematically tuned by electron inductive effects. However, this approach seemed to create an inherent trade-off between the concentration of free ions in solution and the mobility of those ions. End groups with higher electron density coordinate more strongly to Li^+, affording higher lithium salt solubility but hindering the mobility of Li^+. The result is a trade-off between ionic conductivity σ and transference number t^+.

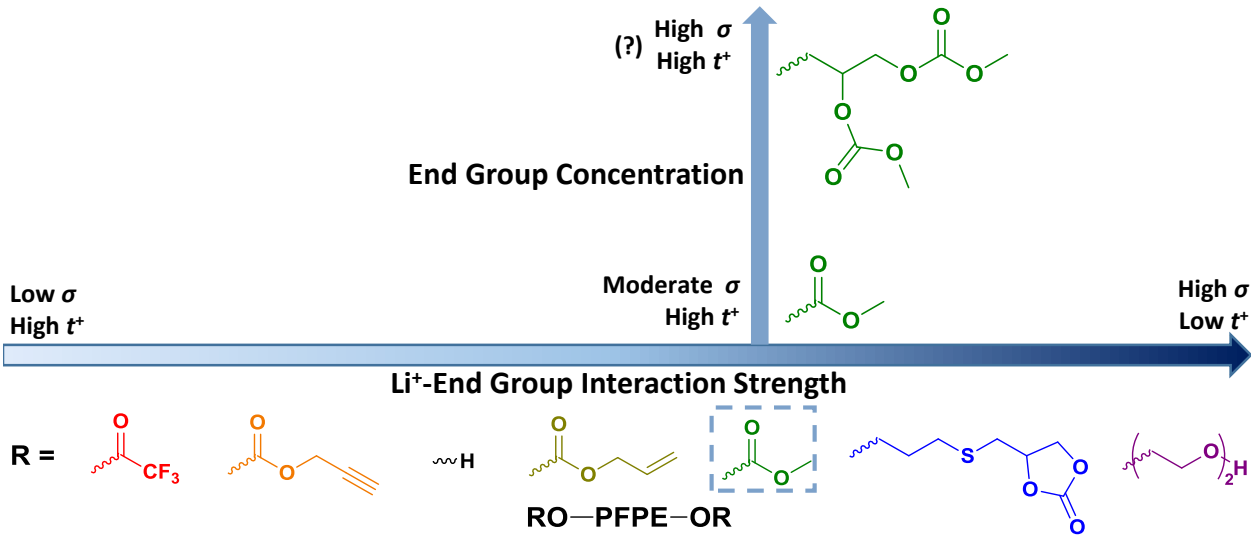

Figure 4.1 Exploration of the effect of end group concentration on ion solvation and transport.

Fortunately, numerous structural parameters can be manipulated to achieve desired polymer properties. Figure 4.1 shows the basic approach that will be discussed in this chapter. We began by selecting a particular end group that was known to enable moderate ionic conductivities and high Li^+ mobility ($t^+ > 0.9$) in PFPE electrolytes: methyl carbonate and hydroxyl end groups meet these criteria.[7] Rather than moving farther down the continuum of end group polarity in an attempt to dissolve more lithium salt and achieve higher conductivity, we elected to increase the concentration of the selected end group. We aimed to increase the *number* of end group-Li^+ interactions for higher conductivity rather than the *strength* of those interactions, which typically results in lower t^+.

A facile route to achieving higher end group concentrations is to simply reduce the molecular weight of a polymer. Thus, Section 4.2 will focus on the electrolyte performance of perfluorinated glycols with degree of polymerization N = 3-4. Although this provided a useful first study on how end group concentration affects PFPE electrolyte performance (and ultimately afforded electrolytes with very promising performance), molecular weight affects other polymer properties such as viscosity and T_g.[8] Therefore, Section 4.4 will discuss our work to isolate the effects of end group concentration on ion transport from those of molecular weight. We achieved this by studying a PFPE material with branched hydroxyl end groups, which has double the end group concentration at a given molecular weight. Finally, Section 4.5 will briefly discuss our attempts to isolate the effects of molecular weight on electrolyte performance. To this end, we synthesized PFPE-polycarbonates in order to increase the PFPE molecular weight while maintaining the same concentration of polar carbonate groups in the electrolyte.

4.2 Experimental

4.2.1 Materials

Perfluorinated triethylene glycol (tradename "C6GDIOL", herein $PFEG_3Diol$), perfluorinated triethylene glycol monomethyl ether (tradename"C7GOL", herein $mPFEG_3Ol$), and perfluorinated tetraethylene glycol (tradename "C8GDIOL", herein $PFEG_4Diol$) were purchased from Exfluor Research Corporation and used as received. Lithium bis(trifluoromethane) sulfonamide (LiTFSI), triethylamine (TEA, 99%), allyl bromide (99%), sodium hydroxide, thioglycerol (97%), 2,2-dimethoxyacetophenone (2,2-DMPA; 99%), ethylene bis(chloroformate) (98%), and methyl chloroformate (99%) were purchased from Sigma Aldrich. LITFSI was dried at 120° under dynamic vacuum for 48 hours and stored in a desiccator prior to use. 1,1,1,3,3-pentafluorobutane was purchased from MicroCare Corporation and dried over molecular sieves prior to use. Fluorolink D10H (Hydroxyl-terminated PFPE, 1480 g/mol, "PFPE-Diol") was purchased from Solvay Solexis and used as received. Trifluoroethanol (98%) was purchased from Oakwood Chemical and used as received. 3-mercapto-1-propanol (97%) was purchased from Acros Organics and used as received.

4.2.2 General Synthesis of Perfluorinated Glycols with Methyl Carbonate End Groups

0.10 mol of commercially available perfluorinated glycol (0.20 mol -OH end groups) and three molar equivalents triethylamine (84 mL, 0.60 mol) were dissolved in 400 mL of 1,1,1,3,3-pentafluorobutane in a 1 L 3-neck round-bottom flask. The solution was cooled to 0°C under nitrogen atmosphere. Methyl chloroformate (46 mL, 0.60 mol) was added dropwise over the course of two hours with rapid stirring, resulting in significant gas evolution and formation of the white triethylamine hydrochloride precipitate. The reaction was stirred overnight under nitrogen atmosphere, and reaction completion was confirmed by FTIR.

The TEA HCl salt was removed by gravity filtration, yielding a pale-yellow solution. The salt was washed 3x with 50 mL 1,1,1,3,3-pentafluorobutane while stirring with a metal spatula to remove residual product. The combined pentafluorobutane solution was then washed 3x with 500 mL water and 1x with 500 mL brine in a separatory funnel. The solution was stirred with activated carbon to remove coloration and dried with magnesium sulfate. After filtering the solids, pentafluorobutane was removed under reduced pressure, yielding a clear, faintly yellow oil. The product was dried under vacuum at 50°C for 2 days.

Perfluorinated Triethylene Glycol-Dimethyl Carbonate ($PFEG_3DMC$)

(Quantitative Conversion; 82% Isolated Yield). ^1H NMR (600 MHz, $(CD_3)_2CO$, ppm) δ = 3.84 (s, 6 H), 4.74 (t, 4 H); ^{13}C NMR (600 MHz, $(CD_3)_2CO$, ppm) δ = 56.15 (s), 65.27 (t) 115.30 (tt), 122.50 (t), 155.39 (s). FTIR (neat): 2967 cm^{-1} (wk, C-H), 1764 cm^{-1} (str, C=O), 1172 cm^{-1} (C-H), 1109 cm^{-1} (C-O).

Perfluorinated Tetraethylene Glycol-Dimethyl Carbonate ($PFEG_4DMC$)

(Quantitative Conversion; 84% Isolated Yield). ^1H NMR (600 MHz, $(CD_3)_2CO$, ppm) δ = 3.84 (s, 6 H), 4.77 (t, 4 H); ^{13}C NMR (600 MHz, $(CD_3)_2CO$, ppm) δ = 56.16 (s), 65.20 (t) 115.54 (m), 122.65 (t), 155.42 (s). FTIR (neat): 2965 cm^{-1} (wk, C-H), 1766 cm^{-1} (str, C=O), 1177 cm^{-1} (C-H), 1107 cm^{-1} (C-O).

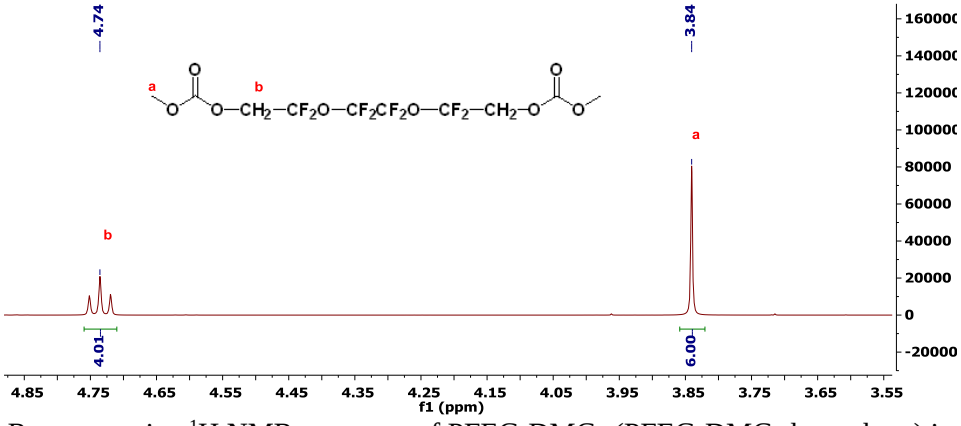

Figure 4.2 Representative ^1H NMR spectrum of $PFEG_{\#}DMCs$ ($PFEG_3DMC$ shown here) in $(CD_3)_2CO$.

4.2.3 Synthesis of $PFPE_{D10H}$-Diallyl Ether Intermediate (PFPE-DAE)

Fluorolink D10H (10 g, 6.6 mmol) was transferred to a 2-neck round-bottom flask equipped with a mechanical stirrer. Aqueous sodium hydroxide solution (70 mL of 6.88 M solution) was added along with two drops of phase transfer catalyst Aliquot 336. The immiscible mixture was heated to 40°C and reacted for two hours under rapid stirring. Allyl bromide (24 mL, 138 mmol) was added, and the reaction was carried out at 40°C for an additional 6 hours. 1,1,1,3,3-pentafluorobutane was used to extract the product (4x, 50 mL solvent each). The extracted product was then washed 5x with 50 mL of deionized water to remove excess allyl bromide and residual sodium hydroxide. The solvent was evaporated, and the product was dried under vacuum at 30°C for 24 hours to obtain the $PFPE_{D10H}$-Diallyl Ether (PFPE-DAE) product as a clear, colorless liquid. (Quantitative Conversion; 79% Isolated Yield). ^{1}H NMR ($(CD_3)_2CO$): 2.84 ppm (m, 4 H), 3.18 ppm (m, 4H), 4.28 ppm (d, 2H), 4.39 ppm (d, 2H), 4.92 ppm (m, 2H). ^{13}C NMR ($(CD_3)_2CO$): 66.90 ppm (t, $CF_2\underline{C}H_2O$). 71.52 ppm (s, $O\underline{C}H_2CH$), 113.30 ppm (m, CF_2CF_2O/ CF_2O), 115.76 ppm (s, $CH=\underline{C}H_2$), 131.83 ppm (s, $\underline{C}H=CH_2$).

4.2.4 Synthesis of Tetra-hydroxy terminated $PFPE_{D10H}$ (PFPE-Tetra-ol)

PFPE-DAE (8 g, 5.1 mmol) and 2 mol eq. thioglycerol relative to the "ene" (2.2 g, 20.4 mmol) were dissolved in a minimal amount of trifluoroethanol (30 mL) along with 2,2-dimethoxy-2-phenylacetophenone photoinitiator (1 mol% relative to -ene). The thiol-ene click reaction was carried out in a UV chamber containing a 365 nm lamp for 5 minutes. The product was then "precipitated" into rapidly stirring water using a blender to remove excess thioglycerol and trifluoroethanol solvent. A hydrogel formed upon precipitation. The hydrogel was dried under vacuum at 50°C overnight, resulting in a clear, colorless oil. The oil was dissolved in a minimal amount of acetone and precipitated a second time to remove residual thioglycerol. The hydrogel

was dried under vacuum a second time, and the resulting oil was washed with dichloromethane to remove the photoinitiator. The product was isolated as a clear, colorless oil.

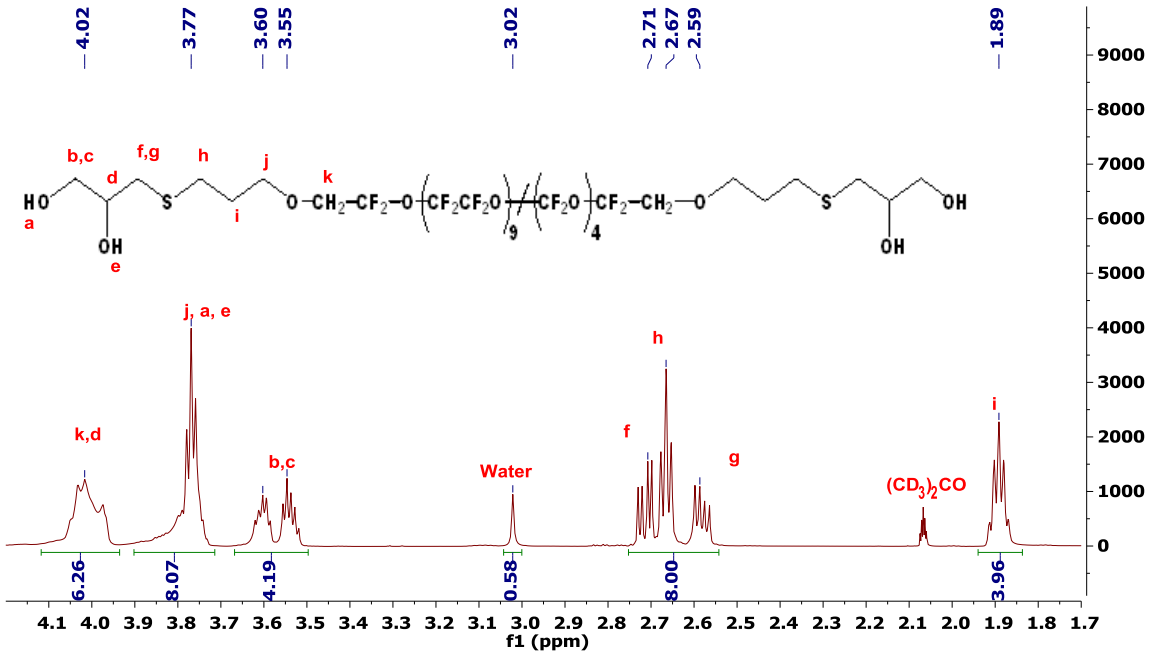

Figure 4.3 ^{1}H NMR spectrum of PFPE-Tetra-ol product in $(CD_3)_2CO$.

(Quantitative Conversion; 68% Isolated Yield). ^{1}H NMR ($(CD_3)_2CO$): 1.87 ppm (p, 4 H), 2.57 ppm (dd, 2H), 2.65 ppm (t, 4H), 2.68 ppm (dd, 2H), 3.53 ppm (p, 2H), 3.58 ppm (p, 2H), 3.75 ppm (m, 8H), 3.90 (m, 2H), 4.01 (m, 4H). ^{13}C NMR ($(CD_3)_2CO$): 29.34 ppm (s, $SCH_2\underline{C}H_2CH_2$). 30.40 ppm (s, $S\underline{C}H_2CH_2CH_2$), 36.02 ppm (s, $S\underline{C}H_2CH(OH)CH_2$), 65.83 ppm (s, $SCH_2CH(OH)\underline{C}H_2$), 69.90 ppm (t, $CF_2\underline{C}H_2O$), 71.77 ppm (s, $SCH_2\underline{C}H(OH)CH_2$), 72.50 ppm (s, $SCH_2CH_2\underline{C}H_2$), 115.04 (m, CF_2CF_2O/ CF_2O).

4.2.5 Synthesis of $PFPE_{D10H}$-Thioether-Diol (PFPE-TE-Diol)

PFPE-DAE (8 g, 5.1 mmol) and 2 mol eq. 3-mercapto-1-propanol relative to the “ene” (1.9 g, 20.4 mmol) were dissolved in a minimal amount of trifluoroethanol (30 mL) along with 2,2-dimethoxy-2-phenylacetophenone photoinitiator (1 mol% relative to -ene). The thiol-ene click reaction was carried out in a UV chamber containing a 365 nm lamp for 5 minutes.

Trifluoroethanol was evaporated under reduced pressure, and the product was dissolved in 1,1,1,3,3-pentafluorobutane. The product was washed several times with water to remove residual trifluoroethanol and 3-mercapto-1-propanol. The product was isolated as a clear, colorless oil.

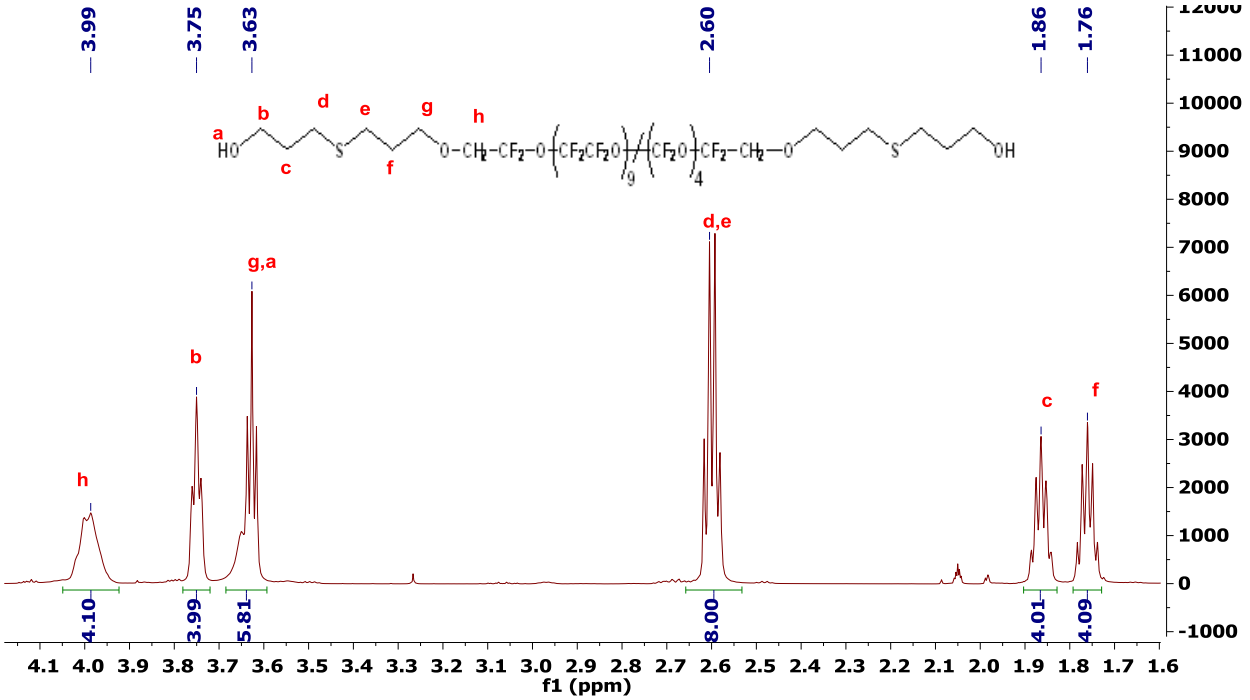

Figure 4.4 ^{1}H NMR spectrum of PFPE-TE-Diol product in $(CD_3)_2CO$.

(Quantitative Conversion; 83% Isolated Yield). ^{1}H NMR ($(CD_3)_2CO$): 1.76 ppm (p, 4 H), 1.86 ppm (p, 4H), 2.59 ppm (t, 8H), 3.63 ppm (m, 6H), 3.75 ppm (t, 4H), 3.99 ppm (m, 4H). ^{13}C NMR ($(CD_3)_2CO$): 28.56 ppm (s, $SCH_2\underline{C}H_2CH_2OH$). 28.85 ppm (s, $OCH_2\underline{C}H_2CH_2S$), 30.34 ppm (s, $S\underline{C}H_2CH_2CH_2OH$), 33.56 ppm (s, $OCH_2CH_2\underline{C}H_2S$), 61.03 ppm (s, $SCH_2CH_2\underline{C}H_2OH$), 69.93 ppm (t, $CF_2\underline{C}H_2O$), 71.79 ppm (s, $O\underline{C}H_2CH_2CH_2S$), 115.06 (m, CF_2CF_2O/ CF_2O).

4.2.6 Synthesis of Ethylene bis(carbonate)-linked $PFPE_{D10}$ [$(PFPE_{D10}\text{-}EBC)_n$]

10 g (10 mmol) of commercially available $PFPE_{D10}$-Diol (20 mmol -OH end groups) and triethylamine (2.8 mL, 20 mol) were dissolved in 100 mL of 1,1,1,3,3-pentafluorobutane in a 250-mL 3-neck round-bottom flask. The solution was cooled to 0°C under nitrogen atmosphere. Ethylene bis(chloroformate) (1.3 mL, 10 mol) was added dropwise over the course of five minutes

with rapid stirring, yielding the white triethylamine hydrochloride precipitate. The reaction was stirred for 4 hours under nitrogen atmosphere, followed by addition of methanol to endcap the material. The TEA HCl salt was removed by gravity filtration, yielding a pale-yellow solution. The pentafluorobutane solution was washed 3x with 200 mL water and 1x with 200 mL brine. Pentafluorobutane was removed under reduced pressure to yield the $(PFPE_{D10}\text{-}EBC)_n$ product as a faintly yellow, viscous oil.

(Quantitative Conversion; 74% Isolated Yield). ^{1}H NMR (600 MHz, $(CD_3)_2CO$, ppm) δ = 4.00 (s, 0.5 H), 4.77 (s, 4 H), 4.50 (s, 4 H); ^{13}C NMR (600 MHz, $(CD_3)_2CO$, ppm) δ = 63.25 (tt), 64.64 (tt), 66.96 (m) 113.13 (m), 149.58 (s), 152.76 (s). FTIR (neat): 2979 cm^{-1} (wk, C-H), 1768 cm^{-1} (str, C=O), 1182 cm^{-1} (C-H), 1084 cm^{-1} (C-O).

4.2.7 Physical Characterization of PFPE Electrolytes

The chemical structures of the functionalized PFPE products were confirmed using ^{13}C and ^{1}H nuclear magnetic resonance spectroscopy (NMR). Quantitative ^{13}C NMR was used to determine the degree of polymerization of $(PFPE_{D10H}\text{-}EBC)_n$. The ^{13}C {^{1}H, ^{19}F} NMR was obtained at a frequency of 150.9028 MHz with relaxation delay d1 = 70 s, 512 scans, ^{1}H decoupling offset = 4 ppm, and ^{19}F decoupling offset = -86 ppm.

The fully dried materials were then stirred with lithium bis(trifluoromethane)sulfonamide (LiTFSI) salt under nitrogen atmosphere. LiTFSI was added in small aliquots until the solubility limit was reached. The LiTFSI solubility limit for each product was determined visually, as salt precipitation leads to heterogeneous, opaque mixtures above the salt solubility limit in PFPE systems. Initially heterogeneous solutions were stirred for at least 24 hours to confirm insolubility, after which PFPE was added in small quantities to the solution until it became transparent once

again. The solution was then vacuum-dried at 50°C for 48 hours to confirm that the solution remained transparent and that water did not confound our characterization.

Differential scanning calorimetry (DSC) thermograms were recorded using a TA Instruments Q200 DSC on samples that were prepared under argon in hermetically sealed aluminum pans. Samples were equilibrated at −120°C, followed by heating at 10°C/min to 50°C and then cooling at 2°C/min to -120°C for two cycles. Midpoint glass transition temperatures (T_gs) were determined from the final heating thermogram. Thermogravimetric analysis (TGA) was recorded using a TA Instruments Q5000 TGA under nitrogen flow (10 mL/min) from 25 °C to 500 °C at a heating rate of 10 °C/min. Closed-cup flash point measurements were performed up to 250°C using an Erdco Rapid Tester small-scale apparatus following ASTM D 3278.

4.2.8 Measurement of Ion Transport Properties

Conductivity samples of the PFEG materials (low viscosity) were prepared by sandwiching a polymer soaked separator, Celgard 2500 (Celgard Company), with a stainless steel shim (MTI Corporation) on either side. The stainless steel shims were 15.5 mm in diameter and 0.2 mm in thickness; Celgard 2500 was cut to 19 mm in diameter and had an average thickness of 25.4 ± 0.6 μm. The thickness of the separator was measured for each sample. The stack was placed into CR2032 coin cells (Pred Materials) that were than hermetically sealed. Three replicate cells were produced and measured for each electrolyte. Conductivity data was collected through ac impedance spectroscopy performed on a Bio-Logic VMP3 potentiostat. The frequency range analyzed was between 1 MHz and 100 mHz at an amplitude of 60 mV. The minimum in a Nyquist plot was taken to be the resistance of the bulk electrolyte. Conductivity was then taken from the fitted R_{el} value using equation 1 for coin cells. In order to account for the porosity of the separator in the coin cells, liquid cell measurements were made with four different electrolytes: $PFEG_3DMC$

with 3 wt% LiTFSI and $PFEG_4DMC$ with 3 wt% LiTFSI, $PFEG_3DMC$ with 20 wt% LiFSI , and $PFEG_3DMC$ with 15 wt% LiBETI at 30 °C. The experimental procedure for liquid cell measurements has been described in full by Teran *et al*. A ratio between the calculated conductivity between the liquid and coin cells were then taken.

$$\sigma_0 = c * \frac{l}{R_{el} * A} \tag{4.1}$$

where *A* is the active surface area of the coin cells in cm^2, *l* is the thickness of the separator in cm, and *c* is a constant derived from the ratio of conductivity of liquid cells to coin cells. An average *c* was taken to be 8.7 with a standard deviation of ± 0.06 from the four independent measurements.

To measure ionic conductivity of PFPE-Tetra-ol and PFPE-TE-Diol (high viscosity electrolytes), stainless steel discs of diameter 1.55 cm and thickness 200 μm (MTI Corp) were used to sandwich a 254 μm thick silicone spacer. A 0.3175 cm hole was cut out of the silicone in order to make space for the polymer electrolyte. The electrolyte was viscous enough such that it did not leak out of the spacer once the sandwich was made. The sandwich was then hermetically sealed within pouch material. Three replicate cells were produced and measured for each electrolyte. Conductivity data was collected through ac impedance spectroscopy performed on a Bio-Logic VMP3 potentiostat. The frequency range analyzed was between 1MHz and 100 mHz at an amplitude of 60 mV. The minimum in a Nyquist plot was taken to be the resistance of the bulk electrolyte, *R*, which was used along with the electrolyte thickness *l* and electrolyte area *a* to calculate the ionic conductivity of the electrolyte σ using the equation below:

$$\sigma = \frac{l}{aR} \tag{4.2}$$

Lithium transference number, t^+, was determined using the potentiostatic polarization method described by Evans, *et al* (equation 4.3).[10]

$$t^{+} = \frac{I_{ss}\,(\,\Delta V - I_0 R_0)}{I_0(\Delta V - I_{ss} R_{ss})} \qquad (4.3)$$

Here, I_{SS} and R_{SS} are the steady state current and electrode-electrolyte interfacial resistance, respectively, ΔV is the voltage applied across the two electrodes, and I_0 and R_0, are the initial current and resistance, respectively. To measure t^+, lithium-lithium symmetric cells were fabricated in 2325 coin cell architecture using a Celgard 2500, 55 percent porous, polypropylene separator. The cells were polarized at 40 mV for 12 h, and interfacial resistance was determined using ac impedance spectroscopy. Impedance was performed using a signal with an amplitude of 10 mV, and frequency varying between 0.1 and 10^6 Hz. The interfacial resistance was measured every hour to ensure that steady state was reached.

4.3 Part 1: Effect of Molecular Weight on Electrolyte Performance

4.3.1 Introduction

A facile route to achieving higher concentrations of end groups is to simply reduce the molecular weight of the polymer. On top of acting as ion solvation sites, high end group concentrations tend to reduce T_g.[8] Naturally, end groups create more free volume than monomers located in the middle of the chain because they are covalently attached at only one end, increasing the translational degrees of freedom. T_g increases as a function of molecular weight according to:

$$T_g = T_{g\infty} - \frac{C}{M_n} \tag{4.4}$$

where $T_{g\infty}$ is the long chain limiting value of the glass transition temperature, C is a constant related to the free volume excess brought by each chain end depending on its nature (typically ranging from 10^4-10^5 K g mol^{-1}) and M_n is the number average molecular weight of the polymer. Importantly, Eq. 4.4 assumes a constant coefficient of friction.

Viscosity is also proportional to molar mass ($\eta \sim M$) in short chains, while longer chains exhibit a viscosity dependence of $\eta \sim M^{3.4}$ due to entanglement effects.[8] This chain length dependence of the viscosity is described by the crossover function

$$\eta \sim \zeta M \left[1 + \left(\frac{M}{M_c}\right)^{2.4}\right] \tag{4.5}$$

where η is viscosity, ζ is the friction coefficient (kg s^{-1}), M is the polymer's molar mass, and M_c is the critical molar mass for entanglements.

Considering the above, we hypothesized that shorter PFPE chains may not only dissolve more lithium salt but also enable higher ion mobility (as summarized in Figure 4.5). We investigated a series of commercially available perfluoroethylene glycols (PFEGs), the low molecular weight analogs of the previously studied PFPEs. We deviate from the commercial trade

names in this section to improve clarity for the reader: Exfluor names their products based on the number of backbone carbons, which changes upon end group functionalization. Instead, we refer to "C6GDiol" as PFEG$_3$Diol (perfluorinated triethylene glycol), for example. The commercially available products, along with their trade names, structures, and IDs in this work are summarized in Table 4.1. Furthermore, when discussing the low molecular weight materials only, we collectively refer to them as PFEGs (perfluoroethylene glycols) to distinguish them from the previously studied, higher molecular weight (Fluorolink) perfluoropolyethers. But when discussing the entire class of materials, we collectively refer to them as PFPEs.

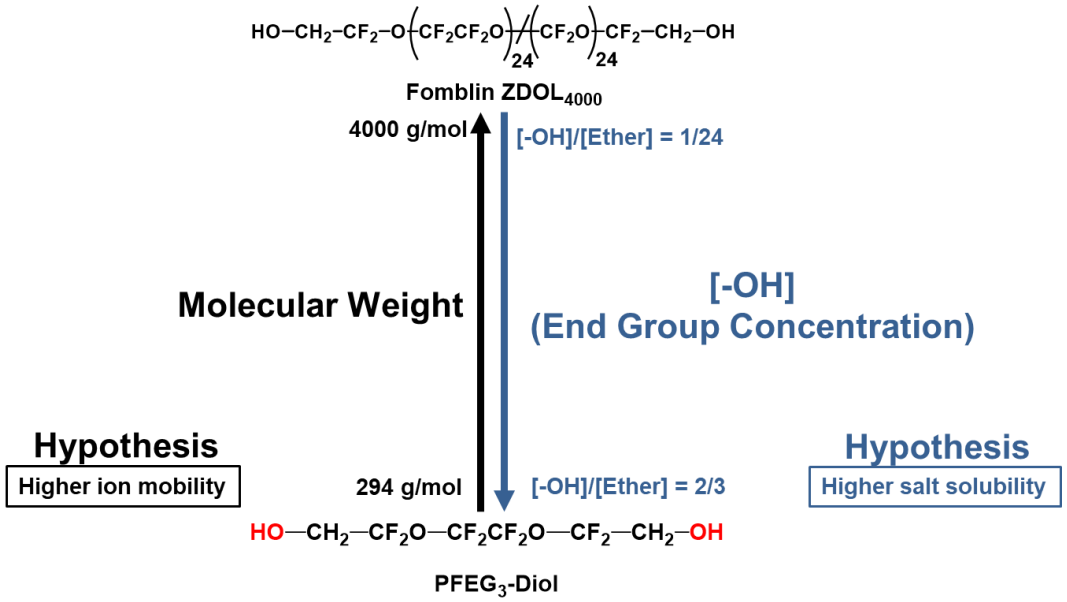

Figure 4.5 Differences in molecular weight and end group concentration across the full range of perfluoroether molecular weights investigated.

Table 4.1 Commercially available perfluorinated glycols from Exfluor Research Corporation.

Trade Name	Name	Compound ID	Structure
C6GDIOL	Perfluorinated Triethylene Glycol	PFEG$_3$Diol	HO—CH$_2$—CF$_2$O—CF$_2$CF$_2$O—CF$_2$—CH$_2$—OH
C7GOL	Perfluorinated Triethylene Glycol Monomethyl Ether	mPFEG$_3$ol	HO—CH$_2$—CF$_2$O(CF$_2$CF$_2$O)$_2$—CF$_3$
C8GDIOL	Perfluorinated Tetraethylene Glycol	PFEG$_4$Diol	HO—CH$_2$—CF$_2$O(CF$_2$CF$_2$O)$_2$—CF$_2$—CH$_2$—OH

4.3.2 Results and Discussion

4.3.2.1 Synthesis and Physical Properties

Unlike the previously studied PFPE systems, perfluorinated tri- and tetra-ethylene glycols are crystalline solids at room temperature (PFEG$_3$Diol T_m = 67°C, PFEG$_4$Diol T_m = 41°C). The Fluorolink systems are random copolymers of tetrafluoroethylene oxide and difluoromethylene oxide units created by β-scission reactions during the photooxidation of tetrafluoroethylene.[11] In contrast, the perfluorinated glycols discussed in this section contain only tetrafluoroethylene oxide repeat units. Though the regularity of the low molecular weight materials may contribute to crystallinity, we propose that hydrogen bonding is the major factor. Perfluorinated triethylene glycol monomethyl ether (mPFEG$_3$Ol), which contains the same backbone as PFEG$_3$Diol but half the number of hydroxyl groups, is a liquid at room temperature. The higher melting point of PFEG$_3$Diol compared to PFEG$_4$Diol further supports this hypothesis. We aimed to mitigate crystallinity by eliminating hydrogen bonding, converting the hydroxyl end groups to methyl carbonate groups as shown in Scheme 4.1 below.

Scheme 4.1 Conversion of PFEG$_\#$Diol to PFEG$_\#$DMC (n = 1 for PFEG$_3$, n = 2 for PFEG$_4$).

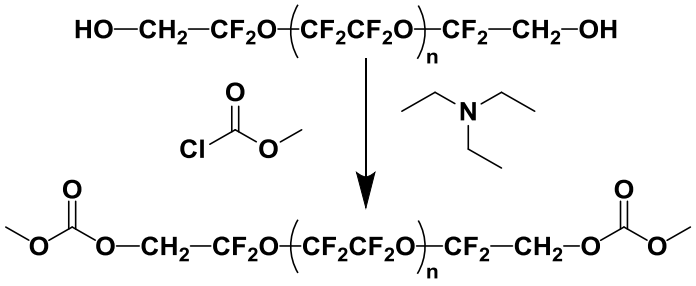

As predicted, the DMC-terminated glycols are amorphous liquids at room temperature. Differential scanning calorimetry was used to analyze the glass transition temperatures (T_gs) and

melting temperatures (T_ms) of the PFEGs. Interestingly, T_gs of the low molecular weight glycols are actually higher than that of $PFPE_{D10}$ (1000 g/mol). As PFPE molecular weight increases, hydrogen bonding or dipole-dipole interactions among end groups are "diluted", lowering the material's T_g.[7] $mPFEG_3Ol$ has the lowest T_g resulting from the low concentration of hydroxyl end groups compared to the other glycols.

Table 4.2 Thermal transitions of PFPE materials.

PFPE	Molecular Weight (g/mol)	T_g (°C)	T_m (°C)
$PFEG_3Diol$	294	--	67
$PFEG_4Diol$	410	--	41
$mPFEG_3Ol$	398	-107	--
D10-Diol	1000	-89	--
$PFEG_3DMC$	410	-77	--
$PFEG_4DMC$	526	-82	--
D10-DMC	1116	-95	--

4.3.2.2 Lithium Salt Solubility

Lithium bis(trifluoromethane)sulfonamide (LiTFSI) salt was then stirred with the fully dried PFEG materials. The LiTFSI solubility limit for each product was determined visually, as salt precipitation leads to heterogeneous, opaque mixtures above the salt solubility limit in PFPE systems.[7] Figure 4.6 shows the maximum lithium salt concentration in each material, expressed in terms of weight percent LiTFSI and as a molar ratio of lithium ions to end groups (R_{max}). As shown in Figure 4.6b, the maximum ratio of lithium ions per hydroxyl and carbonate end group is consistent across a range of molecular weight with one specific exception.

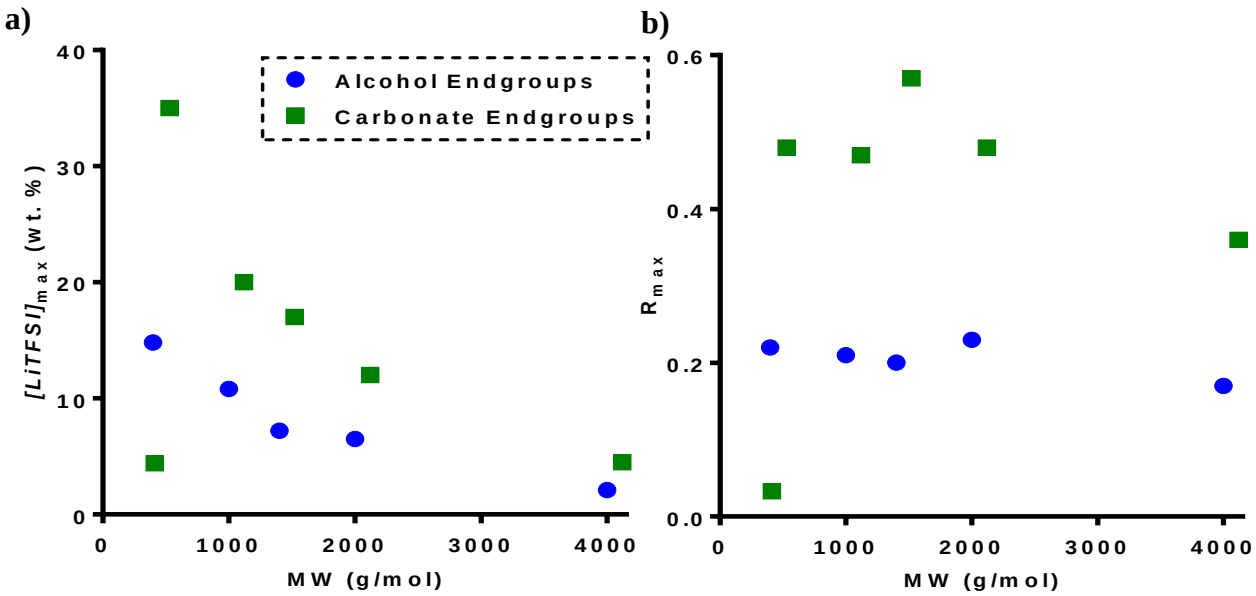

Figure 4.6 Maximum lithium salt solubility in PFPEs of varying molecular weight expressed as a) weight % LiTFSI and b) R_{max} ([Li^+]/[end group]). Data for 1000-4000 g/mol systems obtained from ref. [7].

PFEG$_3$DMC dissolves much less lithium salt (4.4 wt.% LiTFSI, R_{max} = 0.033) than was expected based on its concentration of carbonate end groups. Preliminary density functional theory (DFT) calculations carried out by Dr. Qin Wu at Brookhaven National Laboratory on the Li^+-end group interactions in PFEG$_3$DMC indicate that steric clash prevents all end groups from participating in ion solvation. However, it should be emphasized that these materials are well above their T_gs, making ion solvation a complex, dynamic process that may not be accurately captured by modeling of simple crystal structures.[12] Furthermore, the calculation modeled only the interaction between Li^+ and the PFEGs, neglecting the perfluoroether-anion interactions that we believe to be significant. Regardless, there is a critical molecular weight for ion solvation in PFPE electrolytes, below which the LiTFSI solvating ability of the material decreases significantly.

We added a final perfluorinated material to the lithium salt solubility study in an effort to better understand ion solvation in the low molecular weight system. We purchased commercially available perfluorinated octanediol (C$_8$Diol, T_m = 80°C) and functionalized it with carbonate end groups to form C$_8$DMC, an amorphous liquid at room temperature. C$_8$DMC is closely analogous

to $PFEG_3DMC$, with the only change being replacement of the interior oxygen atoms with CF_2 groups, as shown in Figure 4.7.

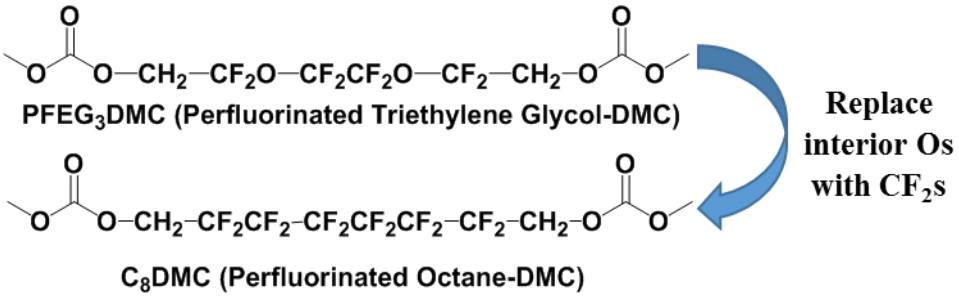

Figure 4.7 Structure of perfluorinated octane-DMC compared to perfluorinated triethylene glycol.

We determined that C_8DMC was unable to dissolve LiTFSI salt, indicating that PFPEs' CF_2CF_2O repeat unit participates in solvation. This is likely not a function of changing solvent polarity. The dielectric constants of PFPEs ($\varepsilon \approx 2.0\text{-}2.2$)[11,13] are similar to that of amorphous poly(tetrafluoroethylene) (PTFE, $\varepsilon \approx 2.1$)[14]: introduction of an ethereal oxygen within the perfluorinated chain has little influence on the electrical properties. Therefore, we propose that there is a favorable CF_2CF_2O-$TFSI^-$ interaction (but not $CF_2CF_2CF_2$-$TFSI^-$ interaction) that supplements the Li^+-end group interaction, enabling lithium salt solubility in PFPE materials. This may also explain the low LiTFSI solubility in $PFEG_3DMC$: aside from steric clash of end groups, the perfluoroether chain may be insufficiently long to accommodate the $TFSI^-$ anion (characteristic length ≈ 8 Å)[15], resulting in ion association and aggregation.

4.3.2.3 Thermal Stability

We recognized that our move to low molecular weight oligomers might mitigate the outstanding thermal stability of PFPE electrolytes. Thermogravimetric analysis (TGA) was used to evaluate the volatility of the PFEGs. Figure 4.8 shows the evaporation profiles of the perfluorinated glycols compared to dimethyl carbonate (DMC) solvent, along with the degradation

profile of $PFPE_{D10}$-Diol. We also performed closed-cup flash point measurements using an Erdco Rapid Tester small-scale apparatus following ASTM D 3278 to evaluate the flammability of the electrolyte. The 5% mass loss temperature ($T_{ML(5\%)}$) and flash points of the materials are listed in Table 4.3.

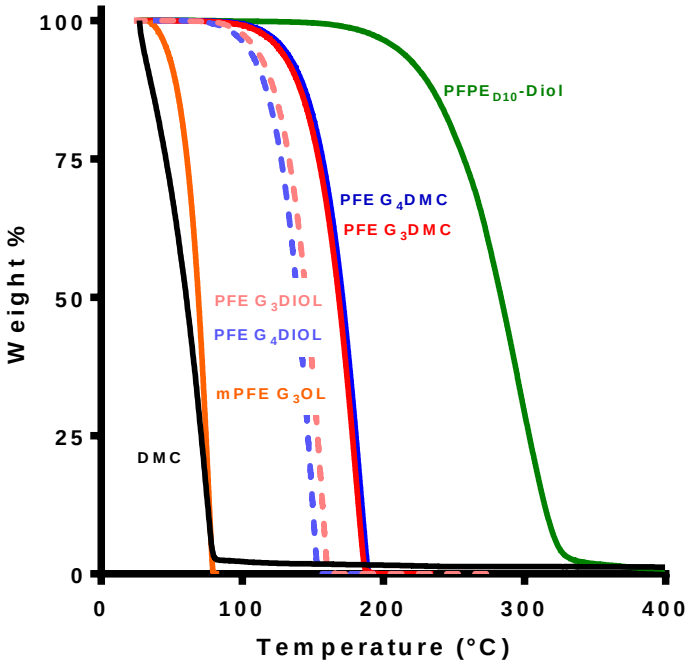

Figure 4.8 TGA of perfluorinated glycols compared to dimethyl carbonate solvent and higher molecular weight $PFPE_{D10}$-Diol.

Table 4.3 5% mass loss temperature and flash point of electrolyte materials.

PFPE	$T_{ML(5\%)}$ (°C)	Flash Point (°C)
DMC	34	18
$PFEG_3$Diol	110	152
$PFEG_4$Diol	104	148
m$PFEG_3$Ol	46	N/A
D10-Diol	210	N/A
$PFEG_3$DMC	126	N/A
$PFEG_4$DMC	129	N/A

No flash point was detected for $mPFEG_3Ol$, $PFEG_3DMC$, or $PFEG_4DMC$ within the experimental window (up to 250°C). It should be noted that the boiling point of $mPFEG_3Ol$ is 140°C, setting the upper limit for flash point measurements of that material. PFEGs are nonflammable and only moderately volatile. Even small molecule DMC solvents are not the component that imposes the high-temperature limit on lithium-ion batteries.[16] Instead, thermal degradation of the salt or SEI layer, along with shrinkage of the battery separator, causes battery failure before DMC vaporization.[17] Thus, the $PFEG_3DMC$ and $PFEG_4DMC$ systems are sufficiently nonvolatile for battery uses. Moreover, their nonflammability is a significant advantage over traditional DMC-based electrolytes.

4.3.2.4 Polymer-Ion Interactions

Measuring the rate of increase of T_g as a function of lithium salt concentration provides insights into the interaction of the polymer with lithium salts. The increase in T_g is attributed to physical, ionic crosslinks that form among polymer chains and lithium ions. Generally, a larger slope of the T_g vs. [LiTFSI] plot indicates stronger, longer-lived, or more numerous polymer-Li^+ interactions. We compared the rate of T_g increase as a function of lithium salt concentration among $PFPE_{D10}$-DMC, $PFEG_3DMC$, and $PFEG_4DMC$ electrolytes. Despite the identical end groups of each material, the rate of T_g increase as a function of lithium salt concentration differed significantly, as shown in Figure 4.9 and Table 4.4.

Table 4.4 Rate of increase in T_g as a function of salt concentration in PFPE-DMC electrolytes.

PFPE	Slope, T_g vs. R (°C)
$PFEG_3DMC$	3.3 ± 2.2
$PFEG_4DMC$	70.1 ± 3.0
D10-DMC	35.7 ± 2.2

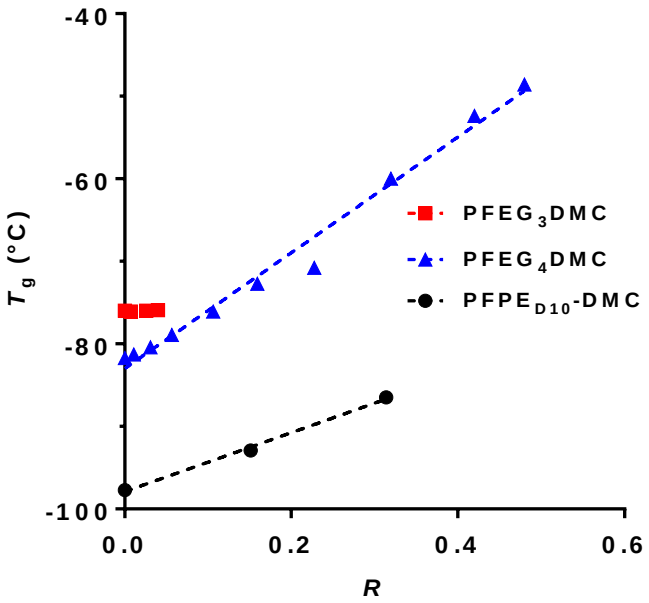

Figure 4.9 Glass transition temperature of DMC-terminated PFPEs as a function of LiTFSI concentration (R=[Li^+]/[end group]).

To better understand the differences in T_g increase among the PFPE-DMC materials, IR spectroscopy was used to probe the interaction between Li^+ and carbonyl oxygen atoms. Consistent with the small increase in T_g as a function of lithium salt concentration, the C=O stretching frequency of $PFEG_3DMC$ exhibited no significant shift upon addition of lithium salt. Peak broadening is apparent in the salt-saturated sample, indicating minimal interaction between the carbonyl oxygen atom and Li^+/ion pairs. $PFEG_4DMC$ and $PFPE_{D10}$-DMC exhibited significant and comparable shifts in stretching frequency as expected based on the materials' similar salt-solvating ability. But despite the comparable strength of interaction between Li^+ and the carbonyl oxygen atoms, $PFEG_4DMC$'s T_g increase is higher than that of D10-DMC. We propose that this is caused by higher end group concentrations in $PFEG_4DMC$, creating closely spaced ionic crosslinks that have greater influences on T_g.

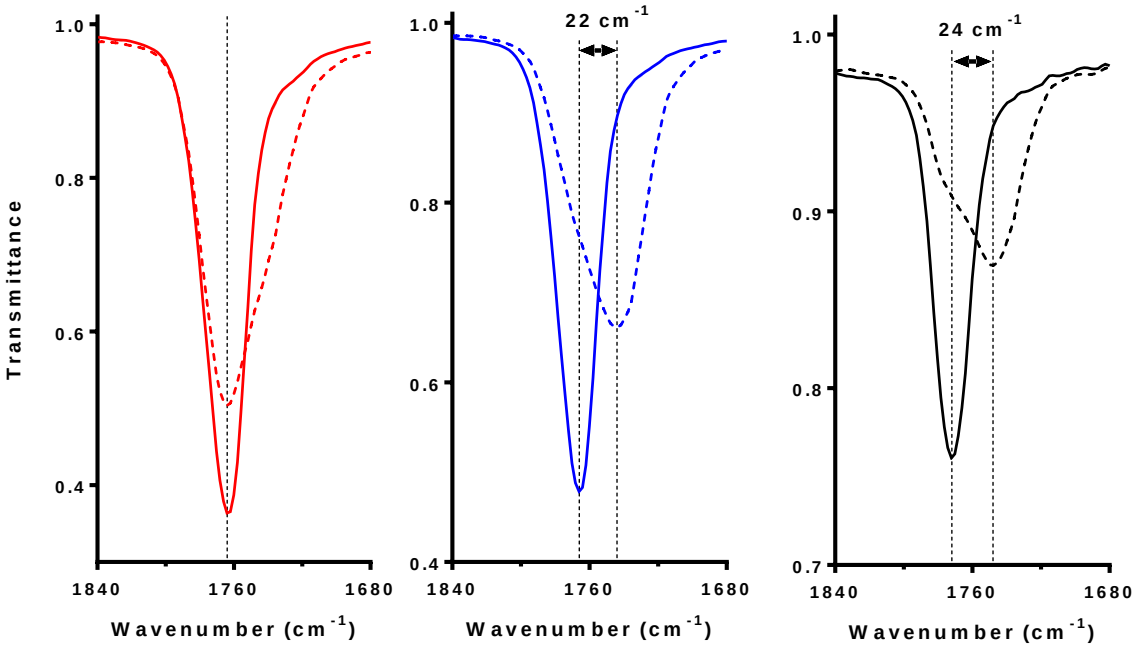

Figure 4.10 IR spectra of PFPE-DMC materials (red: $PFEG_3DMC$, blue: $PFEG_4DMC$, black: D10-DMC; solid = neat, dashed = saturated with LiTFSI).

4.3.2.5 Ionic Conductivity

Ionic conductivity of the PFPE-DMC materials was then measured at 30°C across a range of lithium salt concentrations, as shown in Figure 4.11. At low salt concentrations (~5 wt.% LiTFSI), the ionic conductivity of the PFEGs was more than an order of magnitude higher than that of $PFPE_{D10}$-DMC. However, $PFPE_{D10}$-DMC exhibits a monotonic increase in ionic conductivity as a function of salt concentration, while the fluorinated glycols exhibit maxima in ionic conductivity. As a result, the maximum achievable ionic conductivity in $PFEG_4DMC$ is only ~2.5x higher than that of $PFPE_{D10}$-DMC. In the dilute regime of polymer electrolytes, conductivity increases upon addition of lithium salt due to elevations in the number of available charge carriers.[18] At higher salt concentrations, addition of lithium salt causes conductivity to decrease because elevations in T_g and viscosity more than offset any increase in the number of charge carriers.[19] We propose that LiTFSI reaches its solubility limit in $PFPE_{D10}$-DMC before entering the second (concentrated) regime.

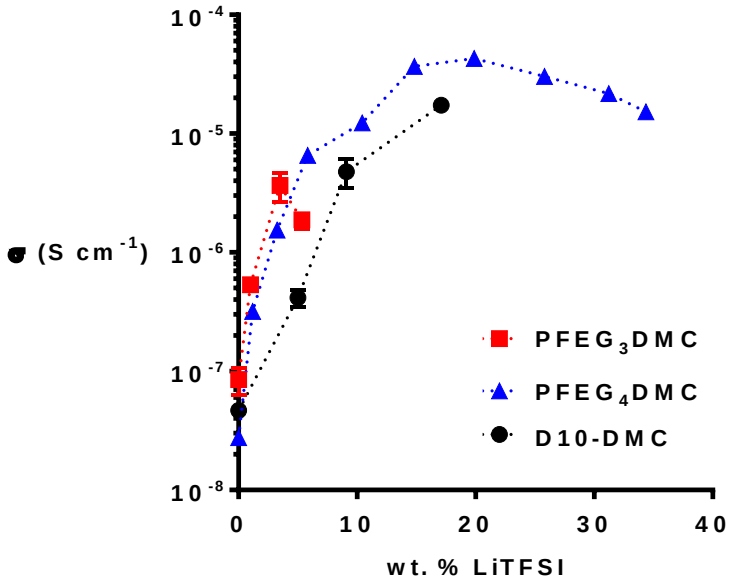

Figure 4.11 Ionic conductivity of PFPE-DMC electrolytes at 30°C as a function of salt concentration.

4.3.2.6 Transference Number

In polymer electrolytes, solvent chains are entangled and immobilized. The prevalent conduction mechanism for Li^+ is ion hopping from solvation site to solvation site along the polymer chain during segmental rearrangements.[20] In small molecule electrolytes, on the other hand, solvent molecules diffuse freely. Vehicular motion occurs: Li^+ diffuses with the solvent molecules in its coordination sphere. Lithium ion transference numbers range from 0.2 to 0.4 in small molecule electrolytes because Li^+ moves at slower speeds with its solvation shell than the relatively "free" anions.[16] Shi and Vincent previously reported that in PEO electrolytes below the critical molecular weight for entanglements (3200 g/mol), vehicular motion becomes a major cation transport mechanism.[4] The PFEG materials are likely below the critical molecular weight for entanglement, indicating that vehicular transport may be a major mechanism for ion transport in the PFEG electrolytes. In theory, this would lower the t^+ value of fluorinated glycols relative to their higher molecular weight analogs, mitigating some of the benefits of perfluoroether-based electrolytes.

The transference numbers of $PFEG_3DMC$ and $PFEG_4DMC$ were measured using the potentiostatic polarization method at 30°C. At ~3.5wt.% LiTFSI, $t^+_{(PFEG_3DMC)} = 0.97 \pm 0.02$, and $t^+_{(PFEG_4DMC)} = 0.98 \pm 0.02$. These values are in good agreement with previously reported values for the transference number of PFPE electrolytes ($t^+_{(D10\text{-}DMC)}$=0.91 at 9.2wt.% LiTFSI, 30°C).[7] In spite of the likelihood that vehicular transport occurs in these systems, Li^+ remains significantly more mobile than the anion. We propose that the perfluorinated PFPE backbone interacts favorably with the fluorinated $TFSI^-$ anion, creating a solvation shell that slows the motion of the anion in an analogous mechanism to the slowed mobility of Li^+ in its solvation shell in commercial electrolytes.[16]

Chapter 3 introduced a hypothesized mechanism for ion transport in PFPE electrolytes, in which Li^+ hops among ion aggregates that are prevalent in these systems.[15] This mechanism presents another possible explanation for the high t^+ values observed in the fluorinated glycols, as Li^+ hopping among ion aggregates is expected to be faster than anion diffusion. It should be noted, however, that efficient Li^+ transport was proposed to only "switch on" at high salt concentrations where ion aggregates are spaced sufficiently close together. To test whether this mechanism applies to the perfluorinated glycols, the dependence of t^+ in $PFEG_4DMC$ electrolytes on LiTFSI salt concentration was measured at 30°C.

As shown in Figure 4.12, t^+ decreased from 0.98 to 0.83 with increasing salt concentration. Contrary to the proposed mechanism for ion transport in other PFPE systems, Li^+ transport actually becomes less efficient at higher salt concentrations. This has been observed in propylene carbonate-based electrolytes[21,22] and is tentatively attributed to ion aggregation yielding the positive triplet, slowing the motion of Li^+. A conflicting report showed that t^+ increases in PEO electrolytes as a function of salt concentration, which was attributed to formation of the negative

triplet, slowing the motion of the anion.[23] While ion aggregation is the likely cause of the reduction in t^+ at high salt concentrations, further work is needed to clarify the transport mechanisms contributing to this phenomenon.

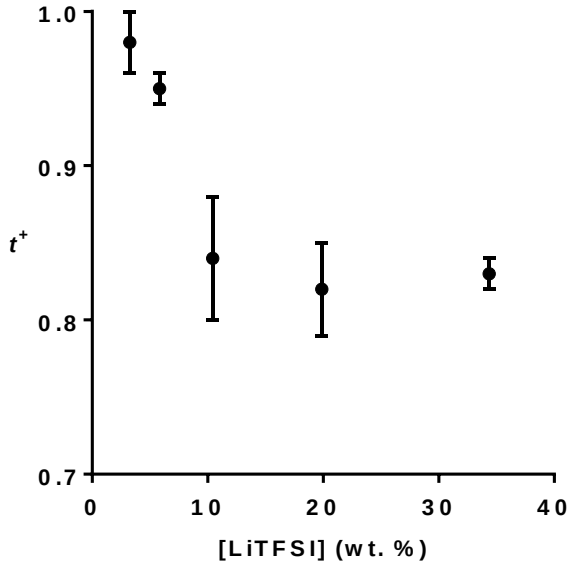

Figure 4.12 Transference number of $PFEG_4DMC$ as a function of LiTFSI concentration.

4.3.3 Summary

Ultimately, the PFEG electrolytes exhibit ionic conductivities that match that of PFPE-EO (Fluorolink E10), which are the most conductive PFPE materials studied to date.[24] Moreover, PFEGs exhibit $t^+ > 0.83$, more than double that of PFPE-EO electrolytes ($t^+ \approx 0.36$)[25] and among the highest reported for electrolytes consisting of lithium salts dissolved in solvents. PFEGs are significantly less volatile than DMC and exhibit no flash points. These materials are promising candidates for LIB electrolytes, and their cell performance is currently being evaluated via cycling and rate capability studies.

4.4 Part 2: End Group Concentration Effects on Electrolyte Performance

4.4.1 Introduction

Section 4.2 showed promising results that higher end group concentrations afford higher lithium salt solubility in PFPE electrolytes, leading to enhanced ionic conductivity. However, the study simultaneously probed the effects of two variables (end group concentration and molecular weight) on PFPE electrolyte performance. In this section, we aim to control for molecular weight and probe only the contributions of end group concentration by functionalizing PFPE of a given molecular weight with branched end groups.

Considering the difficulty of separating polymers with different end groups, synthesis of polymeric materials requires efficient, robust, and facile chemical reactions.[26] To synthesize PFPE with branched end groups, we selected a synthetic route employing the "thiol-ene" reaction, typically considered a click reaction. Yet we encountered unexpected challenges in achieving 100% conversion to the desired products when using equimolar amounts of thiol and ene. Thus, we begin the discussion section of this work with an assessment of our results according to the adapted macromolecular definition for a click reaction. The requirements for click reactions involving one or more polymeric reagents are shown in Figure 4.13.[27] Importantly, our findings indicate that the thiol-ene reaction in PFPE systems should not be considered a "click" reaction.

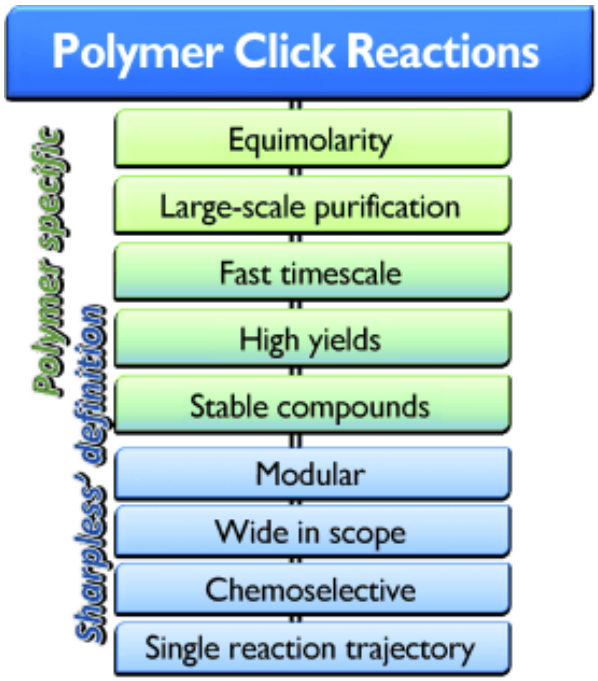

Figure 4.13 Requirements for click reactions involving one or more polymeric reagents (blue: originally defined by Sharpless; green and blue–green: adapted requirement related to synthetic polymer chemistry). Reprinted from ref. [27] with permission from John Wiley and Sons.

4.4.2 Results and Discussion

4.4.2.1 Development of Thiol-Ene Reaction in PFPE Systems

We designed the synthesis of PFPE with branched hydroxyl end groups based on high-yielding thiol-ene reactions reported in the literature.[28,29] The thiol-ene reaction is typically lauded as "click" chemistry, but several reports over the previous decade have suggested that the thiol-ene reaction does not meet the click criteria for polymer-polymer conjugation.[30,31] Even in the case of polymer end group functionalization using small molecule thiols, excess thiol is needed to achieve full conversion.[32–34] Reactions that require an excess of one reagent to offset side reactions are not "spring-loaded for a single trajectory" as Sharpless originally defined in his click criteria.[35] In agreement with these previous reports, development of the thiol-ene reaction for PFPE systems required significant optimization in order to achieve the desired results.

This was unexpected, considering the work that we emulated by Song *et al.* reported successful polymer-polymer conjugation (>90% purity) using PFPE-enes and monofunctional PEG-thiols at equimolar concentrations.[28] Attempts to replicate their results in identical systems using the reported reaction conditions proved unsuccessful. At a minimum, the discrepancy between our results and the previous work points to the need to follow carefully controlled reaction conditions for a given system, which is inconsistent with the original definition for a click reaction.

Thus, we systematically studied the effects of photoinitiator concentration, molecular weight of thiol and ene, stoichiometric ratio of thiol:ene, and atmosphere on the purity of desired PFPE products. We abbreviate the results herein to focus on i) assessing the thiol-ene reaction as a click chemistry in PFPE systems and ii) developing the synthesis of pure PFPE-Tetra-ol. We began by exploring the equimolar reactions among PFPE-enes and thiols of varying molecular weights, as shown in Scheme 4.2. All reactions were carried out with 2,2-dimethoxyacetophenone (2,2-DMPA) photoinitiator (1 mol% relative to the ene). Lower DMPA concentrations caused incomplete conversion of the ene, while higher concentrations increased the formation of side-products from radical recombination, as is well-established in the literature.[31]

Scheme 4.2 Reaction between PFPE-enes and thiols.

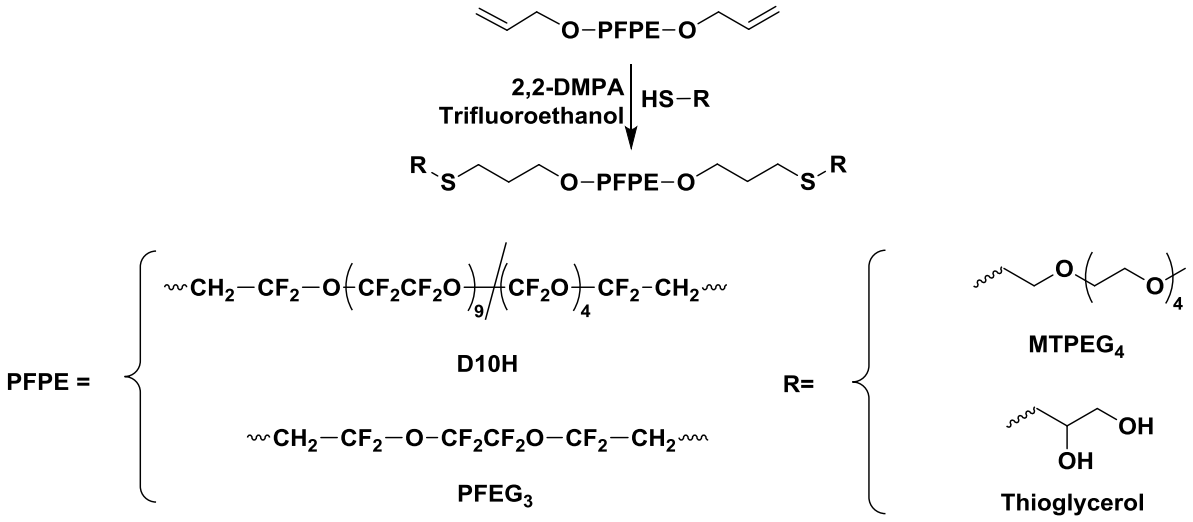

Table 4.5 Reaction efficiencies between PFPE-enes and thiols of varying molecular weight.

PFPE-ene	Thiol	Ratio thiol:ene	% Conversion
$PFEG_3$	Thioglycerol	1:1	97
$PFEG_3$	$MTPEG_4$	1:1	82
D10H	Thioglycerol	1:1	80
D10H	$MTPEG_4$	1:1	51

Table 4.5 shows the reaction efficiency of the thiol-ene reaction in PFPE/thiol systems of varying molecular weight. Low molecular weight coupling (entry 1) proceeds as expected, with nearly quantitative conversion at equimolar concentrations of thiol and ene. Slight increases in the molecular weight of the thiol ($MTPEG_4$, entry 2) reduced the conversion significantly to 82%. Even lower conversions are achieved in the higher molecular weight $PFPE_{D10H}$ system.

On the basis of equimolarity alone, it is clear that the thiol-ene reaction should not be considered a "click"-type reaction for polymer-polymer conjugation in PFPE systems. In other polymer systems, this has been attributed to the chain-length dependence of radical reactivity.[31] Beyond that, the thiol-ene reaction does not meet the "click" criteria for PFPE end group functionalization except for in very low molecular weight systems. We would like to echo the sentiment of the authors of ref. [27], who state, "there is danger that the term 'click' will become meaningless over time and simply a synonym for 'successful'." In the polymer field, it is important to evaluate the "click" term strictly by the guidelines outlined in Figure 4.13.

Table 4.6 Reaction efficiency of PFPE-enes with thioglycerol under various reaction conditions.

PFPE-ene	Thiol	Ratio thiol:ene	Atmosphere	% Conversion
D10H	Thioglycerol	1:1	Air	80
D10H	Thioglycerol	1.25:1	Air	96
D10H	Thioglycerol	1.25:1	Nitrogen	100
D10H	Thioglycerol	2:1	Air	100
$PFEG_3$	Thioglycerol	1:1	Air	97
$PFEG_3$	Thioglycerol	1:1	Nitrogen	97

We then established a set of reaction conditions that would enable 100% conversion of $PFPE_{D10H}$-ene to the thioglycerol-terminated material, as shown in Table 4.6. 25% excess thioglycerol yields 96% conversion to the desired product (entry 2). The same reaction under nitrogen atmosphere yields quantitative conversion to the desired product (entry 3). In contrast, the yield in the low molecular weight system remains unchanged by atmosphere (entries 5,6), consistent with reports of the thiol-ene reaction's oxygen tolerance in most small molecule systems.[36,37] Finally, a larger excess of thiol enabled quantitative conversion of the PFPE material, even in the presence of oxygen (entry 4). Translating the above results to our synthetic design of PFPE-Tetra-ol, we performed the thiol-ene reaction under nitrogen atmosphere with two molar equivalents of thioglycerol to ensure conversion to the desired products.

4.4.2.2 Synthesis of PFPE with Branched End Groups

The above section detailed the reaction development to functionalize $PFPE_{D10H}$ with end groups that enabled us to explore the effects of end group concentration on PFPE electrolyte performance at a constant molecular weight. Scheme 4.3 shows the optimized synthesis for PFPE-Tetra-ol. We functionalized $PFPE_{D10H}$-Diol (1400 g/mol, CF_2CH_2OH-terminated) with allyl ether end groups, followed by "clicking" thioglycerol onto the material to yield PFPE-Tetra-ol.

Scheme 4.3 Synthesis of PFPE-Tetra-ol (f=4) and PFPE-TE-Diol (f=2) by photoinitiated thiol-ene reaction.

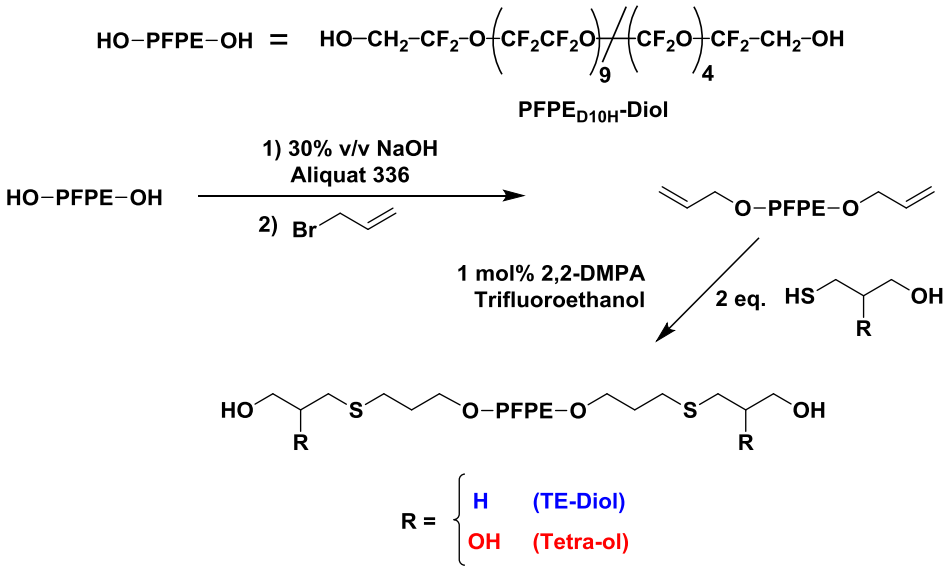

We recognized that the tetra-hydroxy terminated material differed in two main ways from the original diol material: i) the molecular weight of PFPE-Tetra-ol is about 20% higher than $PFPE_{D10H}$-Diol and ii) PFPE-Tetra-ol's hydroxyl end groups have hydrogenated β carbons as opposed to the perfluorinated β carbons of $PFPE_{D10H}$-Diol. The latter factor confounds direct interpretation of end group effects due to the inherent differences in hydroxyl electron density. Therefore, we also synthesized a hydroxyl-terminated control material (PFPE-Thioether-Diol, "PFPE-TE-Diol") to negate these differences in end group polarity and molecular weight (< 2% difference between TE-Diol and Tetra-ol materials). PFPE-Tetra-ol and PFPE-TE-Diol contain the same thioether linkage, have nearly identical molecular weight, and have hydroxyl functionality f = 2 (PFPE-TE-Diol) or f = 4 (PFPE-Tetra-ol), enabling us to determine the effect of end group concentration on electrolyte performance. The effect of the thioether linkage itself can be explored by comparing the performance of the PFPE-TE-Diol (f = 2) product to the original $PFPE_{D10H}$-Diol (f = 2) control.

It is important to note that we were originally interested in studying the effect of end group concentration in both hydroxyl- and carbonate-terminated PFPE systems. However, attempts to functionalize PFPE-Tetra-ol with methyl carbonate end groups to form PFPE-Tetra-carbonate yielded PFPE-diethylene carbonate instead. Intramolecular transesterification results in end group cyclization rather than the targeted branched carbonates, as shown in Scheme 4.4 and detailed in Chapter 3. Therefore, we continued our studies on the hydroxyl-terminated materials only.

Scheme 4.4 Attempted synthesis of PFPE-Tetra-carbonate, resulting in end group cyclization.

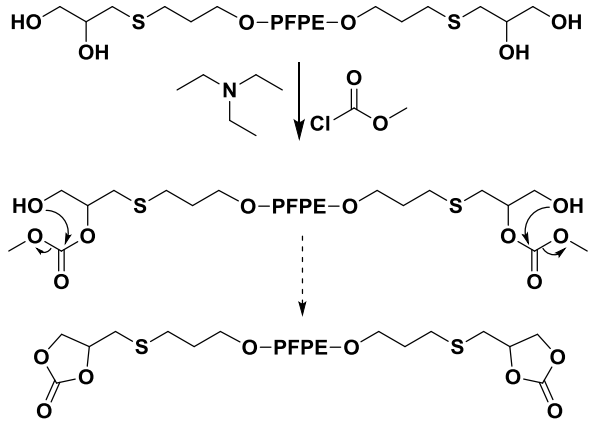

4.4.2.3 Lithium Salt Solubility

Lithium bis(trifluoromethane) sulfonamide (LiTFSI) salt was stirred with the fully dried PFPE materials. The LiTFSI solubility limit for each product was determined visually, as salt precipitation leads to heterogeneous, opaque mixtures above the salt solubility limit in PFPE systems.[7] We normalized the maximum salt solubility as a molar ratio of lithium ions to hydroxyl groups, (R_{max}). Figure 4.14 compares the R_{max} of $PFPE_{D10H}$-Diol (-CF_2CH_2OH end groups), PFPE-TE-Diol, and PFPE-Tetra-ol.

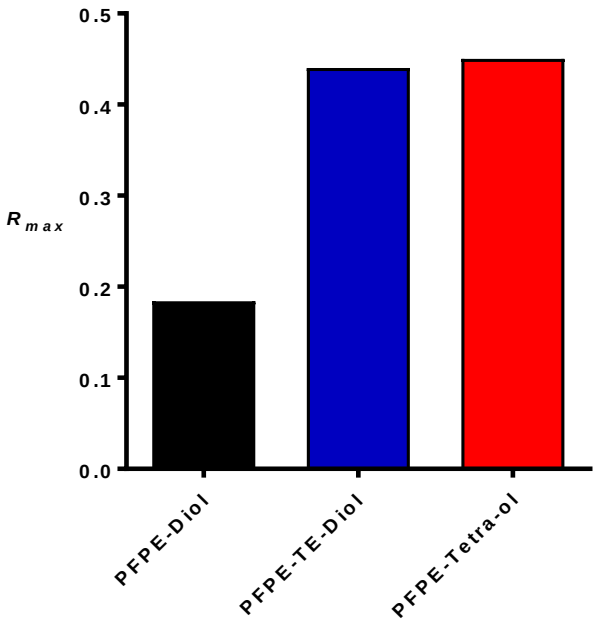

Figure 4.14 Maximum LiTFSI solubility in hydroxyl-terminated $PFPE_{D10H}$ materials.

As expected, the hydrogenated thioether linker increases the solvating ability of PFPE hydroxyl end groups: $R_{\text{max PFPE-TE-Diol}} \approx 0.45 >> R_{\text{max PFPE-Diol}} \approx 0.2$. This solubility enhancement is caused by differences in the electron density of hydroxyl end groups with a perfluorinated vs. hydrogenated β carbon. The interior thioether sulfur atoms and $-CF_2CH_2O-$ oxygen atoms do not contribute significantly to lithium salt solvation in the PFPE-TE-Diol and PFPE-Tetra-ol systems, as evidenced by $R_{\text{max PFPE-TE-Diol}} \approx R_{\text{max PFPE-Tetra-ol}} \approx 0.45$. If either interior S or O atoms contributed to lithium salt solubility, $R_{\text{max PFPE-TE-Diol}}$ would be higher than $R_{\text{max PFPE-Tetra-ol}}$ due to differences in the ratio of interior S and O atoms compared to hydroxyl end groups in the material. The minimal solvation of Li^+ by sulfur atoms is supported by hard-soft acid-base (HSAB) theory in addition to modeling carried out by Johnsson in Li^+-poly(ethylene sulfide) systems.[38] The important implication of the constant R_{max} value in PFPE-TE-Diol and PFPE-Tetra-ol is that the *number* of end group-Li^+ interactions can be increased without significantly affecting the *strength* of end group-Li^+ interactions. Therefore, PFPE-Tetra-ol (f=4) dissolves twice as much LiTFSI salt as PFPE-TE-Diol (f=2) does, doubling the concentration of potential free charge carriers in solution.

4.4.2.4 Ionic Conductivity and Transference

Ac impedance spectroscopy was used to measure ionic conductivity as a function of temperature in the $PFPE_{D10H}$ thioether-containing electrolytes at 9.2 wt.% LiTFSI. As shown in Figure 4.15, the conductivity data nicely captures the effects of both end group polarity and end group concentration on ion transport. The conductivity of a given PFPE material—PFPE-TE-Diol in this case—can be dramatically increased either by increasing the concentration of end groups (PFPE-Tetra-ol) or by increasing the end group polarity (PFPE-DEC). Furthermore, PFPE-Tetra-ol dissolves about 22 wt.% LiTFSI, and therefore even higher ionic conductivities may be achievable in the $f = 4$ system at higher salt concentrations.

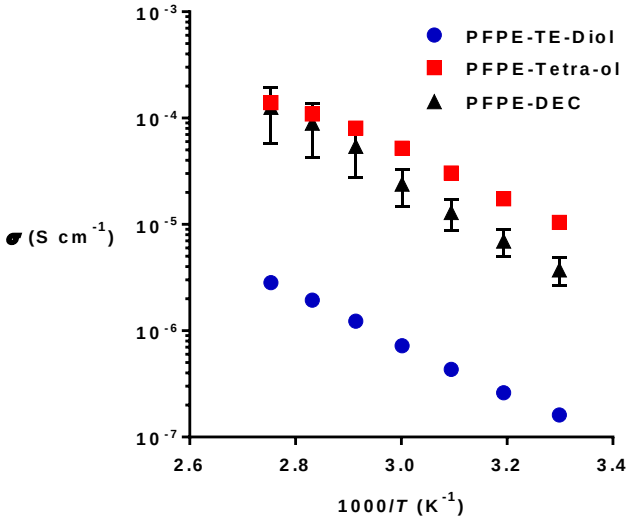

Figure 4.15 Ionic conductivity of $PFPE_{D10H}$ with various thioether-containing end groups at ~9.2 wt.% LiTFSI.

Lithium symmetric pouch cells containing the above electrolytes were made, and the potentiostatic polarization method[10] was employed to measure the transference number. Due to the thickness of the electrolyte and the small active surface area, the cells were too resistive to obtain reliable current responses over time. The cell design is currently being optimized to obtain reliable measurements of t^+. Only then will we be able to definitively evaluate whether increasing end group concentration is a viable route to achieving a high σ, high t^+ PFPE electrolyte. It is clear,

however, that increasing end group concentration enables higher charge carrier concentrations without affecting the strength of Li^+-end group interactions.

4.5 Part 3: Effect of Changing Molecular Weight at Constant Carbonate Concentration

4.5.1 Introduction

Section 4.3 analyzed the effect of PFPE molecular weight on electrolyte performance, which includes the effects of both end group concentration on ion solvation and molecular weight on ion diffusivities. In an effort to better isolate the effect of molecular weight on ion diffusivities, we polymerized the $PFPE_{D10}$-Diol macromonomer using ethylene bis(chloroformate) to yield a PFPE polycarbonate, as shown in Scheme 4.5. By maintaining a constant concentration of polar carbonate groups (2 carbonate groups per PFPE macromonomer), we aimed to eliminate the confounding variable of end group concentration from our molecular weight study.

Scheme 4.5 Polymerization of $PFPE_{D10}$ macromonomer to yield a PFPE polycarbonate.

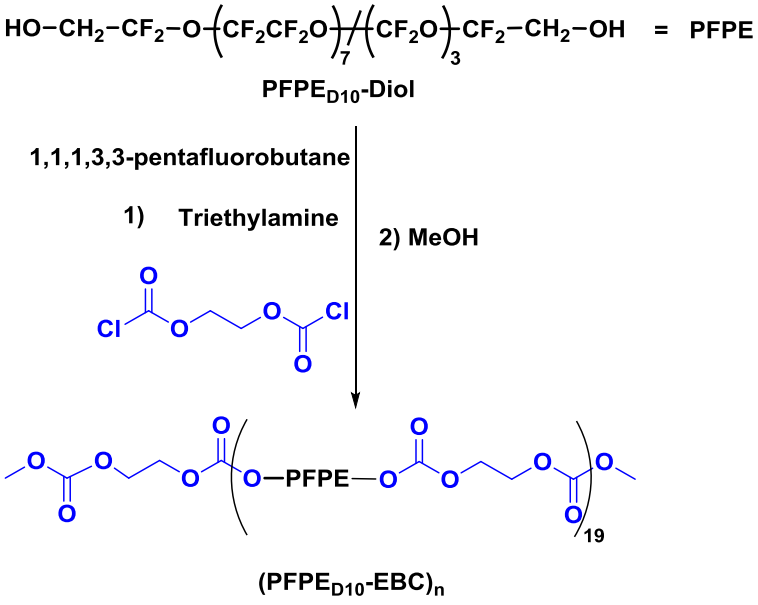

4.5.2 Results and Discussion

4.5.2.1 Electrolyte Synthesis

We synthesized a PFPE-polycarbonate material by mixing a $PFPE_{D10}$-Diol macromonomer (1000 g/mol) with ethylene bis(chloroformate). The ethylene bis(carbonate)-linked polymer $(PFPE_{D10}\text{-EBC})_n$ was insoluble in tetrahydrofuran, precluding analysis using size exclusion chromatography (SEC) to characterize the molecular weight distribution of the product. Instead, quantitative ^{13}C NMR was used to determine the average degree of polymerization by comparing the ratio of interior C=O carbons to terminal C=O carbons, as shown in Figure 4.16. The ratio was determined to be 19:1, indicating that on average, N = 19 (i.e. 19 $PFPE_{D10}$ macromonomers are linked together on average).

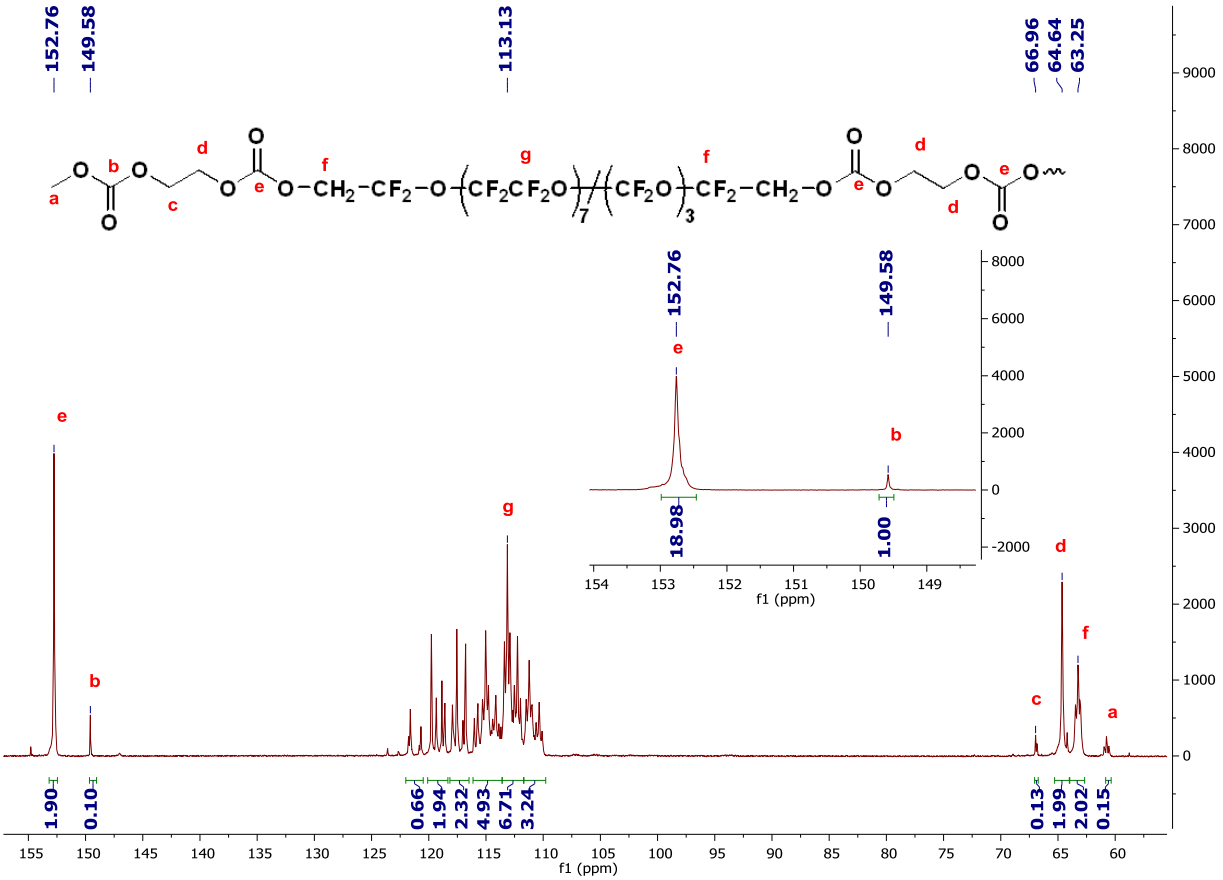

Figure 4.16 Quantitative ^{13}C NMR spectrum of $(PFPE\text{-}EBC)_n$. Inset: carbonyl region of spectrum.

4.5.2.2 Lithium Salt Solubility

We then mixed LiTFSI salt with the PFPE product to determine the maximum lithium salt solubility in the polymer. As shown in Figure 4.17a, the maximum number of lithium ions per carbonate end group was consistent with that of the lower molecular weight PFPE-carbonates. It should be stressed that the calculation of R_{max} accounts for the number of lithium ions per end group only. If interior (linker) carbonate groups contributed to lithium salt solvation, R_{max} would be much higher in the PFPE polycarbonate system than in the PFPE-DMC systems. The consistency of R_{max} indicates that interior polar groups do not significantly contribute to lithium salt solvation.

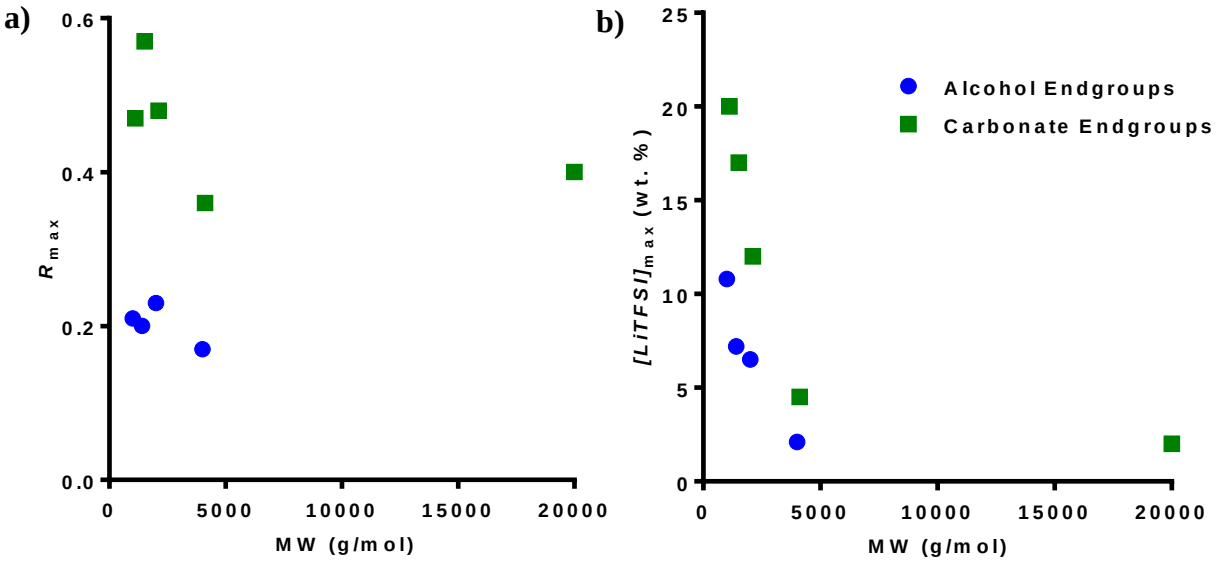

Figure 4.17 Maximum LiTFSI salt solubility in PFPE solvents of varying molecular weight, expressed as a) R_{max}, the number of lithium ions per end group and b) weight percent. Data for 1000-4000 g/mol systems obtained from ref. [7].

Clearly, polar *end groups* are necessary for lithium salt solvation. We attribute this to the accessibility of the end group related to the greater free volume generated by end groups compared

to interior monomers.[6,8,39] Thus, our attempt to alter the molecular weight of the polymer while maintaining a constant concentration of solvating carbonate groups was unsuccessful. Instead, it is necessary to separate the effects of end group concentration and molecular weight on PFPE electrolyte performance by combining the results from Sections 4.2 and 4.4 of this work.

4.6 Conclusions

In this chapter, we reported the effects of increasing the number of Li^+-polymer interactions rather than the strength of those interactions. We determined that the number of free charge carriers contributing to ionic conductivity in PFPE electrolytes is enhanced in materials with higher end group concentrations. Interestingly, studies on PFPE polycarbonates revealed that it is indeed the *end groups,* not simply incorporated polar moieties, that contribute to lithium salt solubility in PFPE electrolytes.

Increasing the concentration of PFPE end groups does not fully circumvent the apparent trade-off between the number and mobility of charge carriers in PFPE electrolytes. Hydrogen bonding and dipole-dipole interactions among carbonate- and hydroxyl-terminated polymers create higher friction coefficients.[6] Thus, although PFPEs with higher end group concentrations dissolve more lithium salts, they also have higher T_gs and thus lower ion mobilities. Despite these factors, perfluorinated glycols exhibit ionic conductivities matching that of the $PFPE_{E10}$ electrolytes reported in Chapter 2 of this work ($5x10^{-5}$ S cm^{-1} at 30°C). Moreover, the transference number of the glycol electrolytes is more than double that of $PFPE_{E10}$ and is among the highest reported in the literature (t^+>0.82). Manipulation of other polymer properties such as morphology may enable practical conductivity levels to be achieved without sacrificing the excellent stability and transference in PFPE electrolytes.

A few results from Part 1 highlight the importance of the perfluoroether backbone in lithium salt solvation. First, there is a critical molecular weight of PFPE (or more accurately, a minimum number of perfluoroether units), below which the combined lithium salt solvating ability of the backbone and end groups drops significantly. We believe that this lower molecular weight boundary is imposed by the requirement for a sufficiently long perfluoroether chain to interact with the perfluorinated $TFSI^-$ anion. Furthermore, LiTFSI is insoluble in perfluorinated octane-DMC, providing additional evidence that the CF_2CF_2O-$TFSI^-$ interaction plays an important role in lithium salt solvation. Chapter 5 will discuss recommendations for future work to tune the perfluoroether-anion interaction and polymer morphology for enhanced ionic conductivity in PFPE electrolytes.

REFERENCES

(1) Pianca, M.; Barchiesi, E.; Esposto, G.; Radice, S. End Groups in Fluoropolymers. *J. Fluor. Chem.* **1999**, *95*, 71–84.

(2) Timachova, K.; Watanabe, H.; Balsara, N. P. Effect of Molecular Weight and Salt Concentration on Ion Transport and the Transference Number in Polymer Electrolytes. *Macromolecules* **2015**, *48* (21), 7882–7888.

(3) Diddens, D.; Heuer, A.; Borodin, O. Understanding the Lithium Transport within a Rouse-Based Model for a PEO/LiTFSI Polymer Electrolyte. *Macromolecules* **2010**, *43* (4), 2028–2036.

(4) Shi, J.; Vincent, C. The Effect of Molecular Weight on Cation Mobility in Polymer Electrolytes. *Solid State Ionics* **1993**, *60* (1–3), 11–17.

(5) Teran, A. A.; Tang, M. H.; Mullin, S. A.; Balsara, N. P. Effect of Molecular Weight on Conductivity of Polymer Electrolytes. *Solid State Ionics* **2011**, *203* (1), 18–21.

(6) Devaux, D.; Bouchet, R.; Glé, D.; Denoyel, R. Mechanism of Ion Transport in PEO/LiTFSI Complexes: Effect of Temperature, Molecular Weight and End Groups. *Solid State Ionics* **2012**, *227*, 119–127.

(7) Wong, D. H. C.; Thelen, J. L.; Fu, Y.; Devaux, D.; Pandya, A. a; Battaglia, V. S.; Balsara, N. P.; DeSimone, J. M. Nonflammable Perfluoropolyether-Based Electrolytes for Lithium Batteries. *Proc. Natl. Acad. Sci. U. S. A.* **2014**, *111* (9), 3327–3331.

(8) Rubinstein, M.; Colby, R. H. *Polymer Physics*; Oxford University Press, 2003.

(9) Teran, A. A.; Tang, M. H.; Mullin, S. A.; Balsara, N. P. Effect of Molecular Weight on Conductivity of Polymer Electrolytes. *Solid State Ionics* **2011**, *203* (1), 18–21.

(10) Evans, J.; Vincent, C. A.; Bruce, P. G. Electrochemical Measurement of Transference Numbers in Polymer Electrolytes. *Polymer (Guildf).* **1987**, *28* (13), 2324–2328.

(11) Marchionni, G.; Ajroldi, G.; Pezzin, G. Structure–Property Relationships in Perfluoropolyethers: A Family of Polymeric Oils. In *Comprehensive Polymer Science and Supplements*; 1989; pp 347–388.

(12) Golodnitsky, D.; Strauss, E.; Peled, E.; Greenbaum, S. Review—On Order and Disorder in Polymer Electrolytes. *J. Electrochem. Soc.* **2015**, *162* (14), A2551–A2566.

(13) Alper, T.; Barlow, A. J.; Gray, R. W.; Kim, M. G.; McLachlan, R. J.; Lamb, J. Viscous, Viscoelastic and Dielectric Properties of a Perfluorinated Polymer, Krytox 143-AB. *J. Chem. Soc. Faraday Trans. 2* **1980**, *76* (0), 205.

(14) Krevelen, D. W. van (Dirk W.; Nijenhuis, K. te. *Properties of Polymers : Their Correlation with Chemical Structure ; Their Numerical Estimation and Prediction from Additive Group Contributions*; Elsevier, 2009.

(15) Timachova, K.; Chintapalli, M.; Olson, K. R.; Mecham, S. J.; DeSimone, J. M.; Balsara, N. P. Mechanism of Ion Transport in Perfluoropolyether Electrolytes with a Lithium Salt. *Soft Matter* **2017**, *13*, 5389-5396.

(16) Xu, K. Nonaqueous Liquid Electrolytes for Lithium-Based Rechargeable Batteries. *Chem. Rev.* **2004**, *104* (10), 4303–4418.

(17) Wang, Q.; Ping, P.; Zhao, X.; Chu, G.; Sun, J.; Chen, C. Thermal Runaway Caused Fire and Explosion of Lithium Ion Battery. *J. Power Sources* **2012**, *208*, 210–224.

(18) Lascaud, S.; Perrier, M.; Vallee, A.; Besner, S.; Prud'homme, J.; Armand, M. Phase Diagrams and Conductivity Behavior of Poly(ethylene Oxide)-Molten Salt Rubbery Electrolytes. *Macromolecules* **1994**, *27* (25), 7469–7477.

(19) Cameron, G. G.; Ingram, M. D. Liquid Polymer Electrolytes. In *Polymer Electrolyte Reviews*; MacCallum, J. R., Vincent, C. A., Eds.; Elsevier applied science; Springer, 1989.

(20) Nitzan, A.; Ratner ', M. A. Conduction in Polymers: Dynamic Disorder Transport. *J. Phys. Chem* **1994**, *98*, 1765–1775.

(21) Zhao, J.; Wang, L.; He, X.; Wan, C.; Jiang, C. Determination of Lithium-Ion Transference Numbers in $LiPF_6$ –PC Solutions Based on Electrochemical Polarization and NMR Measurements. *J. Electrochem. Soc.* **2008**, *155* (4), A292–A296.

(22) Dai, H.; Zawodzinski, T. A. The Dependence of Lithium Transference Numbers on Temperature, Salt Concentration and Anion Type in Poly (Vinylidene Fluoride)–hexafluoropropylene Copolymer-Based Gel Electrolytes. *J. Electroanal. Chem.* **1998**, *459* (1), 111–119.

(23) Koksbang, R.; Skou, E. Transference Number Measurements on a Hybrid Polymer Electrolyte. *Electrochim. Acta* **1995**, *40* (11), 1701.

(24) Olson, K. R.; Wong, D. H. C.; Chintapalli, M.; Timachova, K.; Janusziewicz, R.; Daniel, W. F. M.; Mecham, S.; Sheiko, S.; Balsara, N. P.; DeSimone, J. M. Liquid Perfluoropolyether Electrolytes with Enhanced Ionic Conductivity for Lithium Battery Applications. *Polymer (Guildf).* **2016**, *100*, 126–133.

(25) Chintapalli, M.; Timachova, K.; Olson, K. R.; Mecham, S. J.; Devaux, D.; DeSimone, J. M.; Balsara, N. P. Relationship between Conductivity, Ion Diffusion, and Transference Number in Perfluoropolyether Electrolytes. *Macromolecules* **2016**, *49* (9), 3508–3515.

(26) Sumerlin, B. S.; Vogt, A. P. Macromolecular Engineering through Click Chemistry and Other Efficient Transformations. *Macromolecules* **2010**, *43* (1), 1–13.

(27) Barner-Kowollik, C.; Du Prez, F. E.; Espeel, P.; Hawker, C. J.; Junkers, T.; Schlaad, H.; Van Camp, W. "Clicking" Polymers or Just Efficient Linking: What Is the Difference? *Angew. Chemie Int. Ed.* **2011**, *50* (1), 60–62.

(28) Song, J.; Ye, Q.; Lee, W. T.; Wang, X.; He, T.; Shah, K. W.; Xu, J. Perfluoropolyether/poly(ethylene Glycol) Triblock Copolymers with Controllable Self-Assembly Behaviour for Highly Efficient Anti-Bacterial Materials. *RSC Adv.* **2015**, *5* (79), 64170–64179.

(29) Wang, X.; Ye, Q.; Song, J.; Cho, C. M.; He, C.; Xu, J.; Lu, X.; He, C. Fluorinated Polyhedral Oligomeric Silsesquioxanes. *RSC Adv.* **2015**, *5* (6), 4547–4553.

(30) Koo, S. P. S.; Stamenović, M. M.; Prasath, R. A.; Inglis, A. J.; Du Prez, F. E.; Barner-Kowollik, C.; Van Camp, W.; Junkers, T. Limitations of Radical Thiol-Ene Reactions for Polymer-Polymer Conjugation. *J. Polym. Sci. Part A Polym. Chem.* **2010**, *48* (8), 1699–1713.

(31) Derboven, P.; D'hooge, D. R.; Stamenovic, M. M.; Espeel, P.; Marin, G. B.; Du Prez, F. E.; Reyniers, M.-F. Kinetic Modeling of Radical Thiol–Ene Chemistry for Macromolecular Design: Importance of Side Reactions and Diffusional Limitations. *Macromolecules* **2013**, *46* (5), 1732–1742.

(32) Feldman, K. E.; Martin, D. C. Functional Conducting Polymers via Thiol-Ene Chemistry. *Biosensors* **2012**, *2* (3), 305–317.

(33) Campos, L. M.; Killops, K. L.; Sakai, R.; Paulusse, J. M. J.; Damiron, D.; Drockenmuller, E.; Messmore, B. W.; Hawker, C. J. Development of Thermal and Photochemical Strategies for Thiol−Ene Click Polymer Functionalization. *Macromolecules* **2008**, *41* (19), 7063–7070.

(34) Korthals, B.; Morant-Miñana, M. C.; Schmid, M.; Mecking, S. Functionalization of Polymer Nanoparticles by Thiol−Ene Addition. *Macromolecules* **2010**, *43* (19), 8071–8078.

(35) Kolb, H. C.; Finn, M. G.; Sharpless, K. B. Click Chemistry: Diverse Chemical Function from a Few Good Reactions. *Angew. Chemie Int. Ed.* **2001**, *40* (11), 2004–2021.

(36) Colak, B.; Da Silva, J. C. S.; Soares, T. A.; Gautrot, J. E. Impact of the Molecular Environment on Thiol–Ene Coupling For Biofunctionalization and Conjugation. *Bioconjug. Chem.* **2016**, *27* (9), 2111–2123.

(37) Hoyle, C. E.; Lee, T. Y.; Roper, T. Thiol-Enes: Chemistry of the Past with Promise for the Future. *J. Polym. Sci. Part A Polym. Chem.* **2004**, *42* (21), 5301–5338.

(38) Johansson, P. First Principles Modelling of Amorphous Polymer Electrolytes: Li^+–PEO, Li^+–PEI, and Li^+–PES Complexes. *Polymer (Guildf).* **2001**, *42* (9), 4367–4373.

(39) Annika Bernson; Jan Lindgren; Wei Wei Huang; Roger Frech. Coordination and Conformation in PEO, PEGM, and PEG Systems Containing Lithium or Lanthanum Triflate. *Polymer (Guildf).* **1995**, *36* (23), 4471–4418.

Chapter 5: Recommendations for Future Work

5.1 Introduction

The application of perfluoropolyether (PFPE) materials to lithium-ion batteries represents a fundamentally new approach to battery electrolytes. Further exploration of these interesting systems will not only provide a better understanding of the molecular phenomena governing ion transport in PFPE systems but also enable the materials' full potential to be achieved. In this work, we thoroughly explored the relationship between electrolyte structure/composition and the resulting ion-polymer interactions and ion transport properties. We primarily focused in Chapters 2-4 on the importance of end group polarity, end group concentration, and molecular weight on the Li^+-polymer interactions. Yet much work remains to be done to understand and tune the interaction between the perfluoroether backbone and the perfluorinated anion. Furthermore, introduction of new polymer morphologies via microphase separation may unlock unique ion transport mechanisms. In this chapter, recommendations for future work in these areas are discussed.

5.2 Probing the Interaction between Fluorinated Anions and PFPE

5.2.1 Introduction

Transference numbers in PFPE electrolytes ($t^+ \approx 0.9$) are among the highest measured in lithium-ion battery electrolytes to date,[1] indicating that the perfluoroether backbone interacts favorably with perfluorinated anions. We tentatively attribute this to the fluorous effect, the tendency of perfluoroalkyl chains to segregate in order to minimize energetically unfavorable interactions of the nonpolarizable fluorine atoms with other elements.[2] Additional experimental

observations aside from the near-unity transference numbers provide support for the favorable perfluoroether-anion interaction in PFPE-lithium salt electrolytes:

1. Wong *et al.* reported increased linewidths of the $TFSI^-$ ^{19}F NMR signal in LiTFSI/PFPE solutions compared to LiTFSI/PEO or LiTFSI/D_2O solutions. The broader spectral lines are indicative of either lower $TFSI^-$ mobility or an increase in the number of microenvironments surrounding $TFSI^-$.[3]
2. There is a critical minimum molecular weight of the PFPE backbone, below which LiTFSI solubility drops precipitously. We tentatively proposed that the perfluoroether chains in $PFEG_3DMC$ may be too short to accommodate the $TFSI^-$ anion (characteristic length ≈ 8 Å),[4] resulting in ion association and aggregation. Considering the identical carbonate end groups of the glycols and the small ionic radius of lithium (≈ 0.7 Å), we consider it less likely that differences in the fundamental interactions between the oligomer and Li^+ are the root cause of the drastic differences in salt solvating ability of $PFEG_3DMC$ and $PFEG_4DMC$.
3. Finally, removal of ethereal oxygens from the perfluorinated tetraethylene glycol backbone [i.e. $PFEG_4DMC$ ($-CF_2CF_2O-$) vs. C8DMC ($-CF_2CF_2CF_2-$)] completely eliminates the material's LiTFSI solvating ability despite minimal changes to the dielectric constant.[5] We propose there is a favorable CF_2CF_2O-$TFSI^-$ interaction (but not $CF_2CF_2CF_2$-$TFSI^-$ interaction) that supplements the Li^+-end group interaction.

Electrostatic interactions between Li^+ and hydroxyl or carbonate end groups contribute significantly to LiTFSI solvation in PFPE electrolytes. Yet we propose that this interaction alone is insufficient for lithium salt solvation. A complimentary interaction between the perfluoroether backbone and the perfluorinated anion facilitates counterion solvation, preventing association or

aggregation of the salt on a macroscopic scale. Although there are multiple pieces of evidence supporting this hypothesis, direct spectroscopic evidence of PFPE-fluorinated anion interactions remains to be obtained. To develop commercially relevant perfluoropolyether electrolytes, it will be necessary to gain a fundamental understanding of the perfluoroether-anion interaction and tune that interaction for better performance.

5.2.2 Recommendations for Spectroscopic Analysis of Perfluoroether-Anion Interaction

Infrared (IR) and Raman spectroscopy have been used extensively to probe the interaction between Li^+ and electrolytes.[6-18] Shifts in the vibrational and rotational modes of functional groups contained in both the solvent (ether,[7,9,15] nitrile,[14] carbonate[8,14,16,17,19,20]) and anion (triflate,[10,12–14] sulfonamide,[6–9,17] hexafluorophosphate[15]) have been analyzed to characterize ion-solvent interactions and ion-pairing effects. The above studies focus primarily on the vibrational frequencies of i) solvent functional groups to characterize the cation-solvent interactions and of ii) anion functional groups to characterize ion pairing and aggregation based on "free" anions, contact ion pairs, and triplets.[12,13,21,22]

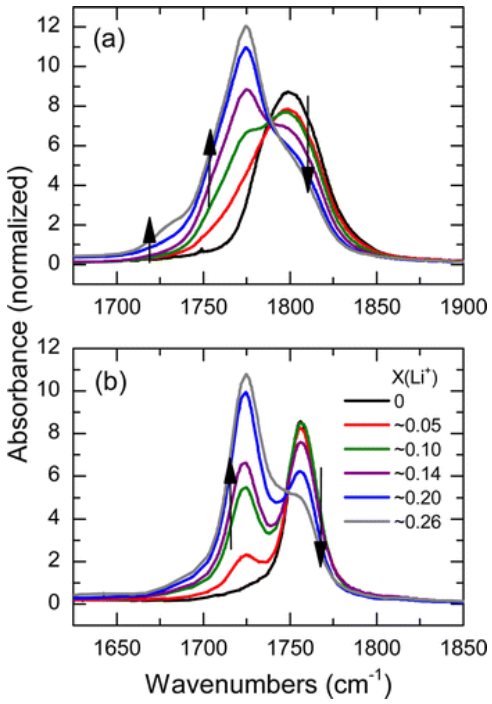

Figure 5.1 FTIR of C=O stretch region. Spectra shown for (a) 1,2 butylene carbonate and (b) dimethyl carbonate at various concentrations of Li^+. Arrows indicate changes in the spectra with increasing salt concentration. Reprinted with permission from ref. [20]. Copyright (2016) American Chemical Society.

IR and Raman spectroscopy may prove to be informative for probing the interaction of the anion with PFPE electrolytes. Analysis of the vibrational frequencies associated with the PFPE backbone (830 cm^{-1} C-O, 1050-1200 cm^{-1} CF_2)[23] as a function of lithium salt concentration may provide further evidence for the perfluoroether-anion interaction, analogous to the frequency shift in the C=O stretch caused by Li^+-end group interactions. The interaction of the solvent with the $TFSI^-$ anion should also change the internal force constants of the anion, shifting all modes to higher frequencies relative to the free ion.[24] A comprehensive study should be carried out to develop a full understanding of the PFPE-anion interaction. We recommend the study to include the following:

First, the frequencies of the "free" $TFSI^-$ anion's vibrational modes should be confirmed (previously reported as $\nu(CF_3)$ = 1190-1240 cm^{-1}).[25] If the stretching frequency of the CF_3 group is found to overlap with the normal modes of the PFPE backbone, alternative modes can also be

explored near 760 cm^{-1}.[14] LiTFSI should be dissolved in aprotic solvents of variable polarity to determine the "free" state of the anion in the absence of solvent effects and ion-pairing effects.[25] Assuming the $TFSI^-$ anion exhibits similar behavior to the triflate anion, the vibrational frequencies of the anion should be consistent and solvent-independent in THF, triglyme, and acetone (polar solvents with low acceptor numbers).[24] It should be confirmed that ion pairing in these solvents is negligible by dissolving $TFSI^-$ complexes with various counterions (e.g. sodium, potassium, magnesium) in each solvent and confirming the CF_3 vibrational modes remain unchanged.

Next, the normal modes of the perfluoropolyether backbone should be established. Vibrational frequencies reported in the literature should be confirmed by obtaining the IR spectrum of neat PFPE.[23] Lithium salts with non-fluorinated counterions such as perchlorate (ClO_4^-) or bis(oxalate)borate [$B(C_2O_4)_2^-$] should then be mixed with PFPE. Provided these salts dissolve in PFPE, this will enable any interactions of the PFPE backbone with Li^+ or with non-fluorinated anions to be quantified based on the changes in the normal modes of the perfluoroether backbone. The backbone's vibrational modes will remain largely unchanged in these solutions if PFPE indeed interacts primarily with fluorinated anions as we suspect. IR spectra of PFPE solutions containing LiTFSI [anion $N(SO_2CF_3)_2^-$] should then be measured. Shifts in the vibrational frequencies of the normal modes for both the perfluoroether backbone and the $TFSI^-$ anion can be analyzed to quantify the interaction between the perfluoroether backbone and fluorinated anions.

The same procedure should be carried out using other lithium salts containing fluorinated anions such as LiFSI and LiBETI (structures shown in Figure 5.2). This will enable the relationship between anion fluorocarbon chain length and interaction strength between the perfluoroether backbone and anion to be established. This systematic spectroscopic study will provide clarity on

the dynamic interaction between PFPE solvents and fluorinated anions of lithium salts, which can then be used to improve the design of future PFPE electrolytes.

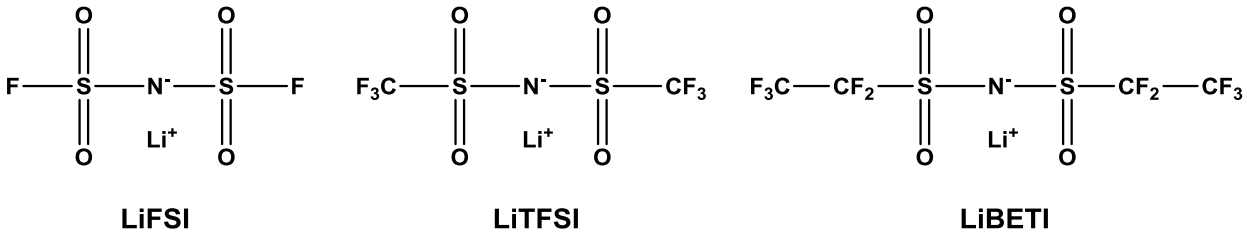

Figure 5.2 Structure of lithium salts with various fluorinated anions.

5.3 Inducing Microphase Separation in PFPE Electrolytes for Unique Ion Transport

5.3.1 Introduction

Wong *et al.* investigated physical blends of $PFPE_{1000}$ and PEG_{400} as electrolyte solvents.[3] In the absence of LiTFSI salt, PFPE/PEG blends containing less than 60 wt.% PFPE phase separated on a macroscopic scale. In contrast, PFPE/PEG mixtures containing over 60 wt.% PFPE were miscible blends that dissolved LiTFSI and produced a uniform ionic environment rather than a combination of ionic environments from pure PFPE and PEG.[3] The uniform ionic environment was intermediate between that of PFPE and PEG, causing the physical blends to exhibit lower conductivity but slightly higher t^+ (0.29 vs. 0.17) than pure PEG electrolytes.

In chapter 2, we reported on our studies of Fluorolink E10, a PFPE material with oligoether end groups. The weight fraction of ether end groups and PFPE backbone were 15% and 85%, respectively, compared to the 20 wt.% PEG_{400} / 80 wt.% $PFPE_{1000}$ reported by Wong *et al*. The electrolyte performance of Fluorolink E10 was similar to that of the PFPE-PEG blends, indicating that the ionic environment was once again uniform.[3,26,27] This was supported by wide-angle x-ray scattering studies carried out by Chintapalli *et al.*, who found Fluorolink E10 is disordered at room temperature and estimated that microphase separation would occur at about 262 K.[28] Despite some

incipient, disordered concentration fluctuations, the ionic environment remains largely homogeneous at room temperature. In short, covalent attachment of short PEG groups to the PFPE backbone does not alter the electrolyte behavior significantly compared to simply blending the PFPE and PEG materials.

5.3.2 Recommendations for Future Work: PEO-PFPE-PEO Triblock Copolymers

Block copolymers, in contrast to polymer blends, do not exhibit macroscopic phase separation due to molecular constraints: the chains are covalently bonded.[29,30] Instead, phase separation is limited to the molecular dimensions. Thus, block copolymer electrolytes are not restricted to the miscibility window of their components in the same way that physical blends might be. PEO-PFPE-PEO triblock copolymers with sufficiently long PEO blocks are expected to microphase separate into two distinct ionic environments rather than producing a uniform ionic environment intermediate between PFPE and PEO.

Several studies have targeted high modulus, high ionic conductivity materials by employing block copolymer electrolytes with conductive PEO domains interspersed within a dimensionally stable matrix.[31-34] Polystyrene-block-poly(ethylene oxide) ("SEO")[33,35] and polyethylene-block-poly(ethylene oxide)[34] are a few examples of commonly studied block copolymer electrolytes. The novel aspect of our approach is that we are targeting a conductive PEO domain interspersed within an anion-trapping domain rather than a high modulus one.

Block copolymers may assemble into body-centered cubic spheres or close-packed spheres, hexagonally packed cylinders, double gyroids, orthorhombic networks, and lamellae.[36] An example of the dependence of ionic conductivity on polymer morphology is provided in Figure 5.3.[37] As discussed in Chapter 3, the self-assembly of block copolymers is determined by the Flory-Huggins interaction parameter χ, the degree of polymerization N, and the block volume

fractions.[36,38] We developed a synthetic strategy to achieve PEO-PFPE-PEO block copolymers with fine control over morphology by coupling PEO blocks of varying molecular weight onto PFPE. The synthesis is outlined in Scheme 5.1. It should be noted that the anionic ring-opening polymerization of ethylene oxide from $PFPE_{E10}$-Diol was repeatedly unsuccessful, consistent with previous reports of complicating chain-transfer reactions in the anionic polymerization of fluorinated epoxides.[39]

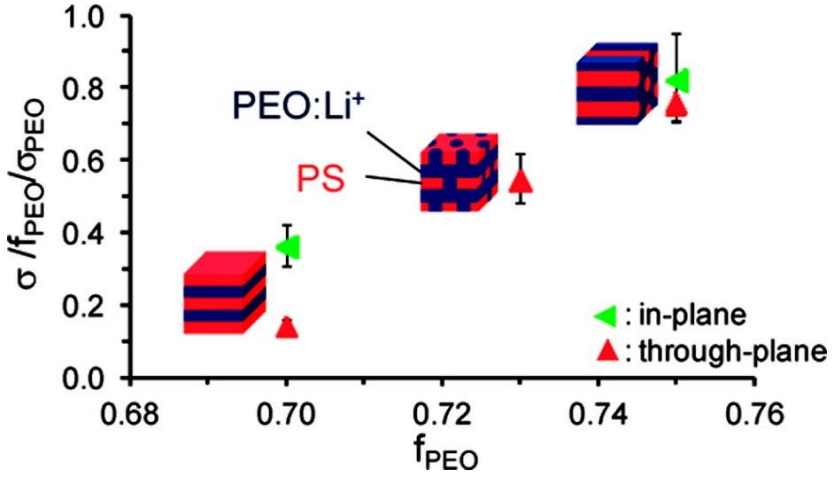

Figure 5.3 Ionic conductivity of SEO electrolytes as a function of polymer morphology. Reprinted with permission from ref. [37]. Copyright (2012) American Chemical Society.

Scheme 5.1 Synthesis of PEO-PFPE-PEO triblock copolymers.

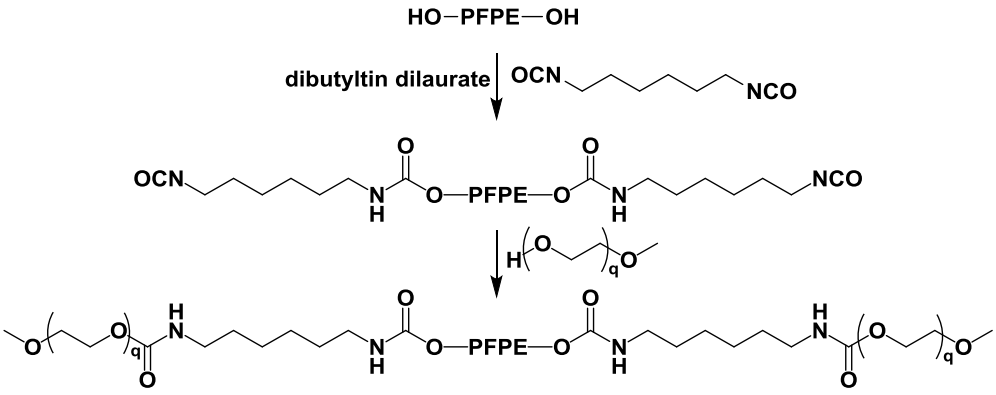

5.3.3 Recommendations for Characterization of PEG-PFPE-PEG Triblock Copolymers

Many of the parameters discussed in this work—maximum lithium salt solubility, thermal stability, ionic conductivity, and transference number—have yet to be characterized in the PEG-PFPE-PEG triblock copolymers. Considering these copolymers become extremely viscous upon addition of lithium salt, we recommend against simply stirring lithium salts with the neat copolymers to determine maximum lithium salt solubility. Instead, following the method of Lascaud *et al*,[40] varying ratios of LiTFSI and PFPE-PEG materials should be mixed in a suitable solvent such as THF at a concentration of 5%, after which the solvent can be removed under dynamic vacuum. DSC thermograms at each composition can be analyzed to establish the phase behavior of the electrolytes at varying salt concentrations, as shown for PEO-LiTFSI in Figure 5.4.[40]

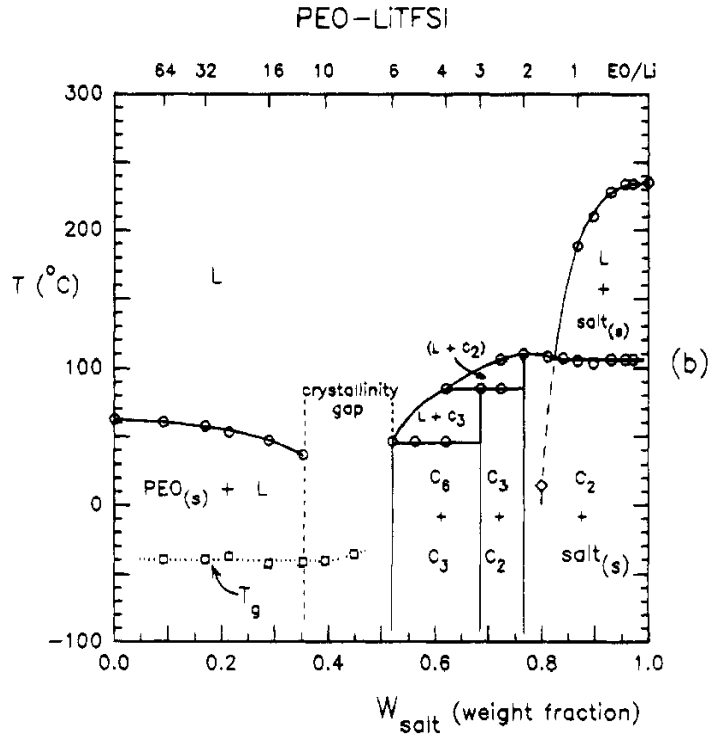

Figure 5.4 Phase diagram of PEO-LiTFSI derived from calorimetric analysis of DSC data. Reprinted with permission from ref. [40]. Copyright (1994) American Chemical Society.

A combination of transmission electron microscopy (TEM),[41] wide-angle x-ray scattering (WAXS),[28] and small-angle x-ray scattering (SAXS)[42] should be employed to explore the microstructures of PEG-PFPE-PEG triblock copolymers as a function of PEG molecular weight. Analysis of x-ray scattering peaks as a function of the scattering vector, *q*, enables identification of polymer morphology. For example, Chintapalli *et al.* determined that the morphology of a polystyrene-poly(ethylene oxide) (SEO) electrolyte was lamellar because the sample exhibited higher order scattering peaks at integer values of the prominent peak (i.e. peaks at q^*, $2q^*$, $3q^*$).[42]

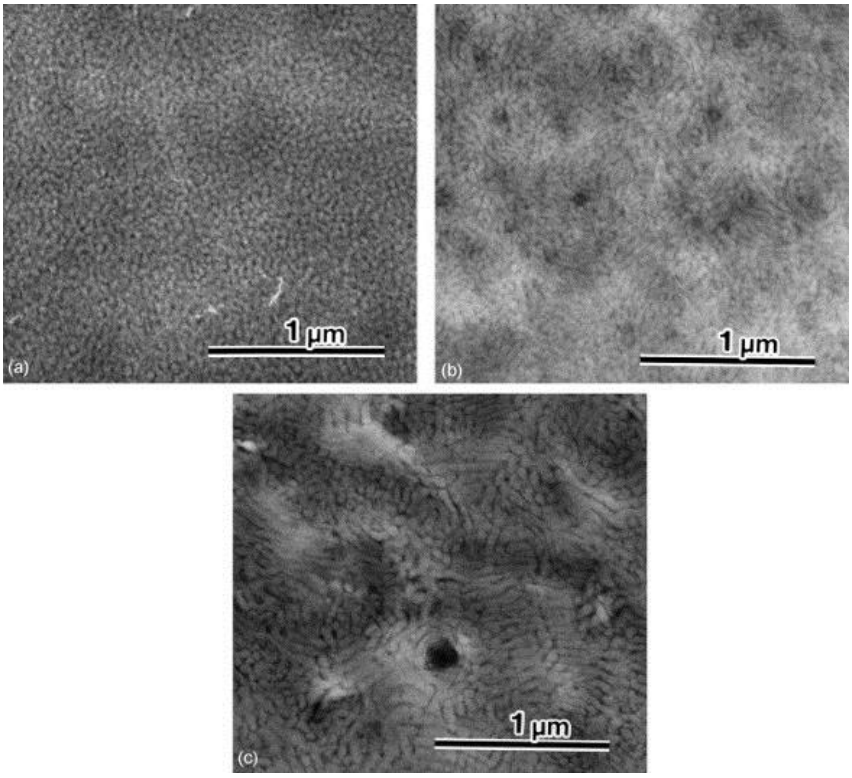

Figure 5.5 TEM images of a polystyrene-poly(poly(ethyleneglycol)methyl ether methacrylate)-polystyrene triblock copolymer at a) 70% b) 50-70% and c) 30-50% PEO content. Reprinted from ref. [41] with permission from Elsevier.

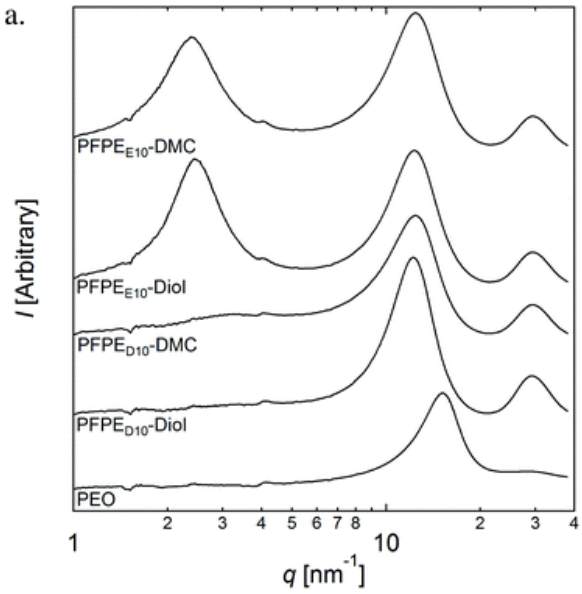

Figure 5.6 WAXS profiles of PFPE and PEO polymers at 30°C. Reproduced from ref. [28] with permission from The Royal Society of Chemistry.

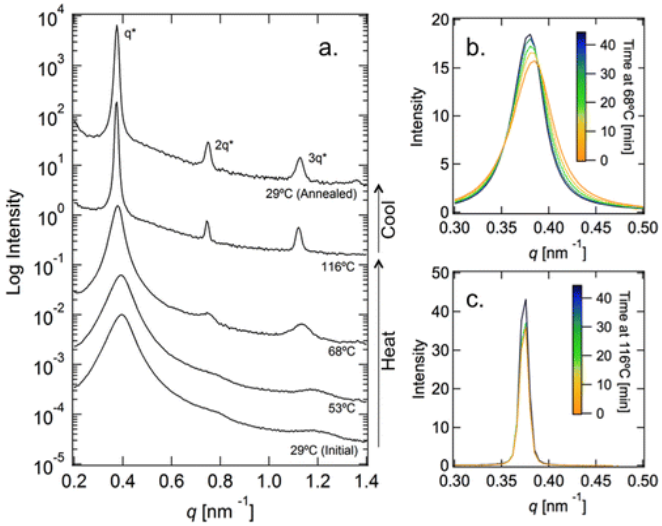

Figure 5.7 SAXS intensity of a polystyrene-block poly(ethylene oxide) lamellar polymer as a function of the magnitude of the scattering vector, *q*, during heating and cooling. Reprinted with permission from ref. [42]. Copyright (2014) American Chemical Society.

After identifying the various polymer morphologies exhibited by PFPE-PEG copolymer electrolytes as a function of PEG chain length and temperature, ionic conductivity and t^+ should also be measured as a function of PEG *N* and temperature. This will provide insight into the effect

of polymer microstructure on ion transport. Inceoglu *et al*. performed in situ experiments wherein ionic conductivity of a polyethylene oxide-poly(styrene LiTFSI) electrolyte was measured concurrently with the SAXS experiment during a heating run.[43] Interestingly, it was determined that ion transport became more efficient at high temperature upon homogenization of the block copolymer microstructure. This study was carried out on a block copolymer electrolyte in which the $TFSI^-$ anion was covalently bound to the polystyrene block, and thus homogenization of the block copolymer microstructure coincided with lithium ion migration into conductive (PEO) domains. This same technique could be carried out on the PEG-PFPE-PEG triblock copolymers to determine how ion transport mechanisms change as a function of electrolyte morphology.

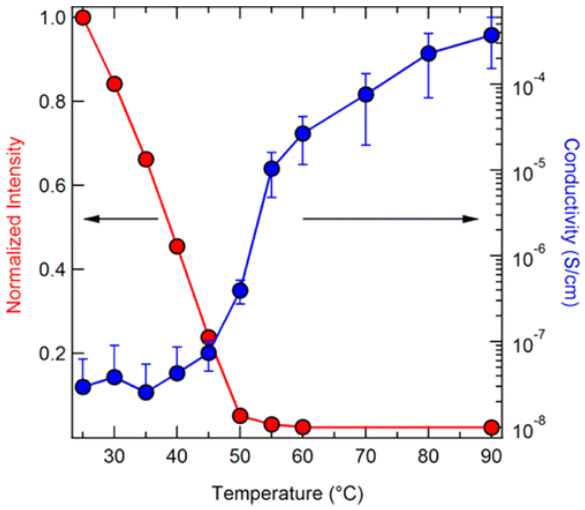

Figure 5.8 Temperature dependence of the ionic conductivity (blue circles) and normalized SAXS intensity at q = 0.228 nm^{-1} (red circles) for PEO–PSLiTFSI(5.0–3.2), r = 0.088. Intensity at each temperature was normalized by the measured value at 25 °C. Reprinted with permission from ref. [43]. Copyright (2014) American Chemical Society.

REFERENCES

(1) Wong, D. H. C.; Thelen, J. L.; Fu, Y.; Devaux, D.; Pandya, A. a; Battaglia, V. S.; Balsara, N. P.; DeSimone, J. M. Nonflammable Perfluoropolyether-Based Electrolytes for Lithium Batteries. *Proc. Natl. Acad. Sci. U. S. A.* **2014**, *111* (9), 3327–3331.

(2) Cametti, M.; Crousse, B.; Metrangolo, P.; Milani, R.; Resnati, G. The Fluorous Effect in Biomolecular Applications. *Chem. Soc. Rev. Chem. Soc. Rev* **2012**, *41* (41), 31–42.

(3) Wong, D. H. C.; Vitale, A.; Devaux, D.; Taylor, A.; Pandya, A. A.; Hallinan, D. T.; Thelen, J. L.; Mecham, S. J.; Lux, S. F.; Lapides, A. M.; et al. Phase Behavior and Electrochemical Characterization of Blends of Perfluoropolyether, Poly(ethylene Glycol), and a Lithium Salt. *Chem. Mater.* **2015**, *27* (2), 597–603.

(4) Timachova, K.; Chintapalli, M.; Olson, K. R.; Mecham, S. J.; DeSimone, J. M.; Balsara, N. P. Mechanism of Ion Transport in Perfluoropolyether Electrolytes with a Lithium Salt. *Soft Matter* **2017**, *13*, 5389-5396.

(5) Marchionni, G.; Ajroldi, G.; Pezzin, G. Structure–Property Relationships in Perfluoropolyethers: A Family of Polymeric Oils. In *Comprehensive Polymer Science and Supplements*; 1989; pp 347–388.

(6) Seo, D. M.; Boyle, P. D.; Sommer, R. D.; Daubert, J. S.; Borodin, O.; Henderson, W. A. Solvate Structures and Spectroscopic Characterization of LiTFSI Electrolytes. *J. Phys. Chem. B* **2014**, *118* (47), 13601–13608.

(7) Brouillette, D.; Irish, D. E.; Taylor, N. J.; Perron, G.; Odziemkowski, M.; Desnoyers, J. E. Stable Solvates in Solution of Lithium Bis(trifluoromethylsulfone)imide in Glymes and Other Aprotic Solvents: Phase Diagrams, Crystallography and Raman Spectroscopy. *Phys. Chem. Chem. Phys.* **2002**, *4* (24), 6063–6071.

(8) Wang, Z.; Gao, W.; Huang, X.; Mo, Y.; Chen, L. Spectroscopic Studies on Interactions and Microstructures in Propylene Carbonate-LiTFSI Electrolytes. *J. Raman Spectrosc.* **2001**, *32* (11), 900–905.

(9) Rey, I.; Lassègues, J. C.; Grondin, J.; Servant, L. Infrared and Raman Study of the PEO-LiTFSI Polymer Electrolyte. *Electrochim. Acta* **1998**, *43* (10–11), 1505–1510.

(10) Ferry, A. Ionic Interactions and Transport Properties in Methyl Terminated Poly(propylene glycol)(4000) Complexed with $LiCF_3SO_3$. *J. Phys. Chem. B* **1997**, *101* (2), 150–157.

(11) Huang, W.; Wheeler, R. A.; Frech, R. Vibrational Spectroscopic and Ab Initio Molecular Orbital Studies of the Normal and ^{13}C-Labelled Trifluoromethanesulfonate Anion. *Spectrochim. Acta Part A Mol. Spectrosc.* **1994**, *50* (5), 985–996.

(12) Huang, W.; Frech, R.; Wheeler ', R. A. Molecular Structures and Normal Vibrations of CF_3SO_3-and Its Lithium Ion Pairs and Aggregates. *J. Phys. Chem* **1994**, *98*, 100–101.

(13) Frech, R.; Chintapalli, S.; Bruce, P. G.; Vincent, C. A. Structure of an Amorphous Polymer Electrolyte, Poly(ethylene Oxide)$_3$: $LiCF_3SO_3$. *Chem. Commun.* **1997**, *0*, 157–158.

(14) Chen, H.-W.; Chang, F.-C. Interaction Mechanism of a Novel Polymer Electrolyte Composed of Poly(acrylonitrile), Lithium Triflate, and Mineral Clay. *J. Polym. Sci. Part B Polym. Phys.* **2001**, *39* (20), 2407–2419.

(15) Burba, C. M.; Frech, R. Spectroscopic Measurements of Ionic Association in Solutions of $LiPF_6$. *J. Phys. Chem. Bournal Phys. Chem.* **2005**, *109* (31), 15161–15164.

(16) Wang, Z.; Huang, B.; Hong, H.; Chen, L.; Xue, R.; Wang, F. Infrared Spectroscopic Study of the Interaction between Lithium Salt $LiClO_4$ and the Plasticizer Ethylene Carbonate in the Polyacrylonitrile-Based Electrolyte. *Solid State Ionics* **1996**, *85* (1–4), 143–148.

(17) Deepa, M.; Agnihotry, S. .; Gupta, D.; Chandra, R. Ion-Pairing Effects and Ion–solvent–polymer Interactions in $LiN(CF_3SO_2)_2$–PC–PMMA Electrolytes: A FTIR Study. *Electrochim. Acta* **2004**, *49* (3), 373–383.

(18) Jobin Yvon SAS, H. Raman Microspectroscopy in Electrochemistry: Study of a Lithium Battery.

(19) Tsunekawa, H.; Narumi, A.; Sano, M.; Hiwara, A.; Fujita, M.; Yokoyama, H. Solvation and Ion Association Studies of $LiBF_4$−Propylenecarbonate and $LiBF_4$−Propylenecarbonate −Trimethyl Phosphate Solutions. *J. Phys. Chem. B* **2003**, *107* (39), 10962–10966.

(20) Fulfer, K. D.; Kuroda, D. G. Solvation Structure and Dynamics of the Lithium Ion in Organic Carbonate-Based Electrolytes: A Time-Dependent Infrared Spectroscopy Study. *J. Phys. Chem. C* **2016**, *120* (42), 24011–24022.

(21) Edman, L. Ion Association and Ion Solvation Effects at the Crystalline−Amorphous Phase Transition in PEO−LiTFSI. *J. Phys. Chem. B* **2000**, *104* (31), 7254–7258.

(22) Ferry, A.; Jacobsson, P.; Torell, L. M. The Molar Conductivity Behavior in Polymer Electrolytes at Low Salt Concentrations; A Raman Study of Poly(propylene Glycol) Complexed with $LiCF_3SO_3$. *Electrochim. Acta* **1995**, *40* (13–14), 2369–2373.

(23) Sung, D.; Gellman, A. J.; Gui, J.; Ma, X. High Resolution Electron Energy Loss Spectroscopy Study of Fomblin Z-Tetraol Thin Films. *J. Vac. Sci. Technol. A J. Chem. Phys. J. Appl. Phys. J. Chem. Phys. J. Vac. Sci. Technol. A* **2005**, *231* (10).

(24) Frech, R.; Huang, W. Anion-Solvent and Anion-Cation Interactions in Lithium and Tetrabutylammonium Trifluoromethanesulfonate Solutions. *J. Solution Chem.* **1994**, *23* (4).

(25) Herstedt, M.; Smirnov, M.; Johansson, P.; Chami, M.; Grondin, J.; Servant, L.; Lassègues, J. C. Spectroscopic Characterization of the Conformational States of the Bis(trifluoromethanesulfonyl)imide Anion ($TFSI^-$). *J. Raman Spectrosc.* **2005**, *36* (8), 762–770.

(26) Olson, K. R.; Wong, D. H. C.; Chintapalli, M.; Timachova, K.; Janusziewicz, R.; Daniel, W. F. M.; Mecham, S.; Sheiko, S.; Balsara, N. P.; DeSimone, J. M. Liquid Perfluoropolyether Electrolytes with Enhanced Ionic Conductivity for Lithium Battery Applications. *Polymer (Guildf).* **2016**, *100*, 126–133.

(27) Chintapalli, M.; Timachova, K.; Olson, K. R.; Mecham, S. J.; Devaux, D.; DeSimone, J. M.; Balsara, N. P. Relationship between Conductivity, Ion Diffusion, and Transference Number in Perfluoropolyether Electrolytes. *Macromolecules* **2016**, *49* (9), 3508–3515.

(28) Chintapalli, M.; Timachova, K.; Olson, K. R.; Banaszak, M.; Thelen, J. L.; Mecham, S. J.; DeSimone, J. M.; Balsara, N. P. Incipient Microphase Separation in Short Chain Perfluoropolyether-Block-Poly(ethylene Oxide) Copolymers. *Soft Matter* **2017**, *13* (22), 4047–4056.

(29) Leibler, L. Theory of Microphase Separation in Block Copolymers. *Macromolecules* **1980**, *13* (6), 1602–1617.

(30) Hashimoto, T.; Shibayama, M.; Kawai, H. Ordered Structure in Block Polymer Solutions. 4. Scaling Rules on Size of Fluctuations with Block Molecular Weight, Concentration, and Temperature in Segregation and Homogeneous Regimes. *Macromolecules* **1983**, *16* (7), 1093–1101.

(31) Gomez, E. D.; Panday, A.; Feng, E. H.; Chen, V.; Stone, G. M.; Minor, A. M.; Kisielowski, C.; Downing, K. H.; Borodin, O.; Smith, G. D.; et al. Effect of Ion Distribution on Conductivity of Block Copolymer Electrolytes. *Nano Lett.* **2009**, *9* (3), 1212–1216.

(32) Minelli, M.; Giacinti Baschetti, M.; Hallinan, D. T.; Balsara, N. P. Study of Gas Permeabilities through Polystyrene-Block-Poly(ethylene Oxide) Copolymers. *J. Memb. Sci.* **2013**, *432*, 83–89.

(33) Singh, M.; Odusanya, O.; Wilmes, G. M.; Eitouni, H. B.; Gomez, E. D.; Patel, A. J.; Chen, V. L.; Park, M. J.; Fragouli, P.; Iatrou, H.; et al. Effect of Molecular Weight on the Mechanical and Electrical Properties of Block Copolymer Electrolytes. *Macromolecules* **2007**, *40* (13), 4578–4585.

(34) Khurana, R.; Schaefer, J. L.; Archer, L. A.; Coates, G. W. Suppression of Lithium Dendrite Growth Using Cross-Linked Polyethylene/Poly(ethylene Oxide) Electrolytes: A New Approach for Practical Lithium-Metal Polymer Batteries. *J. Am. Chem. Soc.* **2014**, *136* (20), 7395–7402.

(35) Yuan, R.; Teran, A. A.; Gurevitch, I.; Mullin, S. A.; Wanakule, N. S.; Balsara, N. P. Ionic Conductivity of Low Molecular Weight Block Copolymer Electrolytes. *Macromolecules* **2013**, *46* (3), 914–921.

(36) Young, W.-S.; Kuan, W.-F.; Epps, T. H. Block Copolymer Electrolytes for Rechargeable Lithium Batteries. *J. Polym. Sci. Part B Polym. Phys.* **2014**, *52* (1), 1–16.

(37) Young, W.-S.; Epps, T. H. Ionic Conductivities of Block Copolymer Electrolytes with Various Conducting Pathways: Sample Preparation and Processing Considerations. *Macromolecules* **2012**, *45* (11), 4689–4697.

(38) Rubinstein, M.; Colby, R. H. *Polymer Physics*; Oxford University Press, 2003.

(39) Smart, B. E.; Farnham, W. B.; Nappa, M. J. Silicon-Mediated Synthesis of Poly(Fluorovinyl Ethers) and Poly(Perfluoroalkenes). In *Progress in Pacific Polymer Science 2*; Springer Berlin Heidelberg: Berlin, Heidelberg, 1992; pp 75–82.

(40) Lascaud, S.; Perrier, M.; Vallee, A.; Besner, S.; Prud'homme, J.; Armand, M. Phase Diagrams and Conductivity Behavior of Poly(ethylene Oxide)-Molten Salt Rubbery Electrolytes. *Macromolecules* **1994**, *27* (25), 7469–7477.

(41) Niitani, T.; Shimada, M.; Kawamura, K.; Kanamura, K. Characteristics of New-Type Solid Polymer Electrolyte Controlling Nano-Structure. *J. Power Sources* **2005**, *146* (1–2), 386–390.

(42) Chintapalli, M.; Chen, X. C.; Thelen, J. L.; Teran, A. A.; Wang, X.; Garetz, B. A.; Balsara, N. P. Effect of Grain Size on the Ionic Conductivity of a Block Copolymer Electrolyte. *Macromolecules* **2014**, *47* (15), 5424–5431.

(43) Inceoglu, S.; Rojas, A. A.; Devaux, D.; Chen, X. C.; Stone, G. M.; Balsara, N. P. Morphology–Conductivity Relationship of Single-Ion-Conducting Block Copolymer Electrolytes for Lithium Batteries. *ACS Macro Lett.* **2014**, *3* (6), 510–514.